A Cluster of Galaxies at z = 0.9

by

Gordon Chattan Ross

B.Sc., University of Victoria 1987

A THESIS SUBMITTED IN PARTIAL FULFILLMENT
OF THE REQUIREMENTS FOR THE DEGREE OF
MASTER OF SCIENCE

in the Department

of

Physics and Astronomy

We accept this thesis as conforming
to the required standard

[redacted]

Supervisor Dr. C. J. Pritchet

[redacted]

Dr. F. D. A. Hartwick

[redacted]

Dr. J. B. Tatum

[redacted]

Dr. A. Zielinski

[redacted]

Dr. D. Crampton

Supervisor: Dr. Christopher J. Pritchet

ABSTRACT

We present a study of faint galaxies in the field surrounding the $z = 0.90$ radio galaxy, 3C 217. Deep broadband and narrowband CCD images were obtained by Pritchet and Hartwick (1987) at the prime focus of the Canada-France-Hawaii 3.6 m telescope and limiting magnitudes of $B = 25.5$, $R = 25$ and $I = 24$ were achieved. Number counts indicate two to four times the number of galaxies expected for a field sample and the distribution of excess counts provides an acceptable fit to a Schechter function at the redshift of 3C 217. The colours and spectral energy distributions of the brightest objects in I were compared with predicted values, which permitted the differentiation of field and cluster galaxies. Many of these cluster galaxies show strong evolution with $B - R$ and $R - I$ colours indicating star formation rates of $\mu \leq 0.5$ in Bruzual's exponential models. However, there are strong K corrections and selection effects that limit the detectability of faint elliptical galaxies. After the strength of these effects were estimated, the sample was transformed to an absolute V magnitude system. The sample shows a fractional content of $20-30\%$ evolving galaxies to a limiting absolute magnitude of $M_V = -19.8$ ($H_o = 100$,$q_o = 0.0$). This is comparable to the blue fraction found in the high redshift clusters ($z \approx 0.5$) in the Butcher-Oemler (1984) sample, but does not appear compatible with the extension of the Butcher-Oemler effect out to $z = 0.9$. Observations 1.0 mag fainter in R would suffice to confirm the elliptical content.

Examiners:

[redacted]

Dr. C.J. Pritchet, Supervisor

[redacted]

Dr. F.D.A. Hartwick, Department Member

[redacted]

Dr. J.B. Tatum, Department Member

[redacted]

Dr. A. Zielinski, Outside Member

[redacted]

Dr. D. Crampton, Outside Member

Contents

List of Figures

Chapter 1

Introduction

Galaxies are the basic units of structure in the Universe. When did they form and what governs their evolution? Galaxies are such fundamental objects that we should study them if only to understand their existence. We can also hope that an understanding of the evolution of galaxies will lead to a better understanding of the Universe that created them.

In our search for an understanding of the evolution of galaxies, we have a powerful tool: the light travel time, or lookback time to distant galaxies. This allows us to see distant galaxies as they were billions of years ago, when their light first began its journey through space. However, the further into the past we look, the fainter the galaxies become. Furthermore, our view of the past does not go entirely unaltered. As light travels though space, the Universe expands and the light waves expand with it. Therefore, when light arrives at our telescopes, it is redshifted, so that our detectors and filters do not measure the same colours as they would for nearby galaxies. This is known as the K correction and the effect depends on both the type of galaxy and its distance.

Galaxies span a wide range of masses, luminosities and colours, but most fall into two main categories. First are the elliptical, or early type galaxies, which are spheroidal in shape and contain mostly old, cool stars. They are red in colour and, at the present epoch, generally reveal no traces of current star formation, or gas and dust that might be associated with star formation Spirals, or late type galaxies, have a more complex structure consisting of a flattened disk, a central bulge and a diffuse outer halo. The central bulge is somewhat similar to elliptical galaxies and both the bulge and halo contain mostly old, cool stars. However the disk contains many young, hot stars as well as gas and dust. Star formation also occurs in the disk, a fact that, along with the younger stars, makes spiral galaxies appear bluer then elliptical galaxies.

On sufficiently large scales, the distribution of galaxies appears nearly uniform. On smaller scales, however, galaxies often form small groups, and occasionally large concentrations, or clusters, of galaxies are seen. Clusters may contain more than 1000 galaxies bound together by their mutual gravitational attraction. In the nearby clusters, the majority of galaxies are elliptical whereas the majority of galaxies outside of clusters, *i.e.* in the field, appear to be spiral. It therefore appears that the present day environment of galaxies plays an important role in their evolution.

The search for evolution in distant galaxies has involved studies of galaxies both in clusters and in the field. Field surveys have the advantage that large, complete samples of faint galaxies are relatively easy to obtain with prime focus plates on 4 metre class telescopes. But because the distances to most individual galaxies are unknown, evolution can only be discerned qualitatively. Attempts have been made to determine redshifts from photometric colours (Koo 1985, Couch *et al.* 1983), but such work is hampered by

the effects of evolution. With the advent of multi-aperture spectroscopy, the problem of determining redshifts for large numbers of faint galaxies is only now being addressed.

Investigations into evolution in cluster galaxies has produced more quantitative results, although these observations are still the source of some debate. Evidence of evolution in cluster galaxies was first observed by Butcher and Oemler (hereafter BO) in their classic 1978 paper. They observed two high redshift clusters, Cl 0024+16 ($z = 0.39$) and the cluster containing 3C 295 ($z = 0.46$), both rich, centrally condensed systems similar to the nearby Coma cluster. Their initial finding was that 40% to 50% of the galaxies in these high redshift systems had relatively blue colours that resembled spiral galaxies, whereas Coma, and other nearby rich clusters, are mainly composed of redder E and S0 galaxies. BO suggested that this was evidence of strong evolution in distant clusters (at large lookback times) and that the blue galaxies were a population of spiral galaxies that would evolve into the early type systems that dominate nearby clusters today.

The publication of these results prompted several follow-up studies of these clusters (*e.g.* Mathieu and Spinrad 1981, Dressler and Gunn 1982, 1983), some of which sharply disagreed with BO. In particular, they felt that the number of background galaxies had been underestimated; since the field is dominated by spiral galaxies, this had resulted in an excess of blue galaxies. Dressler (1985) also found that many blue galaxies that were cluster members did not have the spectral characteristics of normal spiral galaxies. Among these abnormal galaxies was a high incidence of active and emission line galaxies, and unusual E+A galaxies (modeled as a combination of the spectrum of a normal giant elliptical and the spectra of A dwarf stars). They also found that the fractional content of abnormal galaxies among the blue

members varies widely among clusters.

Later work by BO (1984) (see also Couch and Newell 1984) re-examined the issue with a larger sample of clusters out to $z \leq 0.5$, using better membership criteria and a more stringent definition of blue galaxies. They found that the fraction of blue galaxies rises from about 5% for nearby concentrated clusters to 20% by $z \sim 0.5$. There was the appearance of a clear trend, but the scatter was huge; contraryto the general trend the highest redshift cluster, Cl 0016+16 ($z = 0.54$), had a blue fraction of only $\sim 2\%$. The spectral work of Dressler (1986) also shows that a wide variety of blue galaxies can be responsible for the appearance of evolution. There is still much work to be done but it does not appear that any simple model will be sufficient to explain the observations.

Despite the amount of effort that has gone into the study of the high redshift clusters in the BO sample, little has been done to extend their work out to even higher redshifts. Most observations of higher redshift clusters have included only a few of the brightest cluster members (*e.g.* Schild 1984, Spinrad and Djorgovski 1984), so that it is not possible to make direct comparisons with the work of BO. The lack of observations of large numbers of galaxies in clusters at redshifts of $z \sim 1$ is largely due to the faintness of these objects.

In this work, we present the results of a deep, multi-band survey of the field surrounding 3C 217, a radio galaxy at a redshift of $z = 0.9$. We provide evidence for the existence of a cluster at this redshift and examine the extent to which the galaxies in this cluster exhibit evidence of evolution. The distance modulus to 3C 217 is nearly 2 mag greater than the most distant cluster in the BO (1984) sample, a fact that produces a variety of different problems. A decrease of 2 mag in apparent magnitude corresponds to an

increase in the field (foreground/background) content of nearly a factor of 10. The high field content not only increases the possibility of making errors in the selection of cluster members, but also makes clusters difficult to detect because the number density enhancement of the cluster over the background is decreased. This is further complicated by the fact that CCDs are required for observations at this magnitude. Despite the many advantages of these detectors, sky coverage is not one of them! (A single CCD field covers only a fraction of the total cluster area.) Because of the small field size of CCDs, there is no region from which we can determine the field counts independently of the cluster. The expected field content can still be estimated by constructing galaxy number counts, or N(m) diagrams (corrected for both magnitude biases and incompleteness by performing simulations). This allows us to determine the fractional field content as a function of magnitude by comparing the observed number counts with the recent results on field counts from Tyson (1988). The N(m) diagram also proves to be a more effective method of establishing the presence of a cluster than tests that measure spatial number density enhancement.

A major difficulty in the study of high redshift clusters is the K correction, particularly for early type galaxies. These galaxies are strongly dimmed in the bluer bandpasses and will appear much fainter in these filters. We make a careful assessment of the selection effects which may exclude these galaxies from the sample. This is critical since their exclusion will result in an overestimate of the fraction of blue galaxies.

BO (1984) use a $B - V$ colour index to determine the proportion of blue galaxies. However, a single index is unable to distinguish field galaxies that may contaminate the sample. Two colour indices, $B - R$ and $R - I$, plus observations in 5 narrowband filters, are used to make an independent

estimate of the field content which can then be compared to the number of field galaxies expected from published number counts. The differentiation between field and cluster galaxies is made by comparing observed galaxy colours with the redshifted colours of local galaxies (Coleman *et al.* 1980) and those produced by evolutionary models (Bruzual 1981).

Once the cluster galaxies have been determined, they are divided into red and blue populations and the models are used to transform apparent I into the restframe V system. This allows the blue fraction to be determined so that the results are directly comparable to the results in BO (1984) for a cluster at $z = 0.9$. This relatively straightforward calculation requires the incorporation of various competing effects which include incompleteness, magnitude bias, selection effects, field contamination and K corrections.

Chapter 2

Data Reduction

2.1 Observations

The data that were used in this thesis were made with the prime focus camera of the Canada-France-Hawaii 3.6 m telescope (CFHT) using an RCA SID53612 320 × 512 CCD detector (Walker *et al.* 1984). Observations were obtained over seven half-nights in March 1986 by Pritchet and Hartwick (1987). The data were originally used in conjunction with previous observations of the field as part of a search for primeval galaxies.

The observations were made of a high galactic latitude field centred on the radio galaxy 3C 217. A photoelectric *UBV* sequence in this area has been published by Penston, Penston and Sandage (1971). The first optical identification of 3C 217 was made by Laing *et al.* (1978) and the redshift of $z = 0.90$ was determined by Spinrad and Djorkovski (1984).

Broadband images were obtained through filters emulating the Johnson B and the Kron-Cousins R, I systems. Narrow-band filters, with bandwidths $100 - 130$Å, were used to obtain data at 6300Å, 6800Å, 7500Å and 8100Å.

An intermediate bandwidth filter ($\sim$ 500Å bandwith) was used to extend the coverage to 9500Å. Four 4600 s exposures were taken for all filters except I, for which six exposures were obtained, and the 9500Å filter for which three 2400s exposures were taken. Each exposure taken through the same filter was shifted by $\sim 4''$ to enable fringe removal. The frames cover an area of $2.'2 \times 3.'3$ at a scale of $0.''412$ pixel^{-1}. The seeing was consistently good at $\sim 1''$, although the images through the broad filters were somewhat sharper because of optical problems with the narrow band filters.

Data reduction was performed with the reduction package R2D2 at the University of Victoria and consisted of bias and dark subtraction followed by flat-fielding with dome flats and bad column removal. The bias subtraction removes the mean signal per pixel arising from the readout process. The dark subtraction removes the contribution of thermally induced charge in the detector. Flat-fielding corrects for variations in pixel response across the CCD, and requires taking dome flats in all filters since individual pixel response varies widely at different wavelengths. The bad columns are removed and replaced by a linear interpolation along the rows perpendicular to the defect.

The use of thinned CCD's has the advantages of improved response over larger wavelength range and a decrease in the number of cosmic ray events. Unfortunately, these effects are accompanied by an increase in "fringing", particularly for longer wavelength filters. Fringing is due to the wavelength being comparable to the thickness of the CCD, hence the light may be internally reflected many times before being detected, resulting in an interference pattern.

In order to correct for fringing, a mean fringe frame was constructed for each filter by first scaling the unaligned frames to a common sky level

and subtracting this mean sky from each frame. The median of the individual frames was made and the resulting fringe frame was then scaled and subtracted from each frame. This works reasonably well for the following reasons. (i) The observations were made at high galactic latitude, where the number density of discrete images is low. (ii) For all except the 6300Å observations, the fringe amplitude scales closely with the sky level. The 6300Å filter lies on a night sky line which required the fringe amplitude to be measured directly. The separate exposures were scaled directly to this amplitude prior to median filtering.

After being corrected for fringing, the frames were aligned and combined using a median filter. This procedure had the effect of removing almost all cosmic rays and other spatially uncorrelated signals in the final combined frame for each filter.

2.2 Detection of Galaxies

The detection algorithm is identical to that used by Infante (1985) which is in turn based on Kron's (1980) finding technique. The only significant change was that the data frames were convolved with a Gaussian kernel before running the detection routine. The Gaussian used has a full width at half maximum of 1″ which approximates the seeing profile. Since the detection algorithm hinges on the the central pixels of an image, this provides a nearly optimum signal to noise (S/N) for compact images and improved S/N for more extended objects. The detection was done locally and independent of the rest of the frame; this avoids problems due to variations across the frame, *e.g.* errors in the flat fielding. The detection routine was run separately in each of the three broad band filters to avoid colour biases in the

The first step is to create a list of all local maxima (any pixel whose value is greater than that of its eight neighbours). For each maximum, a rectangular area is extracted and divided into three subareas, the middle one centred on the candidate position. The mean intensity of each subarea is determined and the average of the two lowest mean intensities is taken. This helps to remove the contribution of contaminating objects. The mean is then compared with the intensity of a 9 pixel aperture centred on the candidate position. The object is accepted as part of the candidate list if the S/N is above some threshold value.

For large photographic surveys, where the number of candidates is large, the threshold is set fairly high to minimize the number of spurious detections. However this data set involves only a small fraction of the area available to photographic surveys and hence the sample is quite small. Therefore the threshold was set quite low, resulting in a large fraction of the detected objects which are either spurious or simply too faint to allow their signal to be meaningfully determined.

The advantage of this is that the detection procedure does not then make any significant cuts on the data. The S/N cuts are only made after the entire photometric procedure has been carried out on the entire candidate list. This means that the cuts are made on the basis of good photometry and proper sky determination rather than on the necessarily crude detection criteria. The disadvantage is the increase in the amount of computer time required since large numbers of spurious or extremely faint images must be run through the photometric procedure.

2.3 Positions

All objects in the preliminary candidate lists require an accurate determination of their centroid positions before total magnitudes can be measured. This is done using aperture photometry, which determines the centroid via intensity-weighted numerical integration. The values of the centroids X_c, Y_c, are given by:

$$X_c = \frac{\int x\,(I(x,y) - I_s)\,dA}{\int (I(x,y) - I_s)\,dA} \tag{2.1}$$

and

$$Y_c = \frac{\int y\,(I(x,y) - I_s)\,dA}{\int (I(x,y) - I_s)\,dA} \tag{2.2}$$

where $I(x,y)$ is the intensity of pixel (x,y), I_s is the sky background value per pixel, dA is the area element and the integration is performed out to the edge of the aperture. The aperture is centred on the input position from the candidate list and the centroid determined. This then becomes the new input position and the procedure is repeated until the position of the centroid converges.

The integrations (1.1) and (1.2) are performed out to a fixed radius which was chosen as 2.5 pixels. The primary reason for this choice was that this radius is equal to the seeing disk. A larger radius, centred on a particular object, could include other maxima that would be defined as separate objects within the limitations of the seeing. This would result in the aperture being *drawn off* fainter objects by nearby brighter objects during the iterative process of calculating the centroid.

This bias in aperture position will still occur, particularly near very bright objects; the extent of this problem will be a function of the size of the aperture. One can minimize the number of improper mergers of faint images

by decreasing the size of the aperture; however, this would also decrease the fraction of the total light that the aperture contains. The signal-to-noise ratio of a Gaussian image measured by an aperture of radius R, in the sky-noise dominated limit, is given by :

$$\frac{S}{N}(R) = \frac{I_o\left(1 - e^{-R^2/2\sigma^2}\right)}{\sqrt{\pi}\eta_o R} \tag{2.3}$$

where I_o is the peak intensity, σ is the width of the peak and η_o is the noise per pixel. Differentiation yields a maximum at about $R = 1.6\sigma$ so that stellar images, which have $\sigma \approx 1.0$ pix for our plate scale, would have a maximum S/N for a smaller aperture than that chosen. However, since the primary interest is in nonstellar objects, it seems reasonable to use a larger aperture and optimize the S/N for more extended objects. A further consideration is that small differences in the seeing between the different filter bands could cause significant differences in the fraction of light measured if the aperture is cut very close around stellar images. The reason for this is simply that the aperture for optimum S/N occurs at a radius where the signal drops quite rapidly. Changing σ is effectively equal to changing the aperture in a region where $I(r)$ is very sensitive to the radius. A slightly larger aperture will be less sensitive to these differences since a larger fraction of the total light will be measured.

The process of determining accurate centroids will also merge many of the objects for which more than one position was detected, although it can also happen that a single object will contain two or more stable centroids. Once the final coordinates are determined, all positions within one seeing disk are merged into a single object. This represents the final list of candidates for the determination of total magnitudes.

In the procedure described so far, no external S/N noise cuts have yet been made. To a certain extent, the above procedure does make a ragged cut which will depend on parameters such as surface brightness as well as signal strength. However, the vast majority of these objects do not appear to have sufficient signal to make the final S/N cuts. Also any errors in the number of objects in the final list resulting from the detection and photometric procedure are addressed in the simulations (see Section 3.2).

2.4 Kron Photometry

Once accurate centroids have been determined and the merging of "multiple hits" performed, total magnitudes can be determined. Aperture photometry, as discussed in the previous section, works very well for stellar images since the aperture contains a constant fraction of the total signal independent of the magnitude of the object. For resolved images, however, the fraction of the total signal contained in a fixed aperture is a function of various competing factors including size, shape, structure, surface brightness and magnitude.

The two main methods of nonstellar digital photometry are *isophotal* algorithms (*i.e.* Jarvis and Tyson, 1981, Shanks *et al.*, 1984, Tyson, 1988), and *first moment* algorithms (Kron 1980, Koo 1986, Infante 1985). Isophotal magnitudes are calculated out to a radius at which the signal becomes smaller than some predetermined level. Normally this level is set as some fraction of the mean sky noise level. Deep blue photographic work has generally used an isophotal limit of 26.5 mag arcsec^{-2}, whereas with CCD's, the limit has been extended as faint as 29 mag arcsec^{-2} (Tyson 1988).

The advantage of the isophotal method is that isophotal radii are computationally very fast. This is mostly due to the fact that the computation does

not require an accurate determination of the centroid. In some cases, isophotal magnitudes are calculated simply using those contiguous pixels above the threshold. Therefore any initial position within the image boundaries will yield the same magnitude. The disadvantages of this method include the difficulty in estimating the photometric uncertainty and the unknown effectiveness at faint limits, due to the magnitude dependence of the isophotal radius. Although corrections can be made for the light missed in measuring faint objects, the decrease in the isophotal radius with magnitude means that the number of pixels contributing to the the noise also decreases. This creates a Malmquist bias since too many faint objects will escape a signal to noise cut due to an underestimate of the noise. The other disadvantage is that for a given type of galaxy observed at increasing redshift, the radius of integration corresponding to a fixed isophote decreases since surface brightness scales as $(1+z)^{-4}$. This means that the fraction of the total light that is measured within a given isophote is a function of redshift. A further unsettling aspect of isophotal photometry is that the determination of the isophotal radius ignores the information contained in the brighter central regions and depends entirely on the faintest pixels.

Because of the difficulties associated with isophotal photometry, Kron's first moment scheme was used to calculate image magnitudes. The first moment of an image is defined as:

$$r_1 = \frac{\int_1^{r_{up}} r g(r) dr}{\int_1^{r_{up}} g(r) dr} \tag{2.4}$$

where $g(r)dr = 2\pi r I(r) dr$ is the total amount of light in an annulus of constant width dr, $I(r)$ is the intensity at radius r and r_{up} is the upper limit of integration (Kron 1980). The parameter r_{up} does not depend on any external quantities such as the sky background or S/N ratio but depends

directly on the growth function, $g(r)$. This also means that the central portion of the image, where the signal is highest, is given significant weight in the determination of the radius of integration.

The difficulty in applying this method is that the quantity r_1 is a statistical measure of the light distribution and hence does not directly give a value for the radius of intergration. Kron (1980) suggested that an outer integration radius of $2r_1$ gives a good balance between optimum S/N and least amount of missed light. This value has been used by many subsequent authors (Koo 1986, Infante 1985) and is adopted here.

Theoretically, the upper limit of integration r_{up} should be a large distance from the image centroid. In practice, noise fluctuations will tend to dominate $g(r)$ at large values of r; hence r_{up} was set at a fixed value of 3.″3 from the centroid. A variable r_{up} was also tried, determined either from the sky background, or from S/N considerations. These methods were rejected because of differences in noise for observations through different filters. A fixed value allows r_1 to be calculated in a consistent manner for all three frames.

The actual photometry proceeds as follows. For each of the centroid positions supplied from the final lists of candidates, a surrounding circular region is extracted from the data frame. This is then divided into two regions; a circular region centred on the input position extending out to r_{up}, and an outer annulus from which the local sky background and noise are determined. The determination of the sky background is made by an iterative technique which calculates the mean of the pixels and throws out values outside 2.1σ from the mean. Within a few iterations the mean tends toward the mode as the distribution of intensities becomes symmetric and the solution converges.

The inner circular area is further subdivided into 1 pixel wide annuli

with 8 radial sectors. This radial division allows the application of an excision algorithm which gives an improved treatment of blended images in semi-crowded fields. The excision is done by taking the mean of the radial sectors for each annulus and the value of those sectors that lie outside the distribution is replaced with the mean of the remaining sectors. While not as sophisticated as the deblending techniques used in stellar photometry (*e.g.* in DAOPHOT), stellar deblending depends on the common, self-similar, profile of stellar images. The deblending of galaxies is rather more difficult because of the variety of image profiles encountered and it is not always possible to apply deblending algorithms in a consistent manner. For example, the light along the major axis of very elongated images could be interpreted as contamination by the algorithm.

The deblending also depends on the number of sectors chosen and the statistics are hardly robust regardless of the choice. The larger the number of sectors chosen, the less reliable the information contained in each sector. Following Kron (1980) and Koo (1981), eight sectors was used as a reasonable compromise between a large number of sectors and a large number of pixels contained in each sector. Excision was not applied within one seeing disk radius because of the lack of information available in each sector. This also means that the algorithm is fully operational only in areas that contain objects that would be classified as distinct. Stable centroid positions within a radius of one seeing disk would have been previously merged into a single object. The inner cutoff for the excision means that the light at any of these centroid positions would not be excised.

After the sky background value has been subtracted from the pixels in the inner area, the value of $2r_1$ is determined from equation (1.4); this sets the limit of the intensity integration. Within this limit the region is subdivided,

the excision algorithm applied and the total magnitude determined. For very faint objects the growth function may become negative within $2r_1$ in which case a fixed aperture (with a radius equal to the seeing disk) is used to determine the magnitude. (This is essentially the same as the aperture photometry used in the determination of the centroids, with some differences in how the sky is calculated.) The noise per pixel is calculated from the width of the converged distribution of sky intensities and thus the photometric uncertainties can be determined from the number of pixels within a radius of $2r_1$, or within the seeing disk in the case of the default aperture.

The use of a default aperture gives greater completeness for faint magnitudes but at the cost of introducing a new set of biases. Not only will the Malmquist bias operate differently on the aperture photometry, but its effect will also depend on the shape of $g(r)$ which, along with the local noise distribution, triggers the use of the default aperture. To some extent the effects of the Malmquist bias can be accounted for by running simulations, although there is insufficient data available to allow simulations with a dependence on image compactness. The simulated galaxies consist of the median image of all galaxies of a certain magnitude, and the more galaxies used, the greater the reduction in the noise. This is extremely important since the S/N cuts strongly affect the completeness at faint magnitudes.

2.5 Classification

In order to analyze the galaxy content of the frames, the foreground stellar (unresolved) images must be removed. The fractional stellar content drops rapidly for magnitudes fainter than $B \approx 22$, but can significantly contaminate the bright population.

Stars have very simple profiles consisting of a scaled point spread function (PSF), while galaxies have a wide variety of shapes and radial surface brightness profiles. Star/galaxy classifiers follow two main approaches: *parametric classifiers*, which retain information on the light distribution (Jarvis and Tyson 1981); and *non-parametric classifiers*, which measure the central compactness using statistical moments (Kron 1980). Parametric classifiers are significantly more complex to implement and somewhat difficult to interpret beyond star/galaxy separation. This is particularly true towards the faint end, where details of the light distribution become buried in the noise. From the extent to which the extra details (concerning image shape) provided by the parametric classifiers are used by previous workers, their use does not seem to have justified the extra effort involved.

The star/galaxy classifier adopted here is a non-parametric form adopted by Kron (1980). It operates as a statistical measure of the central concentration of an image. To be exact, it is the intensity weighted inverse squared moment of the image, defined as

$$(r_{-2})^{-2} = \frac{\int_1^{r_{up}} r^{-2} g(r) dr}{\int_1^{r_{up}} g(r) dr} \tag{2.5}$$

where $g(r)$ and r_{up} are defined as previously. Stars have maximum compactness and values of r_{-2} that are independent of magnitude. The brighter galaxies are well resolved and have r_{-2} values greater than those for stars. For fainter galaxies, the value of r_{-2} tends to decrease and the separation between the two classes of objects becomes blurred by the noise. This effect is caused by a variety of factors. For example, high redshift galaxies will have a surface brightness lowered by $(1+z)^4$ and hence the nucleus becomes dominant, thus making such objects appear more compact. Perhaps the strongest effect is from the Malmquist type biases. Faint objects in the

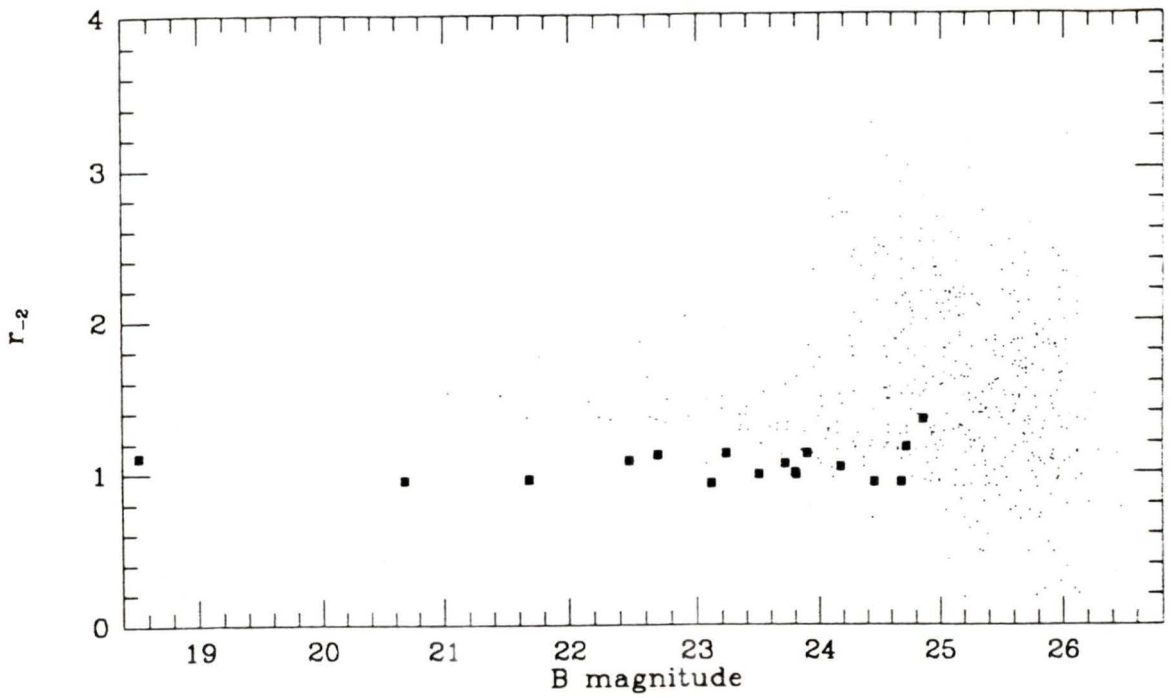

Figure 2.1: Galaxies are indicated by dots and stars by filled squares. The stars that lie above the general distribution have been identified either by their red colours or small r_{-2} values in other filters that have better statistical weight.

sample are more likely to be found on positive noise fluctuations. These fluctuations tend to be sharply peaked and hence they bias the values of r_{-2} to smaller values. Fortunately, at the depth of these frames, the number of stars decreases rapidly toward the faint end where the galaxies appear to increase in their central concentration.

In photographic work, r_{-2} is normally plotted as a function of magnitude, since the value increases at the bright end because of saturation of the images and decreases at the faint end because of the effects of noise. For our data, Figures 2.1-2.3 show a consistent r_{-2} value over nearly 5 mag in all three

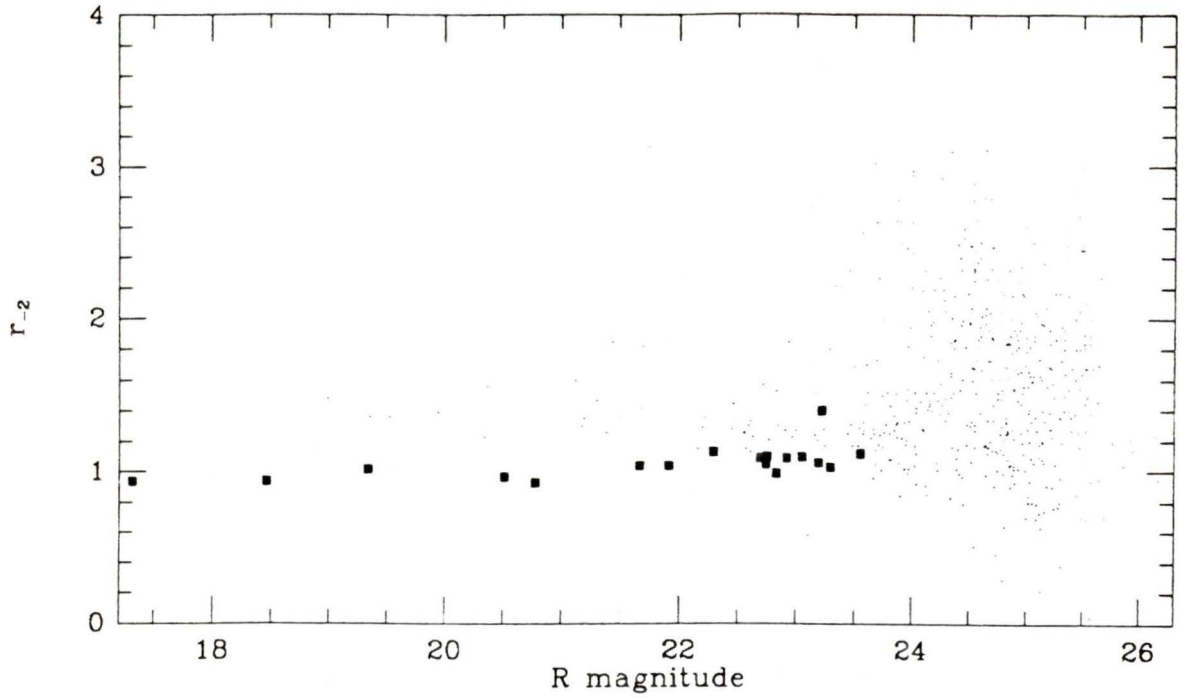

Figure 2.2: r_{-2} vs. magnitude for the R filter. Symbols are the same as in Figure 2.1.

filters. Saturation effects are not apparent at the bright end, but the scatter at the faint end begins to increase significantly about 2 mag above the limit. This is similar to what is observed on photographic plates, except that the scatter on plates begins at a magnitude bright enough that the star/galaxy fraction will still be significant. Tyson (1988) used parametric classifiers on CCD data more than a magnitude fainter than ours, giving him a greater statistical weight for objects of similar magnitude. From his star counts over a much larger area, the number of stars fainter then $R = 23.5$ mag for our observed area is expected to be ≤ 1.

The nearly constant r_{-2} over a wide range of magnitude allows good comparisons to be made between different filters. Therefore, the primary

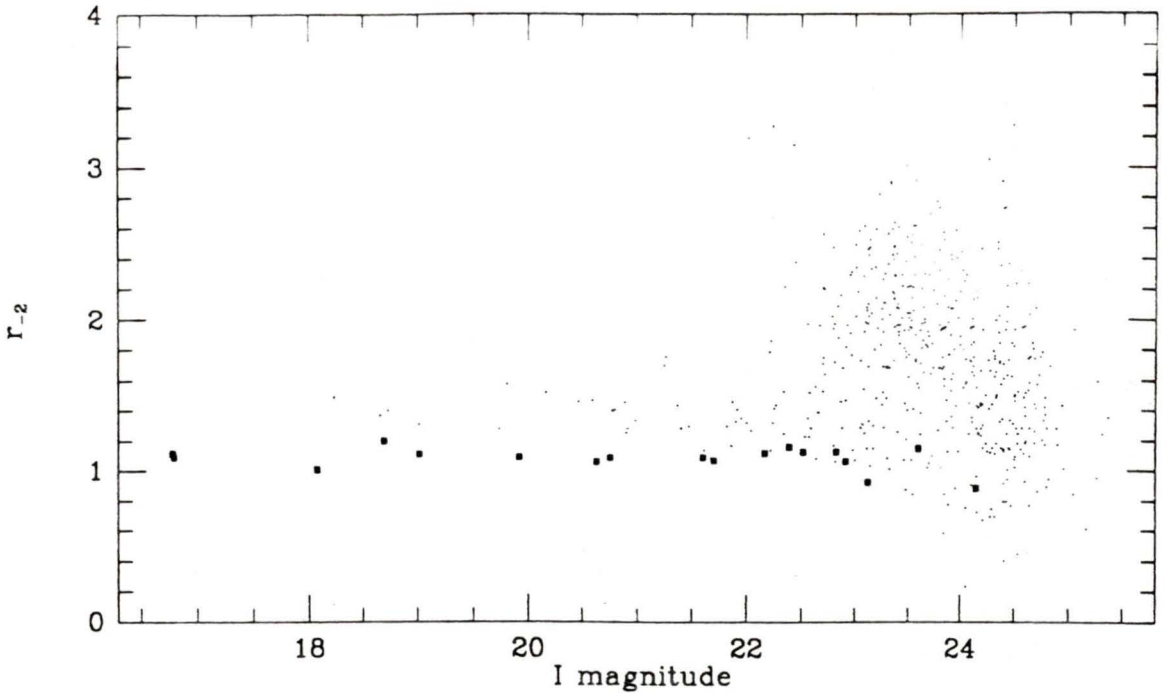

Figure 2.3: r_{-2} vs. magnitude for the I filter. Symbols are the same as in Figure 2.1.

method of star/galaxy separation is in figures 2.4 and 2.5, which show the r_{-2} values for objects from two different frames. To avoid confusion at the faint end only objects brighter than 23.5 in R were plotted. Of course this does allow a colour bias to affect the classification since some of the objects will be much fainter in B or I and hence their values of r_{-2} will be more subject to noise. This has to some extent been accounted for as can be seen in the objects that are classified as stellar despite the fact that they lie outside the main distribution. Two other objects lie outside the distribution and these have been classified as stars because of their extremely red colours.

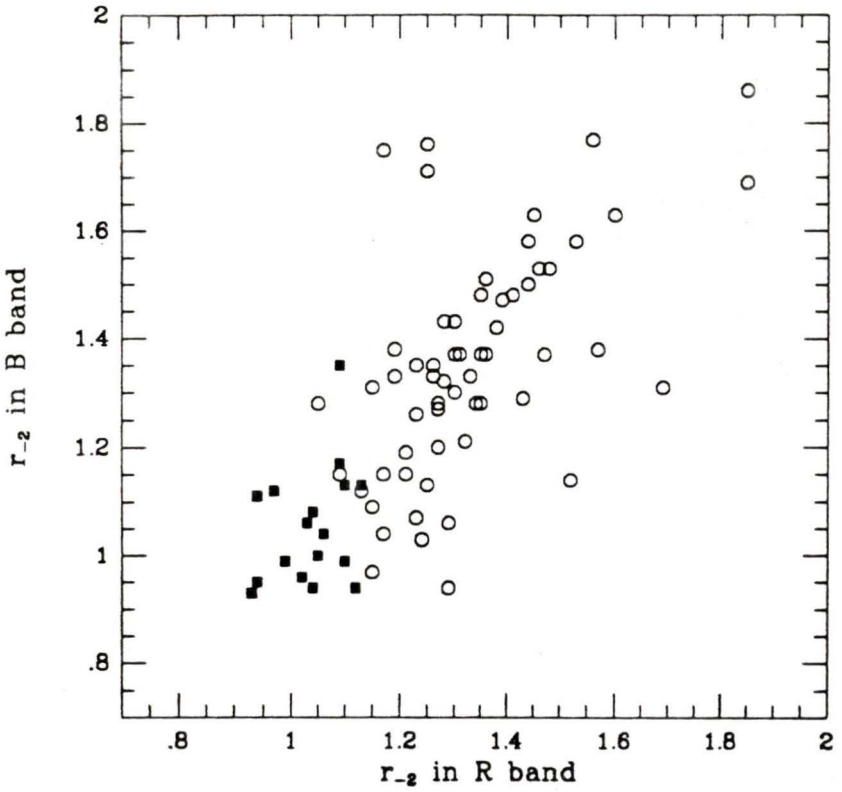

Figure 2.4: Intensity weighted inverse squared moments, B filter vs. R filter. Open circles indicate galaxies, filled squares indicate stars. Only objects brighter then 23.5 R mag are included. Stars outside the stellar envelope have very red colours resembling M stars

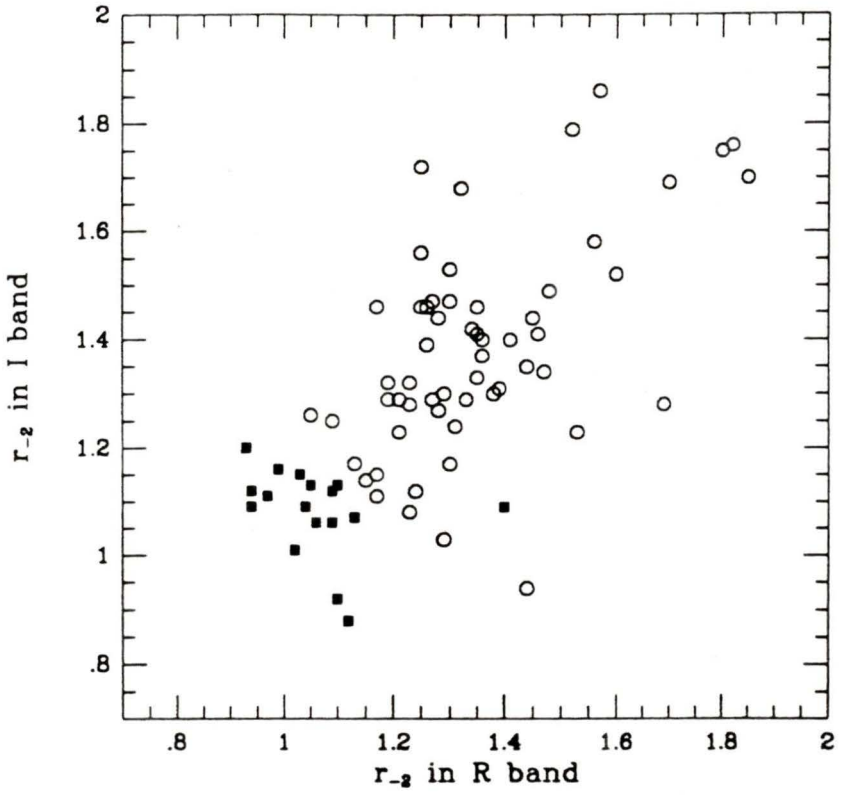

Figure 2.5: Intensity weighted inverse squared moments, I filter vs. R filter. Symbols are the same as in Figure 2.4.

2.6 Calibration

The calibration of deep, 4 metre class CCD frames can present some difficulties. Photometric standards are spaced on scales that greatly exceed the $2.'2 \times 3.'3$ field size. Furthermore, despite the CCD's large dynamic range, most standards are still too bright to be incorporated into deep observations. Certainly the best approach is a separate observing program that ties the available stars in the field to nearby photometric standards. Because of constraints on the availability of telescope time and the somewhat uncertain nature of faint galaxy photometry, a less rigorous approach was adopted here.

Penston *et al.* (1971) made photoelectric UBV observations of blue objects in the region surrounding the radio position for 3C 217 in the hope of obtaining an optical identification, and also to provide a faint photometric sequence for this area. Their star f lies in our observed area and at $B = 18.53$, it is the brightest unsaturated object in the field. The colours of star f were compared with objects in the stellar spectrophotometric catalogue of Gunn and Stryker (1983), hereafter GS83. Only one of their stars had colours that matched that of star f to within 1σ of the combined uncertainties in both $U - B$ and $B - V$. Detailed spectrophotometric information for this star was obtained from Stryker (1986), and was used in calibrating both the broad and narrow band filters.

Two different approaches were attempted in calibrating the broadband magnitudes. The first uses GS83 broadband values which are calibrated to Johnson standards. These values are then converted to our Kron-Cousins R , I using the transformations found in Bessell (1979). The second method uses the AB magnitudes for the Johnson filters which convert directly to

flux (Oke and Gunn 1983). The fluxes can then be converted to our B , R , I using the absolute flux calibration of the two systems. While the two methods are not entirely independent, the first uses the colour terms in the calibration, whereas the second essentially performs a bandwidth correction. Both methods agree to within 0.01 mag which suggests that the calibration is at least self-consistent. The narrow bands were flux calibrated by taking the mean AB magnitude over the equivalent width at the effective wavelength of the filter.

Because the calibration is based on a single observation of one star, the main concern is whether the Penston UBV sequence is correct and that their Johnson filter system is consistent with that of GS83. The latter has at least qualitative support in that we were able to find equally good matches between the GS83 standards and the other stars observed in the 3C 217 field; however, without additional observations, there is no independent means of verifying the colours of star f .

Even if there has been an error which resulted in the misidentification of star f in the GS83 catalogue, the systematic error in the calibration will only be of the same order as the error since a small error will only suggest a slightly different spectral type. Penston *et al.* estimate their uncertainty at ± 0.015 mag per filter; hence even a 3σ error in the observed colours will result in a systematic error of ≤ 0.1 mag. This roughly corresponds to the mean uncertainty in colour for galaxies at ~ 23.5 in R and over two-thirds of the detected galaxies are fainter then this. This illustrates the dominance of random photometric errors for the large majority of objects.

The only other published observation of this field has been by Spinrad and Djorgovski (1984) who determined a spectrophotometric magnitude for 3C 217 of $R = 21.30$. We obtain a nearly identical $R = 21.31$, and while

differences in the filter system may cast some doubt on this agreement, it does suggest that our calibration is accurate to within 0.1 mag

While calibrating the data using a single star can hardly be considered ideal, the degree of accuracy obtained can easily be sufficient for galaxy photometry. Stars have simple profiles which allows consistent photometry to be relatively straightforward to obtain. Stars are also local objects and free of such effects as K corrections that alter the observed colours. Furthermore, the physics of stars is comparatively well understood and agreement between theory and observation can be reached with uncertainties of order 0.01 mag.

On the other hand, galaxy photometry has none of these advantages. The images are resolved and have a wide range of profiles that may or may not be symmetric about the image centre. Nor is there a consistent method for determining apparent magnitudes among observers. There is also the problem of distance which alters the colours and cannot be corrected unless redshifts are known. Even if the redshifts were known, galaxies are composite objects and hence can produce their observed colours in a variety of different ways. All this makes for a good deal of uncertainty about what is actually observed, making the calibration accuracy of order 0.1 mag quite sufficient.

Chapter 3

Simulations

3.1 Input

At faint magnitudes, the observations become increasingly affected by incompleteness and by systematic and random errors in flux measurement. These errors arise primarily from decreasing signal-to-noise levels, although many other factors, such as the presence of bright objects in the field and the effectiveness of the photometry, are also important. Simulations were performed in order to evaluate these errors as a function of magnitude so that the data could be properly interpreted.

Performing simulations is the most widely used method of correcting faint galaxy samples. Simulations generally involve adding template galaxies onto a field of noise and then testing the detection and photometry routines on these fields. The template objects consist of either simulated galaxies (Hall and Mackay 1984, Infante 1985), or real objects (Koo 1986, Tyson 1988). Simulated objects may be a simple combination of a stellar profile with exponential wings, but the best use of simulated objects is for testing

theoretical models. This can provide a wealth of information about the relationship between the observations and the intrinsic nature of the objects; however it does require a number of external assumptions and hence may not be the best way to determine the errors in the data.

The advantage of using real galaxies taken from the actual data is that the template objects will be intrinsically linked to the objects that they are simulating. They are also readily accessible and do not require complex modeling, scaling or other assumptions that would contribute to the uncertainty. The disadvantage is that the noise must be removed from real objects before they will make suitable template galaxies. This can be achieved by using bright galaxies and decreasing their intensity to mimic faint objects, with noise being reduced along with the intensity. Implicit in this approach is the assumption that faint galaxies are just dim versions of the bright galaxies. This is not necessarily the case. For example, a high redshift spiral galaxy will have a different light distribution from a nearby one because of the difference in the K corrections for the disk and bulge.

To avoid these assumptions, we have used template galaxies that consist of the median image of all the galaxies within each half magnitude interval for each of the three broadband frames. These means that the simulations test the data using objects that share the *average* properties of the galaxies at that particular magnitude and colour. The noise was effectively reduced by the square root of the number of galaxies used (typically ~ 50 in the faint intervals, reducing the noise by a factor of ~ 7). Fewer galaxies were available for the brightest simulations, but the noise is less important for these objects since none were classified as undetected from the signal to noise cuts.

The alternatives in the simulation of objects also apply to the construction of noise fields. Template objects can be added either onto fields of

randomly generated noise, with a σ that matches the sky noise, or onto the real data fields. Simulated noise fields tend to be used in conjunction with simulated data and work well when the purpose is to determine the detectability of a modeled object. One disadvantage in their use for correcting real data is that they either fails to account for variations in noise across the fields, or requires mapping out the noise levels. More importantly, they do not make corrections for the presence of other objects in the field which affects both the completeness and the bias. While adding the template objects at random locations in the real data frames does tend to involve significantly more computation time, it does take full account of both the noise variations and the presence of bright objects in the field.

The objects included in the median images are well isolated within the upper limit of integration, r_{up}, but not necessarily in the annulus where the sky is calculated. Hence the median sky annulus is probably somewhat noisier then the median image itself, due to contamination. This noise will be added to that in fields so that the calculated background noise for the simulations was somewhat higher than for the real data. This could affect the results because the additional noise would alter the completeness through the signal to noise cut. In calculating the photometric uncertainty, we subtracted off the noise per pixel in the template objects from that in the detected simulations. Although this correction makes a considerable difference to the values of the corrections, its effect on the galaxy counts is negligible. This is because the decrease in the bias caused by more faint galaxies (*i.e.* those with a lower S/N) will be accompanied by an increase in the completeness. These two effects tend to cancel each other out, and the counts are relatively unaffected (see section 4.2).

This is not a perfect solution since there will still be some remnant noise

in the template objects. Considering only the signal to noise, the detection of objects with additional noise is equivalent to looking at fainter objects. The implication is that the template objects would require a correction in their magnitude to account for the extra noise they add in. However, considering that the correction would be of order ≤ 0.1 of the σ in the mean magnitude for the detected galaxies, an attempt at this second order correction does not seem warranted.

A more important consideration would be the apparent size of the template galaxies. The simulations by Koo (1986), showed that the 50% completeness limit occurred ~ 0.5 mag brighter for extended galaxies than for compact galaxies, although fainter galaxies were better described as compact images. These simulations were performed using bright objects that were dimmed in intensity and hence it was possible to choose an extended object for use in faint simulations. Our simulations use the median image of objects that are being simulated at that particular magnitude and will share the mean compactness at that magnitude. It would have been possible to create two or more template objects of different spatial extent at each magnitude; however this would have increased the noise in each of the objects. As discussed previously, the noise in the template image is difficult to account for properly and increasing it would serve only to reduce the confidence in the simulations. If a larger sample of objects were available, this might be an interesting alternative, although making corrections based on both magnitude and spatial extent would be considerably more complex.

3.2 Output

Our simulations consisted of the template galaxies being individually added onto the real data frames at 500 random locations, at half magnitude intervals in all three filters. The detection routine is run at each position and centroids determined for all objects detected in that region. An object is considered detected if a final position is found within one seeing disk of the input position, if there are no brighter, real objects at that position, and if the object has sufficient signal to noise. This routine is essentially the same as for the real data except for the position check against input position and position/magnitude check against the list of real objects.

The results of the simulations are shown Figures 3.1-3.3 in terms of the corrections to the data. The corrections to the data take two main forms: *completeness corrections* and *bias corrections*. The completeness corrections are a measure of the fraction of the *true* number of galaxies that would be required to produce the observed number, at any given magnitude. The sample is nearly complete for the brighter galaxies with the only mitigating factor being the overlap of even brighter objects, either stars or galaxies. Naturally, as the galaxies become fainter, their completeness drops since there are more bright objects relative to the objects of interest. Towards the faint end, this slow drop in completeness becomes dwarfed by the effects of the decreasing signal to noise level. When the signal becomes small enough, negative fluctuations in the noise are sufficient to prevent detection and eventually only those objects that lie on positive noise fluctuations are found. As the signal continues to decrease, larger noise peaks are required for detection and hence fewer objects are found. Simulations performed on an artificial noise field (Hall and Mackay 1984, Koo 1986) tend to show only this steep drop in the

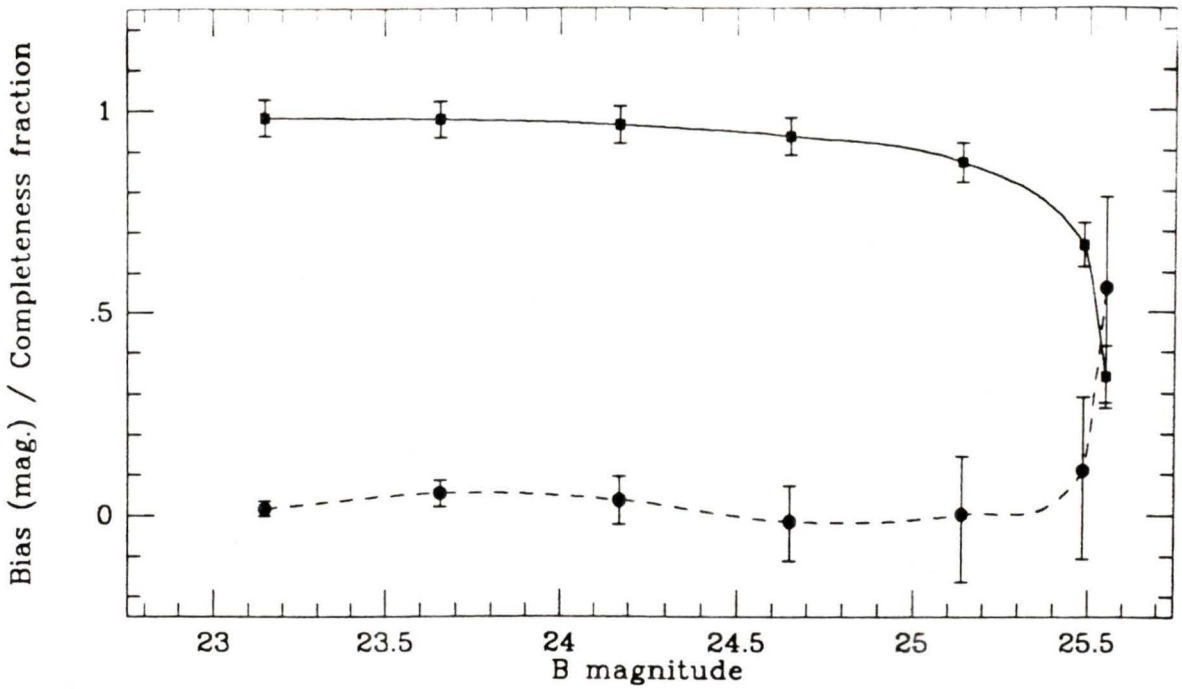

Figure 3.1: Completeness and bias corrections as a function of B magnitude. The solid line is a spline fit to the completeness corrections and the error bars represent $\sqrt{n}$ errors. The dashed line is a spline fit to bias corrections and error bars are the mean photometric errors.

completeness at the faint end. The brighter galaxies tend to be detected at the 100% level since no account is made of confusion with other objects in the field.

The bias corrections are linked to the drop in completeness at the faint end and are essentially due to the Malmquist effect. Since the galaxies that are detected will be those that lie on positive noise fluctuations, they will appear systematically too bright. There are more faint galaxies than bright galaxies, so the number of faint galaxies scattered into the sample will be higher than the number of bright galaxies scattered out of the sample.

At the bright end, the bias corrections are small compared with the mean

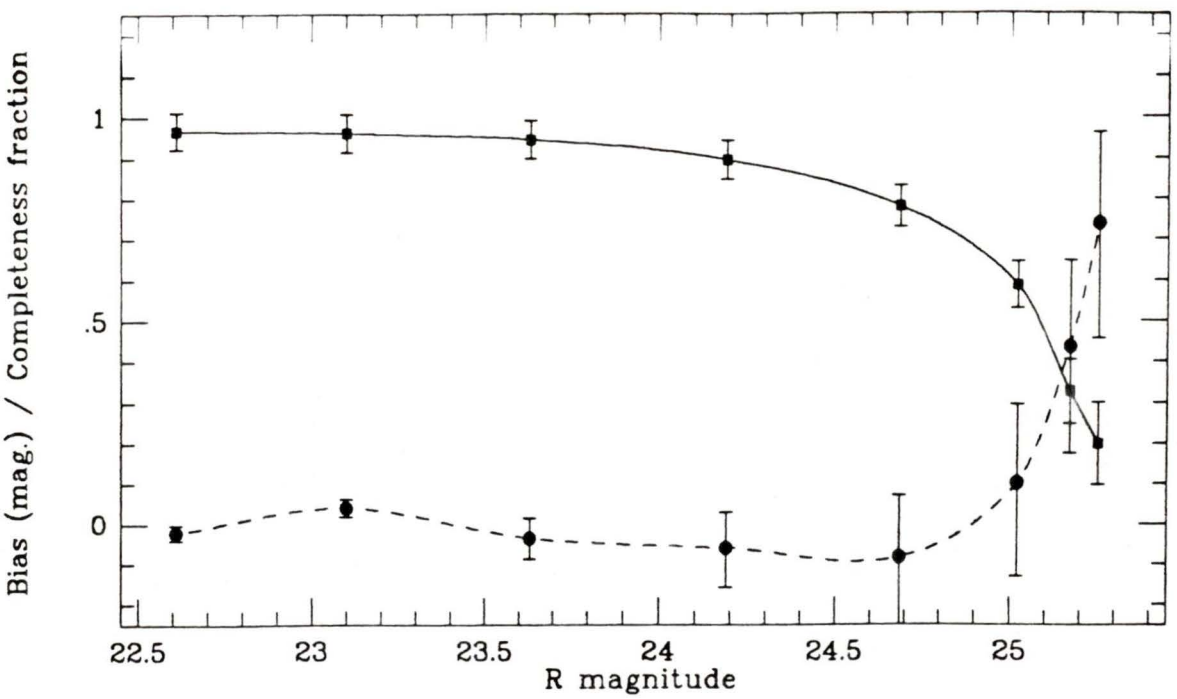

Figure 3.2: Completeness and bias corrections as a function of R magnitude. Symbols are the same as for Figure 3.1.

photometric errors and relatively constant, except that all filters show a slight drop before the onset of the Malmquist bias. The implication is that the total light is being underestimated at these magnitudes, probably because of noise affecting the growth curve $g(r)$, and causing equation 2.4 to determine a value of r_1 that is too small. This effect is strongest in the I band and is possibly the result of slightly poorer seeing.

The corrections become somewhat more complex when more then one filter is involved. This is required when examining number counts for objects that appear in two adjacent filters (section 4.4) or for determining mean colours (section 5.2). Because noise can shift the centroid position of an image, the total completeness will be given by the completeness of the object at its magnitude in each filter, with an additional factor that takes account

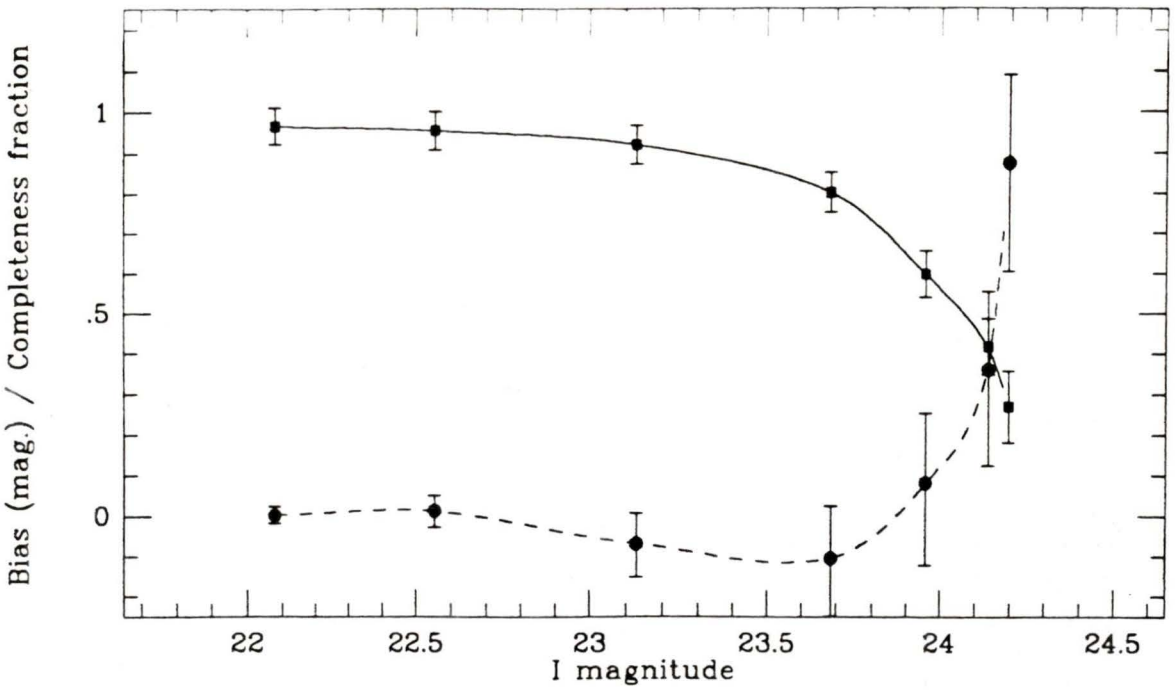

Figure 3.3: Completeness and bias corrections as a function of I magnitude. Symbols are the same as for Figure 3.1.

of the probability of both filters registering detections within a distance of one seeing disk. Rather then calculating this factor separately, the positions from the final simulation lists in each filter were matched against those in adjacent filters for all combinations of magnitudes of input objects. This gives a three dimensional version of the completeness curve with two of the axes in terms of magnitude. This is not required for the bias curves since the magnitudes of the simulations at a given position in different filters are completely independent.

These two component corrections do not make allowance for objects of extreme colour or for colours excluded near the faint end limits of a particular filter. In order for objects to receive a completeness weighting, it must first be seen in both filters. For example, by $R = 24$ mag, objects having $R - I \leq 0.0$

will have an I completeness below the 50% limit. Since the uncertainties in both the simulations and the I magnitude become very large beyond this point, no meaningful corrections can be applied. Such corrections would require assumptions about the true colour distribution. This is beyond the scope of these simulations, although the simulations do help to delimit the region of the colour-magnitude diagram affected by incompleteness.

Chapter 4

Counts

4.1 The N(m) Diagram

Differential number counts provide a standard tool for astronomers interested in the properties of faint field galaxies. The main advantage of studying number counts is that complete faint samples are relatively straightforward to obtain. The main disadvantage is that the various effects of redshift, galaxy type, and evolution make interpretation difficult.

Number counts, or N(m) tests, were pioneered by Hubble (1936) in an early attempt to measure the curvature of space. This test is actually fairly insensitive to space curvature since the sensitivity to the deceleration parameter varies only as z^2. This means that the effect of space curvature is seen only at high redshift, but Hubble was unaware of this since the proper expression of the redshift-distance relation for any spatial curvature had not yet been determined (Mattig 1959).

The early 1980's brought about a revival of faint field galaxy surveys. This was made possible by the development of faster fine-grained photo-

graphic emulsions, rapid and automated digitizing microphotometers and tremendous gains in computing power. Theoretical studies of galaxy evolution demonstrated that luminosity and spectral evolution would dominate the effects of cosmology. Perhaps a further spur was the observations of Butcher and Oemler (1978), who found that two "Coma-like" clusters at $z = 0.39$ and $z = 0.46$ had enhanced populations of blue galaxies with respect to the nearby Coma cluster. The possibility that evolution had been observed in the relatively recent past, combined with the availability of the tools with which to obtain and to interpret the observations, prompted many to undertake the investigation of field galaxies for evidence of evolution. Studies include papers by Tyson and Jarvis (1979), Peterson *et al.* (1979), Kron (1980), Koo (1981), Shanks *et al.* (1984), Hall and Mackay (1984), Infante (1985) and Koo (1986).

The primary effect seen in number count studies of faint galaxies is the flattening of the log N - magnitude slope due to the expansion of the universe. As bright as $B = 20$, surveys find only about one quarter of the galaxies that would be seen in the absence of expansion (Kron 1982). The evolution of galaxies will tend to increase the slope of the counts but the increase must be untangled from the effects of redshift. The redshift of distant galaxies means that a particular filter measures light from a different part of the spectrum; this effect is commonly known as K dimming, or the K correction (depending on the context). Intrinsically blue galaxies suffer less from K dimming than intrinsically red galaxies, thus changing the observed mixture of blue and red galaxies as a function of magnitude. This presents a major difficulty in modeling counts in the absence of evolution since the slope of the predicted counts is quite sensitive to the adopted blue-to-red ratio and the luminosity-colour relation. The "no-evolution" counts predicted by Tinsley (1980) and

Koo (1981) differ by 40% at $B = 23$ when both models are normalized to the same number of galaxies at the bright end.

More recent estimates of the no-evolution counts in B give log N(m) slopes in the range 0.34 to 0.36 (Ellis 1987). Recent observations in B bandpasses find slopes in the range 0.40 (Infante 1985) to 0.48 (Shanks *et al.* 1984). Despite the differences in the slope of the counts determined by various authors, the observed counts are consistently higher then those predicted by no-evolution models. This has been interpreted as indicating that evolution in field galaxies has been detected. The observed decrease in the slope of number counts at longer wavelengths (Koo 1986, Tyson 1988) also appears to support this conclusion. (The number of galaxies increases at a greater rate in the bluer bandpasses; the extra galaxies are blue, implying evolution.) However, the uncertainties in both the models and the observations allow little hard information to be obtained about the nature of the evolution. The redshift at which the onset of evolution becomes important, and the primary galaxy types responsible, remain unknown.

4.2 Observed Counts

The raw and corrected number counts for our observations are shown in Figure 4.1-4.3 for all galaxies with a S/N $\geq 3:1$. The completeness and magnitude bias corrections are made using a spline fit to the results of the simulations, and are applied to the individual galaxies *before* binning. The completeness weighting was applied to the galaxies before the bias corrections because the completeness was determined as a function of the observed (not true) magnitude of the objects. The error bars represent the $\sqrt{n}$ of the unweighted counts.

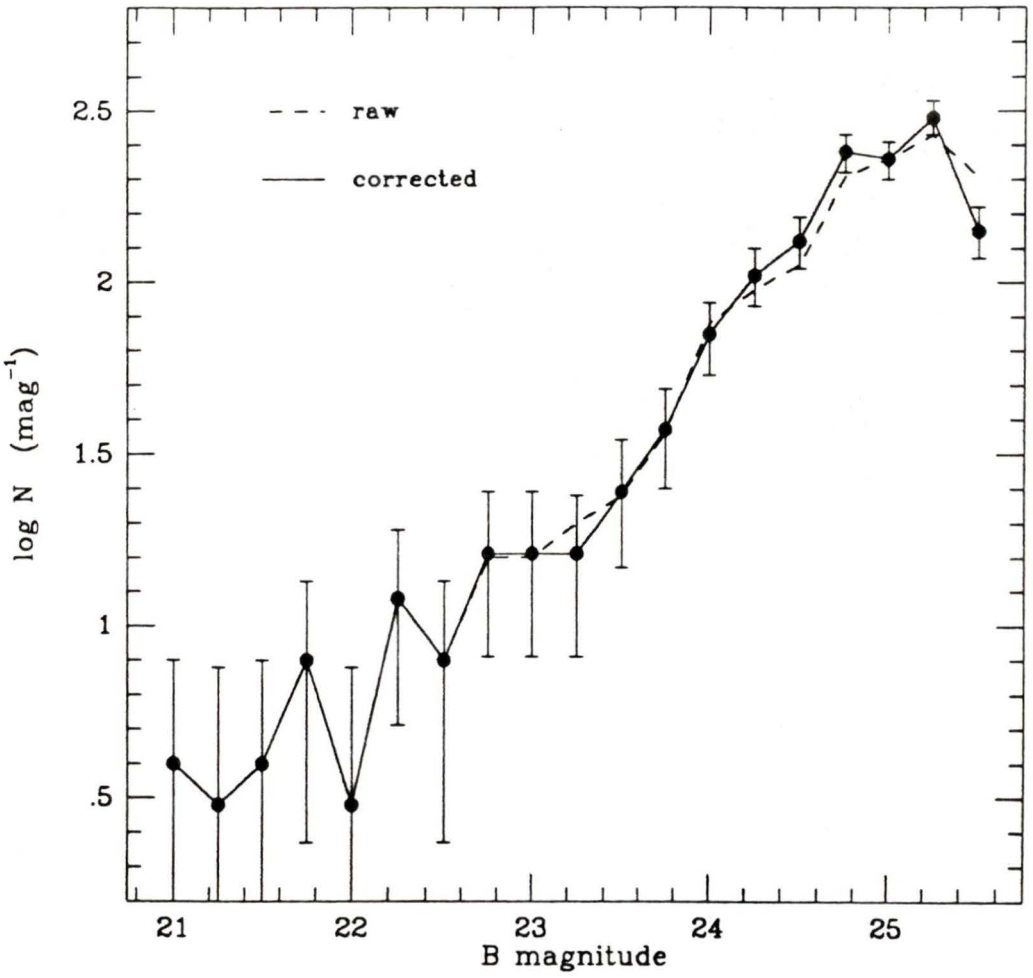

Figure 4.1: Raw and corrected log counts for the *B* filter. The counts are in 0.25 mag bins and are normalized to a mag^{-1} scale. The error bars represent the $\sqrt{n}$ errors. The counts are for an area of 1 CCD field (6.6 arcmin^2).

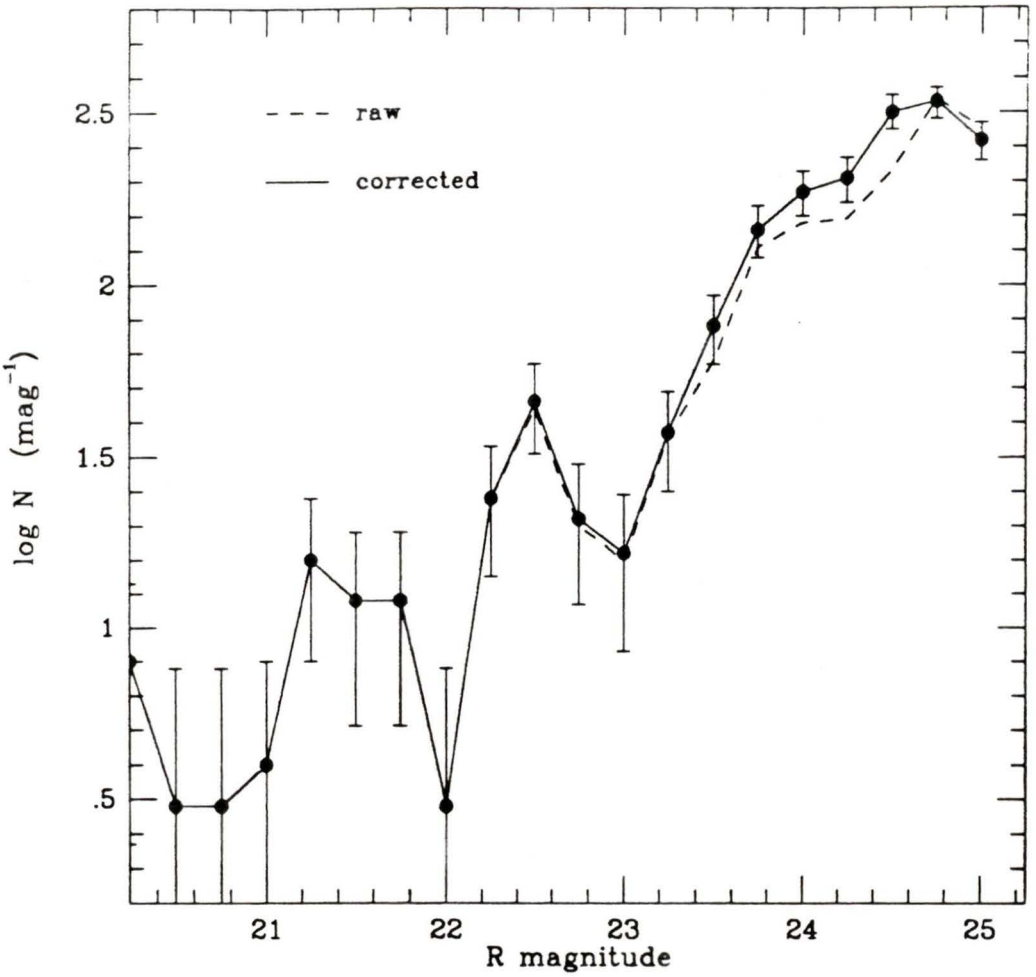

Figure 4.2: Raw and corrected log counts for the R filter. The counts are in 0.25 mag bins and are normalized to a mag^{-1} scale. The error bars represent the $\sqrt{n}$ errors. The counts are for an area of 1 CCD field (6.6 arcmin^2).

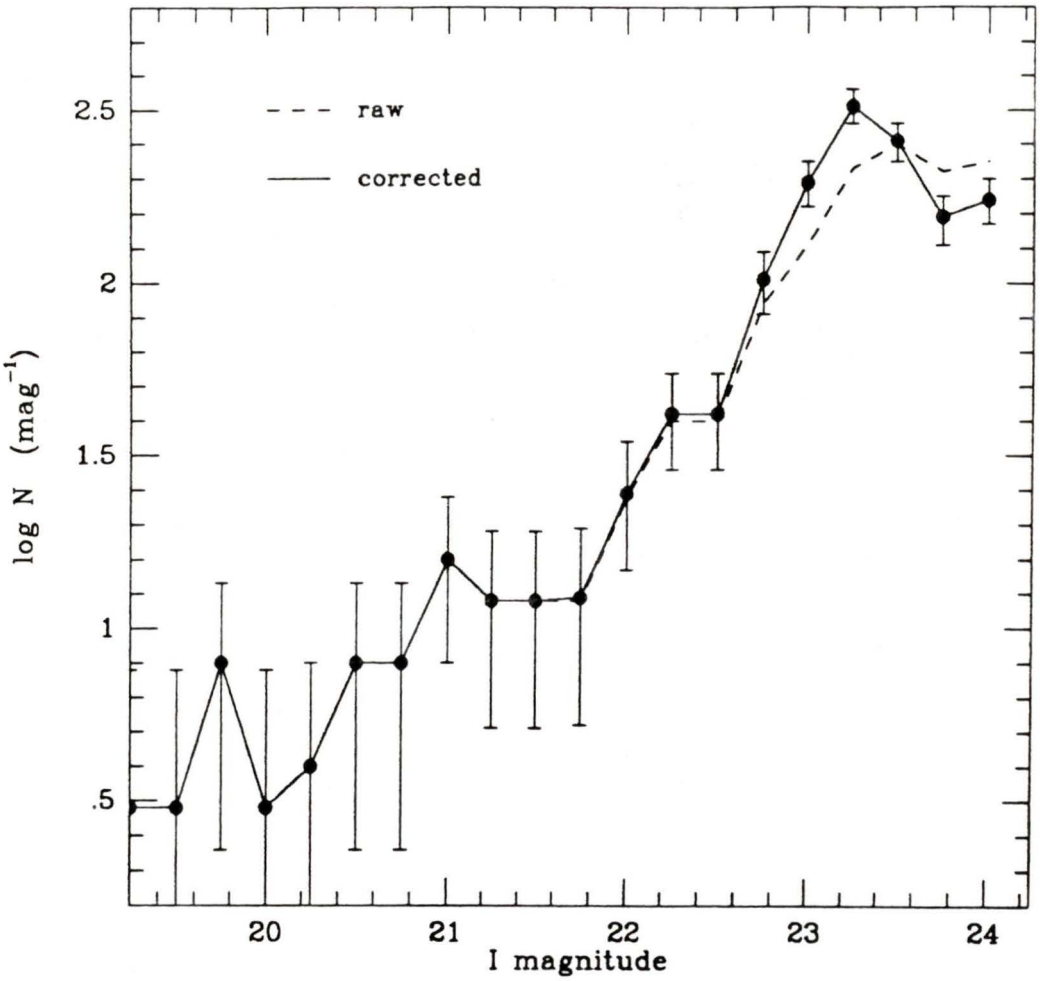

Figure 4.3: Raw and corrected log counts for the I filter. The counts are in 0.25 mag bins and are normalized to a mag^{-1} scale. The error bars represent the $\sqrt{n}$ errors. The counts are for an area of 1 CCD field (6.6 arcmin^2).

The application of the corrections appears less dramatic at the the faint end than might be expected, because of the competing effects of the two corrections. While the completeness correction increases the weight of faint objects, the bias correction moves the objects into fainter bins where the effect of the increased weight is absorbed by the overall increase in the counts with magnitude. The net effect is to shift the counts higher but also to fainter magnitudes, thus maintaining the same general shape. The largest change between raw and corrected counts appears in the I band at about 23 I mag. Referring back to Figure 3.3, this is an effect of the negative bias in the corrections which shifts the galaxies to brighter magnitudes.

A simple test of the shape of N(m) diagrams was made by increasing the level of S/N cut from 3 : 1 to 4.5 : 1, the results of which are shown in Figures 4.4-4.6. Changing the S/N reduces the effects of the random errors, since the noise is limited to a smaller fraction of the signal. The higher cut was also applied to the simulations as well so that the corrections were appropriate to the data. This tended to reduce the negative magnitude bias, since the onset of the Malmquist bias occurs much sooner. The increased signal to noise cut also reduced the faint end limit of the data, with all three frames showing the 50% completeness limit about $\sim$ 0.5 mag brighter. The counts remain essentially unchanged except for differences in the faintest bins. This could easily be due to uncertainties in the corrections since at this point the incompleteness is large and the bias is nearly equal to the bin width.

The counts in Figures 4.4-4.6 have been normalized to units of deg^{-2} mag^{-1} and the counts found by Tyson (1988) were also plotted for reference. The 0.25 mag binning of our data results in considerable scatter at the bright end due to the small number of objects. The bright end counts are generally consistent to within the $\sqrt{n}$ errors, although the agreement might be improved

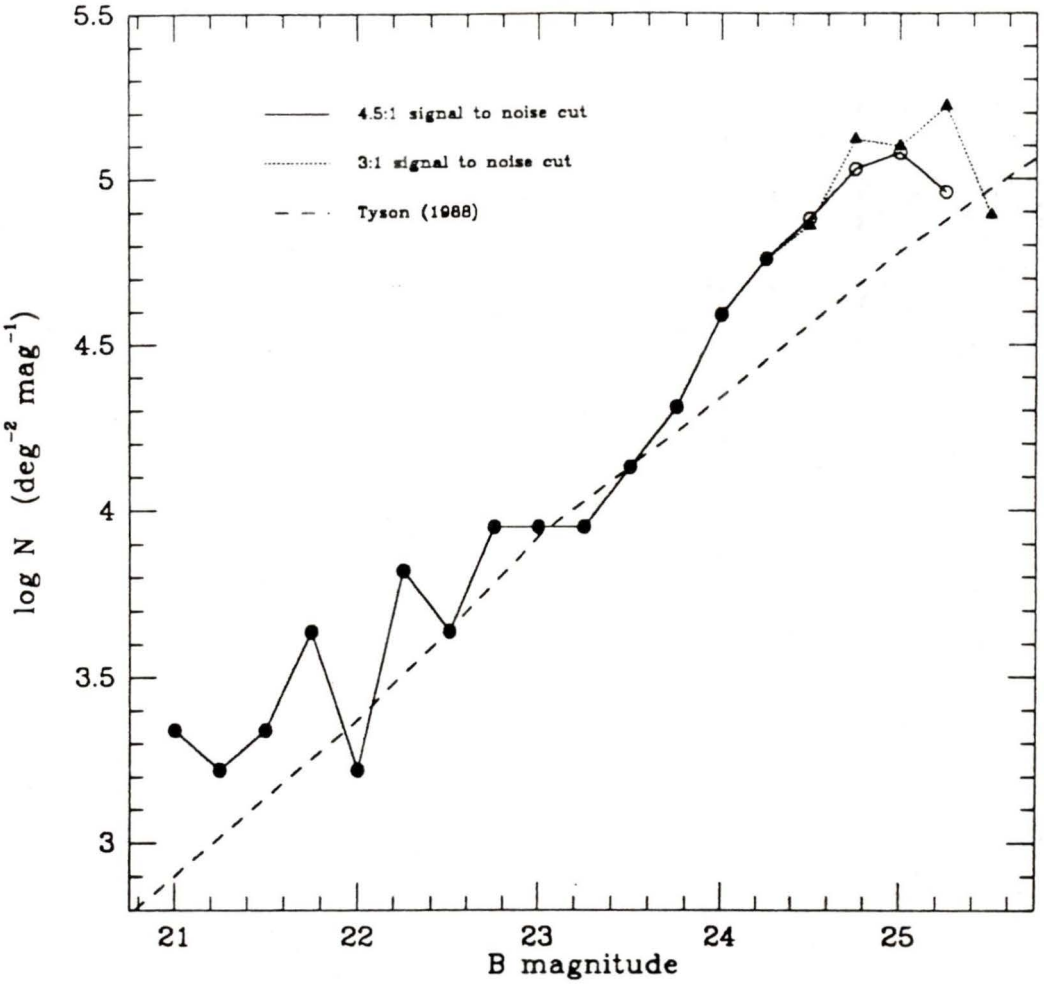

Figure 4.4: Comparison of log counts for a 3 : 1 and 4.5 : 1 S/N cut in B . The counts are normalized to a deg^{-2} mag^{-1} scale. The dashed lines are the counts from Tyson (1988).

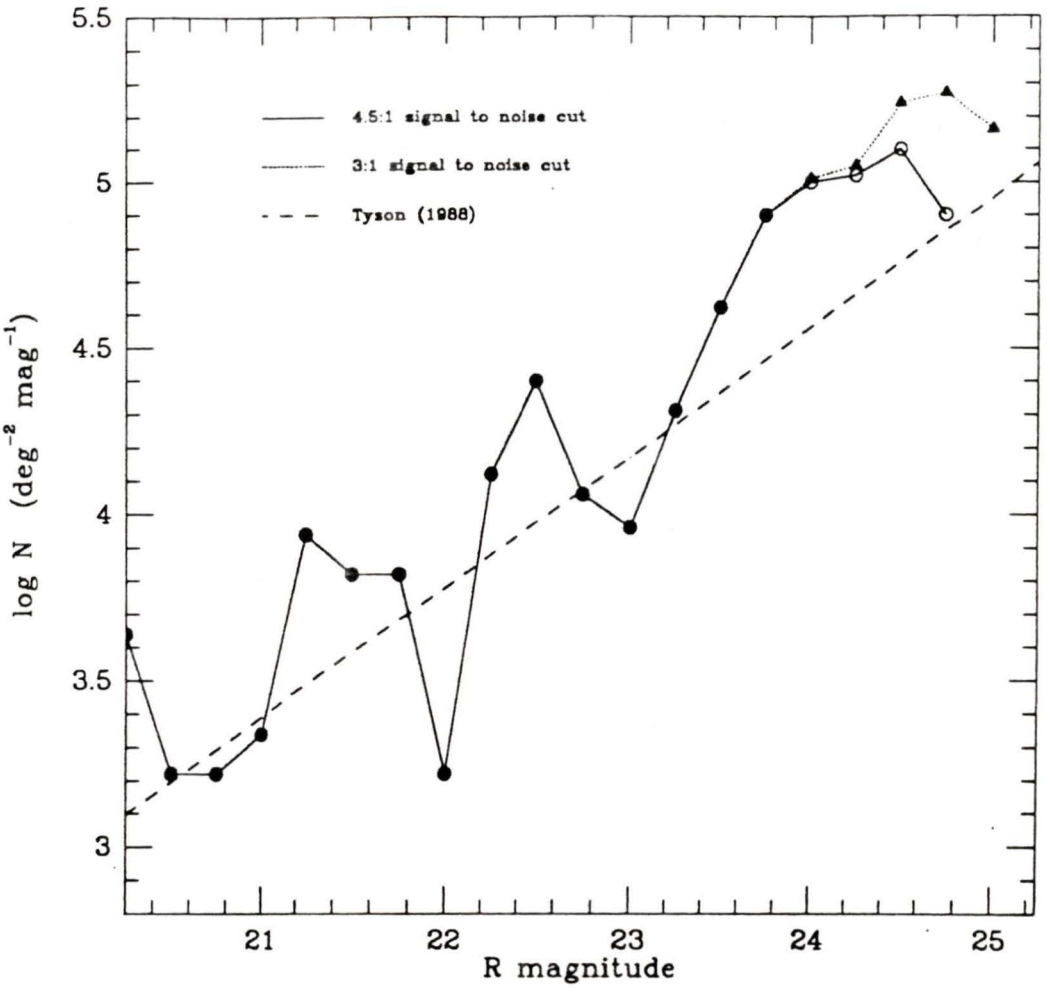

Figure 4.5: Comparison of log counts for a 3 : 1 and 4.5 : 1 S/N cut in R . The counts are normalized to a deg^{-2} mag^{-1} scale. The dashed lines are the counts from Tyson (1988).

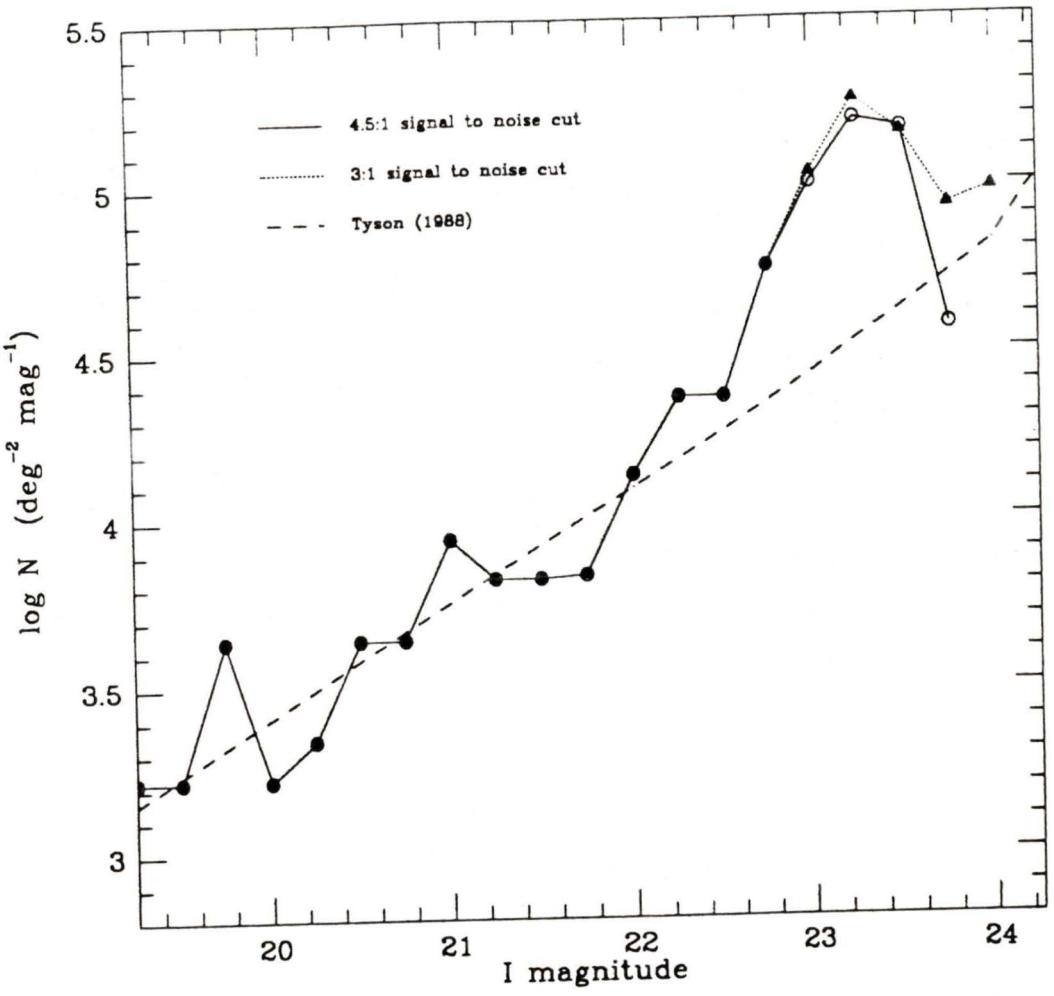

Figure 4.6: Comparison of log counts for a 3 : 1 and 4.5 : 1 S/N cut in I. The counts are normalized to a deg^{-2} mag^{-1} scale. The dashed lines are the counts from Tyson (1988).

by small shifts in the zero point.

The faint counts show a discrepancy compared with Tyson's values. At fainter magnitudes, the counts are sufficiently high to give reasonable confidence in the values (*i.e.* the errors are much smaller than the counts) and the excess is considerably greater then the expected error. All three bands contain a greater than Euclidean rise that persists over a magnitude before decreasing in slope. The steepness of the rise is greatest in I and least in B, which is opposite to the normal trend of slope with wavelength. The peak of the excess lies about 0.4 dex above Tyson in B, 0.5 dex in R and 0.6 dex in I.

4.3 A Faint Cluster

The most probable explanation for the steep rise and observed excess is the presence of a faint cluster of galaxies centred on the radio galaxy 3C 217 at a redshift of $z = 0.9$. The distribution of the excess counts gives a poor fit to a single power law slope, a result which would seem to rule out an origin arising solely from an error in the absolute number density. However, if we treat Tyson's counts as the field population and the excess as the cluster members, then shifting the zero points of Tyson's slopes could strongly alter the implied number of members.

Photographic work has shown substantial variations in the absolute number densities of faint galaxies in different surveys. A collaboration between Ellis and Koo (Ellis 1987) showed that the mean difference in isophotal and Kron magnitudes was insufficient to explain the observed variations (*i.e.* the variations cannot be solely due to different measuring techniques used by different authors). Ellis also reduced a set of five plates covering 1 deg^2 areas

and found sufficient scatter to explain the differences between groups. He concluded that large scale clustering was primarily responsible.

This would bode ill for absolute number count densities obtained from CCD surveys since these detectors cover only a small fraction of the area available to photographic plates. However, Tyson reports the variations between his 12 CCD fields to be only of order 10%. The solution to this apparent discrepancy may lie in the fainter magnitudes accessible to CCDs. The spectroscopic surveys by Koo (1988) and Broadhurst *et al.* (1990) found that field galaxies with $B \leq 21$ have a strongly clumped distribution in redshift which is sufficient to dominate and cause strong field-to-field fluctuation in the counts. However, in the fainter CCD surveys, the sample will include an increasing number of these structures which will serve to smooth out their distribution. This may explain the observed lack of variation between fields.

This remains somewhat speculative until fainter redshift surveys become available. Also required are additional faint field surveys to confirm lack of variation in absolute number density for deep CCD fields. However, with the information presently available, we can expect only small variations in the field density, a result which makes it highly unlikely that the observed excess of faint galaxies in our field can be accounted for strictly by shifting the zero point or the slope of the number counts.

An error in calibration could also change the absolute number density if the magnitude scale were calibrated too high or too low. However the shift in the zero point of the counts would be equal to the calibration error times the slope of the counts. This requires an error of order 1 mag to account for the excess. The agreement of our data with the published magnitude of 3C 217 rules out errors of this size. The estimated uncertainty in calibration of order ~ 0.1 mag has a negligible effect on the zero point of the number

counts.

Quite aside from the fact that the discrepancy is too large to be due to a zero point error, the counts themselves do not provide a good fit to a straight line in the log N - magnitude domain. Koo (1986) pointed out that failure to correct the number counts for the Malmquist bias will result in an observed slope that is too steep. These corrections have been performed, although the question arises as to whether the biases have been properly accounted for. However, the form of the corrections appears well behaved and is fairly well understood. The simulations were treated in a nearly identically manner to the real data, and every effort was made to follow the detection and reduction procedure outlined in Chapter 2. The counts with an increased S/N cut are virtually identical, even in the I band where the negative bias is decreased by more than a factor of two. As a test, the negative magnitude bias in the I corrections was arbitrarily eliminated; this resulted in the height of the peak being decreased by < 0.1 dex.

The small numbers and scatter at the bright end make it somewhat difficult to determine the extent to which these counts are consistent with Tyson's normalization. Figures $4.7 - 4.9$ show the number counts plotted on a linear scale to emphasis both the magnitude of the excess at the faint end and the difficulty in determining a normalization from the small number of objects at the bright end.

The integrated number densities are generally consistent at magnitudes brighter than the rise of the excess. The integrated bright end counts are slightly higher than Tyson for $R < 23.0$ although the scatter in the R count seems particularly high. Also, some of the brighter cluster galaxies, including 3C 217, will contribute to the bright end counts and therefore some excess is perhaps expected. (In section 5.4, we study the brightest galaxies in I more

carefully, and find that cluster members add significantly to the bright end counts)

The increase in the steepness of the rise in counts with wavelength can be understood in terms of the K corrections for the different filters. Coleman *et al.* (1980) show that for $z = 0.9$, the K corrections for E type and Scd type galaxies differ by ≥ 3.0 mag in B , whereas the difference is only ~ 1.3 mag in R and ~ 0.9 mag in I . A large difference in the K corrections between galaxy types should serve to spread out the distribution of a cluster in the N(m) diagram. The I filter would be expected to show the steepest rise because it is much less affected by the K corrections.

While the excess number counts appear to be best explained by the presence of a faint cluster, examination of the data reveals no significant central concentration. Several attempts were made to enhance a radial density gradient using a variety of selection criteria based on magnitude, colour and/or the presence of (or lack of) objects in more than one filter. That we failed to produce any significant density gradient is perhaps not too surprising, since the field population accounts for $40 - 50\%$ of the total number of galaxies in the frames. From the models of Cappi *et al.* (1989), this 2 : 1 ratio of total to background galaxies corresponds to a cluster detection probability of only ~ 0.05. Although these models apply to the probability of cluster detection when the position is not known, it does indicate the difficulty in determining presence of a cluster when the field content is high. Proper selection criterion can reduce the fraction of the background galaxies but probably no better than a 4 : 1 ratio is achieved. (the effects of various selection criteria on this ratio is somewhat difficult to estimate). The largest excess, at the peak of the I band distribution, still represents only a 0.3 probability of cluster detection.

It is conceivable that there may be little or no gradient across the frame because of the size of the area surveyed. If the cluster is centred on 3C 217 at redshift $z = 0.9$, we can determine the luminosity distance from (Mattig 1959)

$$d_L = \frac{c}{H_o {q_o}^2} \left\{ z q_o + (q_o - 1)[(2 q_o z + 1)^{0.5} - 1] \right\} \tag{4.1}$$

and the metric size from

$$s = \frac{\theta d_L}{(1+z)^2} \tag{4.2}$$

This gives the metric area surveyed as $(0.65 \times 0.98) h^{-2}$ Mpc^2 at $z = 0.9$. H_o and q_o determine the cosmology and here are taken as 100 km s^{-1} Mpc^{-1} and 0.0 respectively. θ is the angular size and the h is the Hubble constant in units of 100 km s^{-1} Mpc^{-1}. For a typical cluster core radius of $r_c \approx 0.50$ Mpc (Koo 1988), the cluster core takes up almost the entire area surveyed. If the cluster has a flattened core distribution this means that a significant number density gradient across the field may not be present, and would certainly be difficult to detect with the high level of contamination from the field. This also suggests that number counts are more sensitive to the presence of high redshift clusters than spatial tests, which fail to function in the presence of a populous background.

Early type systems (E's and S0's) represent a high percentage of the galaxies in nearby clusters. These galaxies also tend to be more virialized and show a higher degree central concentration than later type galaxies. However, early type galaxies at a redshift of $z = 0.9$ are strongly dimmed by K corrections. This may also inhibit the detection of a central concentration.

4.4 The Luminosity Function

The primary purpose in determining the luminosity function is to see if the fit to the excess counts yields a characteristic absolute magnitude, M^*, that is roughly consistent with a cluster at $z = 0.9$. At high redshifts, the luminosity function will be somewhat altered by differences in the K corrections for individual cluster members. Because of the high field contamination it is not practical to adopt the Monte Carlo approach to membership used in relatively nearby clusters (Oegerle and Hoessel, 1989). It is possible to make some determination of cluster membership (see Chapter 5), but only at the brighter magnitudes where photometric errors are small and the colours can be accurately determined. For our purposes, the uncertainty in the field correction is too high to give any greater confidence over the application of a single K correction to M^*.

The standard Schechter (1976) luminosity function has the form

$$\phi(M)dM \sim 10^{-0.4(\alpha+1)M} e^{-10^{0.4(M^*-M)}} dM \tag{4.3}$$

where α is a free parameter that determines the faint end slope. The faint end slope of our counts depends on corrections that are large and have considerable uncertainties. Also the background increases faster than α which would hamper its determination. Following Felten (1985), we have adopted a value of $\alpha = -1.25$ which simplifies the task of determining M^*. For the apparent magnitudes in the B and R filters, we estimate values of $m_B^* = 24.9 \pm 0.5$ and $m_R^* = 24.2 \pm 0.4$. The count density normalization for the two fits is consistent to within 25%.

The distance modulus was determined as $m - M = 43.0$ using equation 4.1. Adopting the K corrections for an Sbc type galaxy at $z = 0.9$ (Coleman

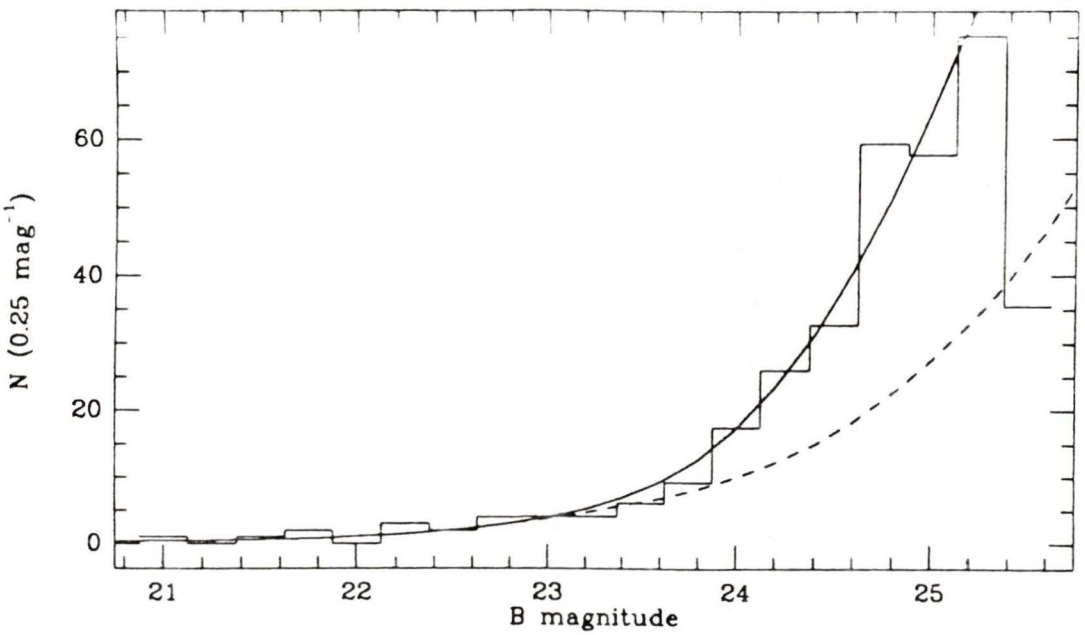

Figure 4.7: Counts vs. B magnitude. The dashed line indicates Tyson's (1988) observations. The solid line shows the addition of a Schechter function to Tyson's counts.

et al. 1980) yields values of $M_B^* = -19.9 \pm 0.5$ and $M_R^* = -20.2 \pm 0.4$. The value for M_B^* shows good agreement with that determined by Kirshner *et al.* (1983) and Schechter (1976), who obtained M_B^* values of -20.1 and -19.9 respectively. Good agreement is also found with Oegerle and Hoessel (1989) who determine a median value for nine clusters at $M_R^* = -20.4$ using a fixed value of $\alpha = -1.25$.

The agreement is somewhat uncertain since a judicious choice of K corrections could match a wide range of values of M^*. Although the bright end of the luminosity function in nearby clusters is dominated by early type galaxies, the K corrections for elliptical galaxies at this redshift are large and these galaxies will be dimmed considerably relative to spiral galaxies. And while Im type galaxies are seen to comprise a significant fraction of local

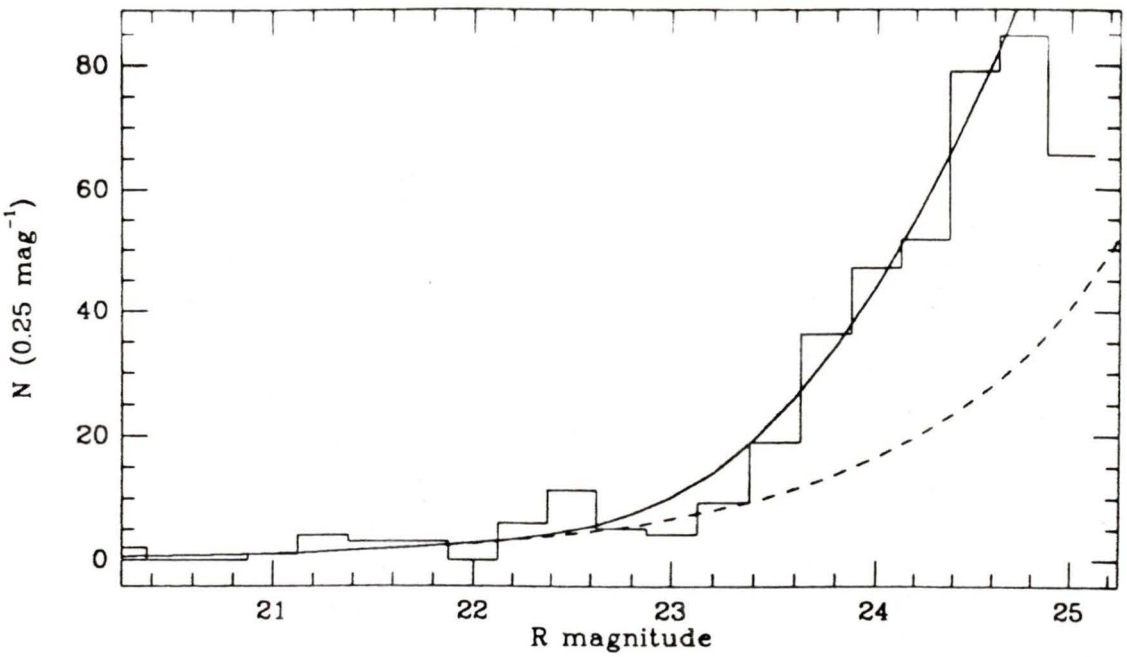

Figure 4.8: Counts vs. R magnitude. The dashed line indicates Tyson's (1988) observations. The solid line shows the addition of a Schechter function to Tyson's counts.

cluster members, their small K corrections are insufficient to overcome their intrinsically fainter magnitudes. Therefore, despite some reservations about the assumptions made in applying the K corrections, the agreement of our M^* values with published values is consistent with the excess counts being produced by a cluster at the redshift of 3C 217.

It is somewhat unexpected that even though the K corrections are smallest in the I band, the excess appears least like a Schechter function. For the I counts in Figure 4.9, the initially very steep rise in counts and the decrease by 23.5 in I creates some uncertainty as to the best fit. Fitting to the steep rise presumes that the galaxies are underweighted in the faintest bins, which implies a number density normalization of over three times that found in the fit to B and R bands. On the other hand, fixing the number density to

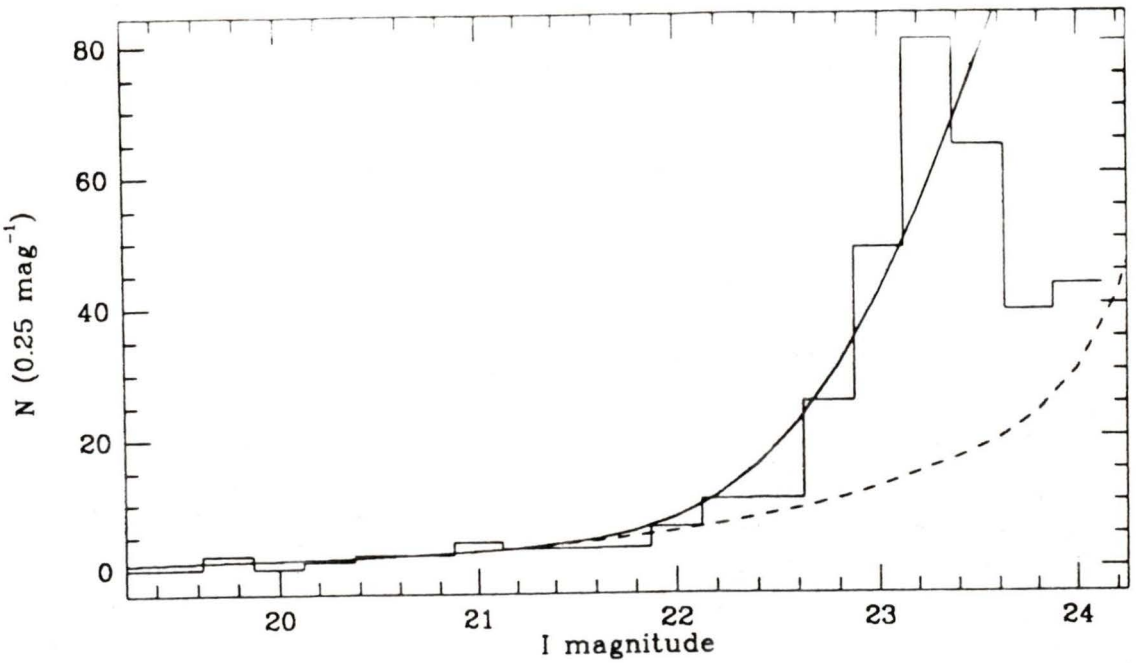

Figure 4.9: Counts vs. I magnitude. The dashed line indicates Tyson's (1988) observations. The solid line shows the addition of a Schechter function to Tyson's counts.

values consistent with that found for the other filters gives a more gradual increase in counts than has been determined.

4.5 Counts of Filter Matched Galaxies

A further test of the behaviour of the N(m) diagram is made by determining the counts using only those galaxies with detected positions in two or more filters. This test provides a check on the robustness of the observed distribution as well as providing some insight into the effects of colour on the distribution. As discussed in section 2.2, using objects detected in two filters requires completeness corrections that depend on the observed magnitude in both filters. To avoid the excessive weighting for an object with a very faint counterpart (and hence a very uncertain correction), no object was given a

weight greater than 2.0.

Figure 4.10 shows N(m) diagrams for galaxies appearing in both the B and R filters as well as their single filter counterparts. The B counts are consistent to within $\sqrt{n}$ errors at all magnitudes. There is a slight lowering of the counts which may be due to an underestimation of the incompleteness for objects of extreme colour. This consistency lends some confidence to the corrections since just over half of the objects appear in both filters.

The R counts show a consistent match over the steep rise, although the faint end is decreased somewhat from the single filter values. This is most likely due to completeness effects since the incompleteness in B starts to affect the shape of the distribution by $R = 24$. The effect of colour on the distribution will be seen in Chapter 5.

Figure 4.11 shows much stronger effects for the counts of R and I matched galaxies. Although the steep rise in R remains undiminished, the counts then drop down to the level of Tyson's values and the position of the peak shifts brighter to $\sim 24R$. The higher I peak is reduced by nearly 0.3 dex although its position is unchanged. The reduction of the peak also decreases the rise in counts, although it remains steeper then Euclidean.

Even though these counts show a considerable decrease in number, the excess is not entirely removed. Both diagrams show a peak excess of more than twice Tyson's values, which is still considerably greater than the expected errors. Nor is the difference in the count levels due to spurious detections since over a third of the galaxies that do not appear in I are detected in B . A more probable explanation is that the difference is due to the colours of these objects affecting the completeness. Completeness effects arising from colour are perhaps expected to play a greater role in Figure 4.11 since the

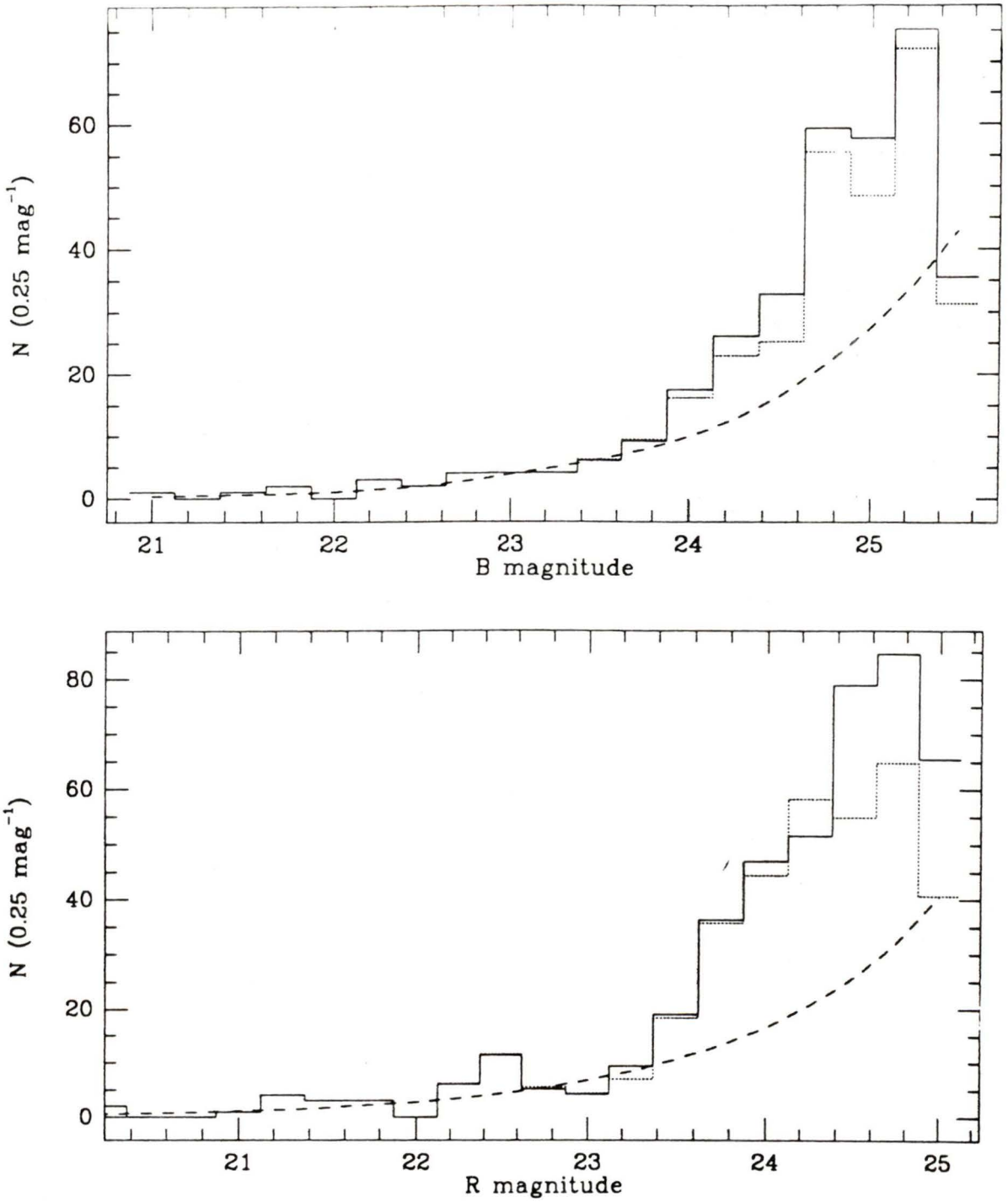

Figure 4.10: The B and R counts for galaxies appearing in both filters. The single filter counts and Tyson's values are also plotted.

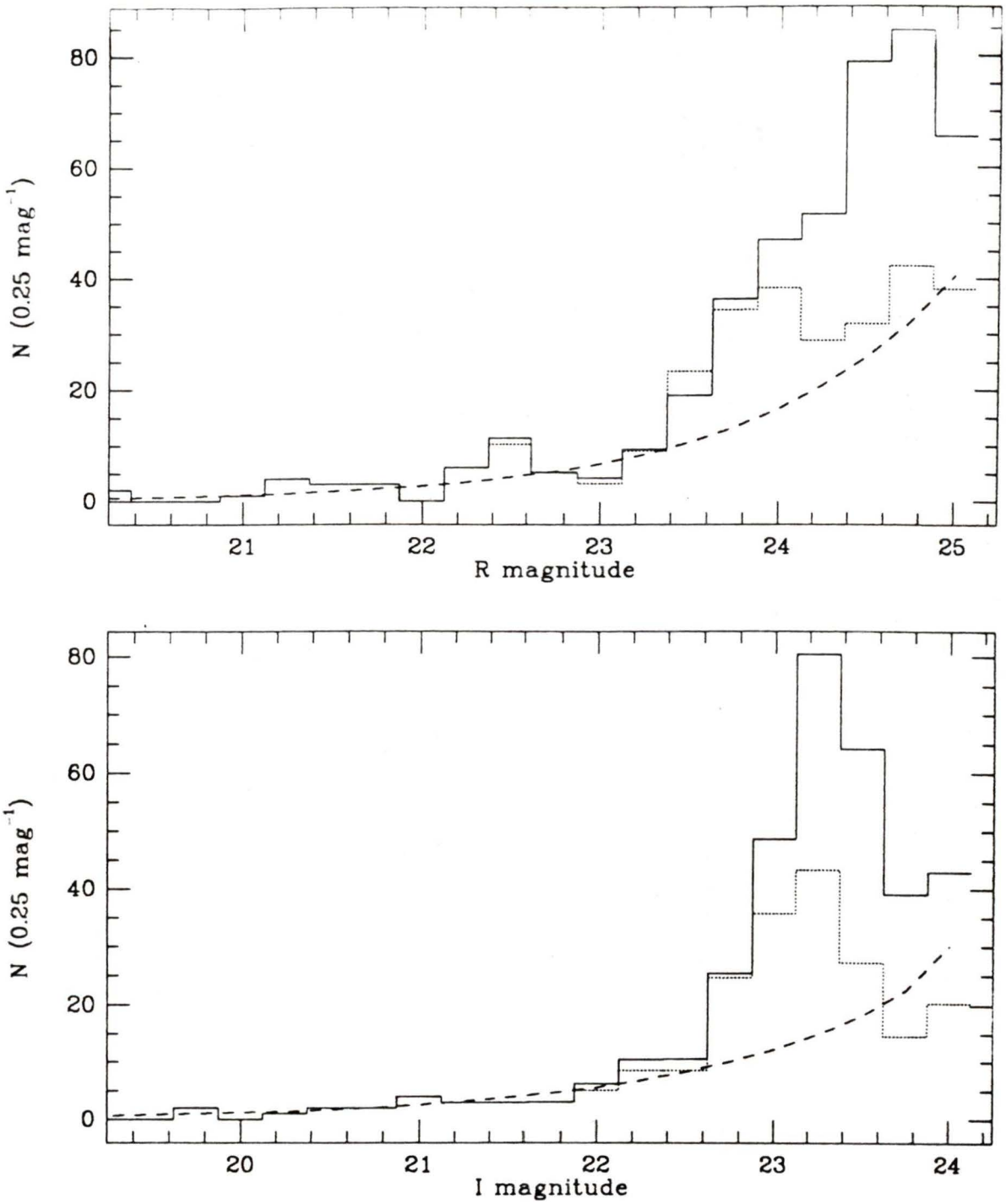

Figure 4.11: The R and I counts for galaxies appearing in both filters. The single filter counts and Tyson's values are also plotted.

difference in limiting magnitude is greater between R and I than between B and R .

In addition to the seeming reconciliation of the faintest R counts with Tyson's values, what is interesting about the counts of R and I matched galaxies is that the size and shape of the excess becomes roughly similar. The implication is that the excess in the two N(m) diagrams is due to the same population of galaxies. The difference in the magnitude of the two peaks is $R - I \sim 0.5$, which could be identified as the median colour of the population. For the galaxies fainter then 24 R mag, this colour corresponds to the point at which the completeness limits in the I band begin to affect the distribution (see Figure 5.2) - a fact which could explain the decrease in the counts.

This test seems to imply that at least a portion of the peak is somehow associated with the bright end of the R band excess. A large fraction of the I galaxies fail to match despite the fact that the excess in R extends to fainter values. At a redshift of $z = 0.9$, the rest wavelength of the I filter lies just above the 4000Å break. This means that it would be sensitive to galaxies with a relatively large break, *i.e.* early type systems, which may not be seen in the other filters. If the elliptical and spiral galaxies were at about the same I magnitude, they could produce a peak that was significantly more spread out, via K corrections, in the bluer filters.

There are two problems with this scenario. The first is that the Schechter function provides a reasonable fit to the B and R residuals. At a redshift of $z = 0.9$ the I band corresponds roughly to the rest frame B , while the other filters will be deeper into the ultraviolet. Therefore, the I counts are less sensitive to both K corrections and evolutionary effects and should give a better description of the distribution. For the B and R counts, this would

imply that the shape of distribution was in fact due to differences in the K dimming of the various galaxy types.

The other problem is that despite the larger peak excess in the I band counts, the integrated excess is about equal to that in R . The expectation is that there ought to be significantly more galaxies in the I residuals since they contain not only the objects that comprise the R excess but also the objects that are not seen in R .

This problem can be avoided if the faint end of R and I counts are composed largely of different objects. The I galaxies that do not appear in R would be objects with a relatively large values of $R - I$ and hence run up against the completeness limit in R . The R galaxies that fail to appear in I would have colours less than or equal to 0.5 mag, the difference in the matched R and I peaks. These would be flat spectrum galaxies with possible evolutionary effects. The colours of our distribution appear to show an excess of galaxies that are bluer in $R - I$ than those typically observed in the field.

4.6 Summary

There are several important features obtained from our N(m) diagrams. The primary result is that we see number counts that exceed the expected values by a factor of two. The excess is characterized by a greater than Euclidean rise in the counts that steepens in the longer wavelength filters (with peak excesses of 2.5 to 4.0 times the expected values). The use of a higher signal to noise cut on the data does not affect this conclusion, indicating that the excess is real. The most plausible explanation of the excess is the presence of a high redshift cluster of galaxies in the field.

A Schechter function, with $\alpha = -1.25$, was fitted to residuals obtained by subtracting off the expected background from the observed counts. The fitted M^* values give good agreement with published values in B and R after correcting for a distance and K dimming corresponding to the $z = 0.9$ redshift of 3C 217. The I counts fail to provide an acceptable fit to a Schechter function despite the smaller K corrections for this filter.

A possible explanation is that the filters are sensitive to different populations. The I band samples a population of red galaxies not seen in the shorter wavelength filters because of K dimming. The R filter sees a population enhanced by evolution but too faint to be seen in I because of its flat $R - I$ colours.

Chapter 5

Colours

5.1 Determining Colours

Multi-band photometry provides the Rosetta Stone for the interpretation of stellar objects. This is because stars have broadband photometric colours that correspond closely to their spectral type. Observations of stars are relatively straightforward since stars share a common point spread function, and stellar astrophysics provides a well understood theoretical basis for interpreting stellar colours. For faint galaxy surveys, the impact of multi-colour measurements has been equally important, but the results have been somewhat less satisfying and their interpretation has often been the source of controversy. The problem lies with the increased number of variables inherent in the observation and interpretation of faint galaxy colours.

Galaxies are classified according to morphological type and although these types do have characteristic spectra and colours, the intrinsic scatter within a particular classification is far greater than for stellar classification. Naively, the range of morphological types mimics an evolutionary sequence

in that higher rates of star formation are seen in later type galaxies. However, it is generally believed that later type galaxies do not evolve into earlier types (except possibly by mergers) and that the evolution associated with lookback time will have a different effect on the colours. Also, a burst of star formation involving only a small fraction of the population of a galaxy can easily dominate the observed colours. There is also the factor of redshift which distorts the observed colours because of differences in the K corrections between filters. Although we are examining a cluster at known redshift, we do not know *a priori* the redshift of a particular galaxy. The task is to use the colour observations to separate the competing effects of galaxy type, evolution and redshift.

A separate consideration in determining colours is photometric error. Because galaxies are resolved, their images contain more noise than stellar objects at the same magnitude. The determination of colours combines two independent measurements of magnitude which sums the noise in quadrature, making the reduction of noise of primary importance.

The determination of magnitudes by the Kron method is an attempt to measure the total amount of light for objects that may extend over more than 200 pix (35 arcsec^2). The noise in these measurements can be reduced by using aperture photometry (as described in section 2.3). This does not provide a good measure of the total magnitude because of the variations in the surface brightness profiles between different galaxies. However, colours are measured by the relative brightness of an object in two filters and hence it is not necessary to measure all the light since the same fraction of light will be missed in both filters. This requires that an object has roughly similar profiles in both filters, an assumption which is not always the case; but tests indicate that the mean errors are smaller than obtained using total

magnitudes (Koo 1986).

5.2 Colour Distribution

The difficulties associated with the interpretation of the colour distribution require a careful assessment of selection effects. This is particularly important with high redshift galaxies since the K corrections through different filters can produce large changes in the observed colours. The initial samples consist of all objects detected in the required filters. ("Detected" means that the objects were not only detected in these filters, but also have sufficient signal-to-noise for their Kron magnitudes to be meaningful.) This allows us to examine how the selection effects determine which objects are seen in various filters, since the completeness limits of the data have already been calculated from the simulations.

The colour-magnitude diagrams are shown in Figures 5.1 and 5.2, both of which include estimates of the 50% completeness limits. Figure 5.1 shows that fainter galaxies are, on average, bluer; this effect is best seen in R , but is still apparent in B . However, the trend in R may be affected by the $B-R$ completeness limit (the diagonal line) which impinges on the distribution fainter than $R = 23.5$. Although there are relatively few objects on the faint side of this limit, there is some uncertainty in the exact position of the limit. A 1σ change in the limit could change its effect on the distribution.

Completeness in B prevents only the bluer galaxies from being seen and the distribution looks somewhat flatter. Fainter than $B = 23.5$, there is no strong appearance of a blueing trend. While the brighter galaxies undoubtedly become bluer with magnitude, estimating the extent to which this trend continues to fainter magnitudes is hampered by incompleteness.

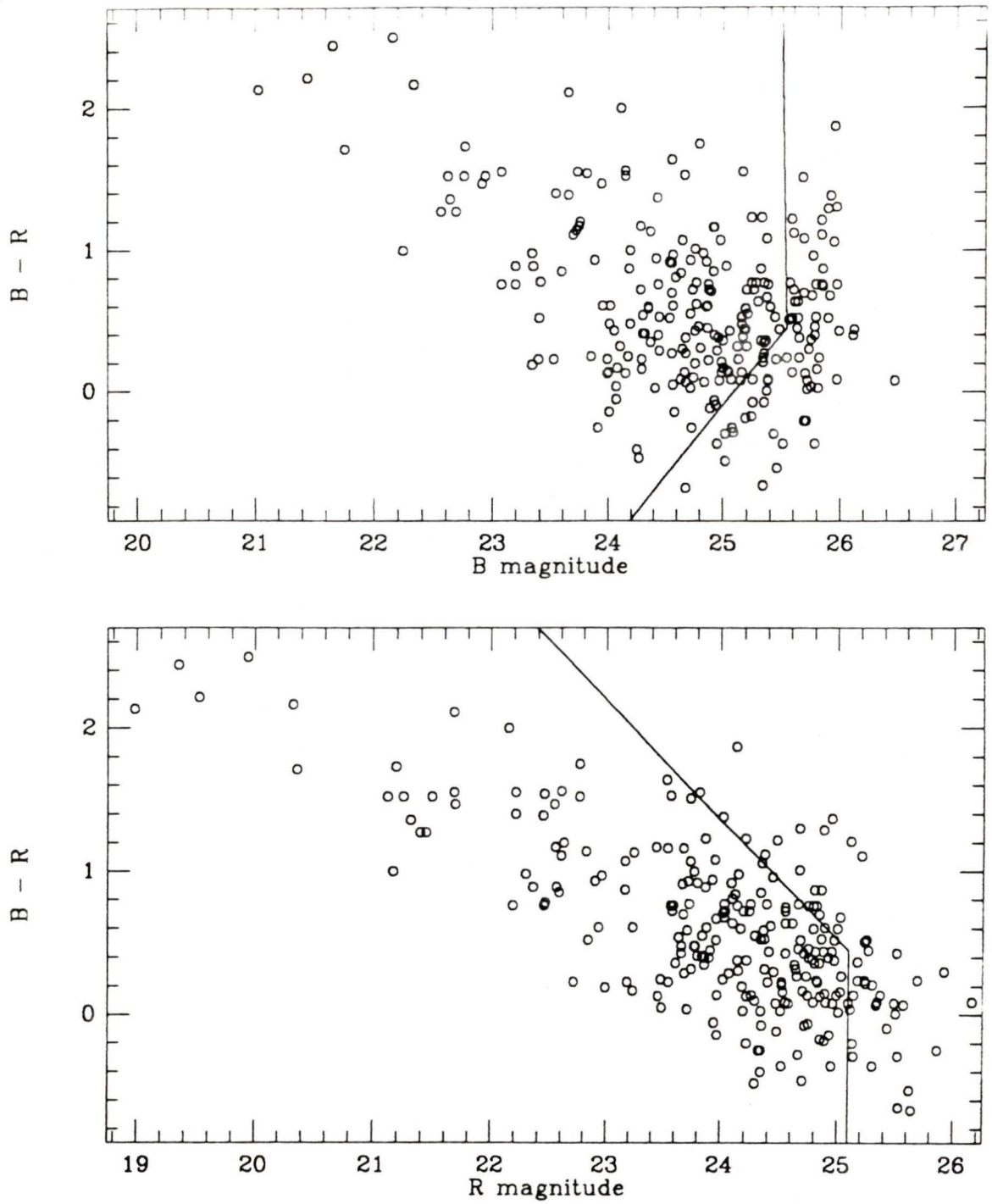

Figure 5.1: $B - R$ vs. B and $B - R$ vs. R . The solid lines are estimates of the 50% completeness limits.

Figure 5.2 also shows a slight trend toward bluer $R - I$ colours as magnitudes become fainter. The trend appears to continue in the R band despite incompleteness effects for galaxies with small values of $R - I$ fainter than $R = 24$. No evidence of this trend is seen in Tyson (1988), which shows an essentially flat distribution of $R - I$ colours.

Figures 5.1-5.2 represent the colour-magnitude counterparts to the filter matched N(m) diagrams (Figures 4.10-4.11). This allows some insight into how samples that include colours (which combine the selection effects in two filters) alter the number of galaxies observed.

In Figure 5.1, the completeness limits due to the $B - R$ colour do not appear to have a strong effect on the distribution. There are few objects fainter than these limits and the trend of the distribution seems to be through the magnitude limit (vertical line) rather than the colour limit (diagonal line). The number counts of the galaxies found in both B and R show little difference from the counts determined from the objects found in a single filter. There is some decrease towards the faint end which is probably due to the upper limit of a factor of 2 on the completeness correction.

For the galaxies that appear in both R and I, there is a much larger decrease in the single filter counts. The R band counts in particular are strongly affected. However, in Figure 5.2 it is apparent that the trend of the distribution moves across the $R - I$ completeness limit. There are many galaxies fainter than this limit and these will be underweighted (due to the upper limit on the completeness correction), resulting in the decrease seen in the filter matched number counts.

There is also a significant decrease in the I band counts for objects appearing in R and I, but there are few galaxies in Figure 5.2 that are fainter than the $R - I$ completeness limit. Unlike the R band, the decrease in counts

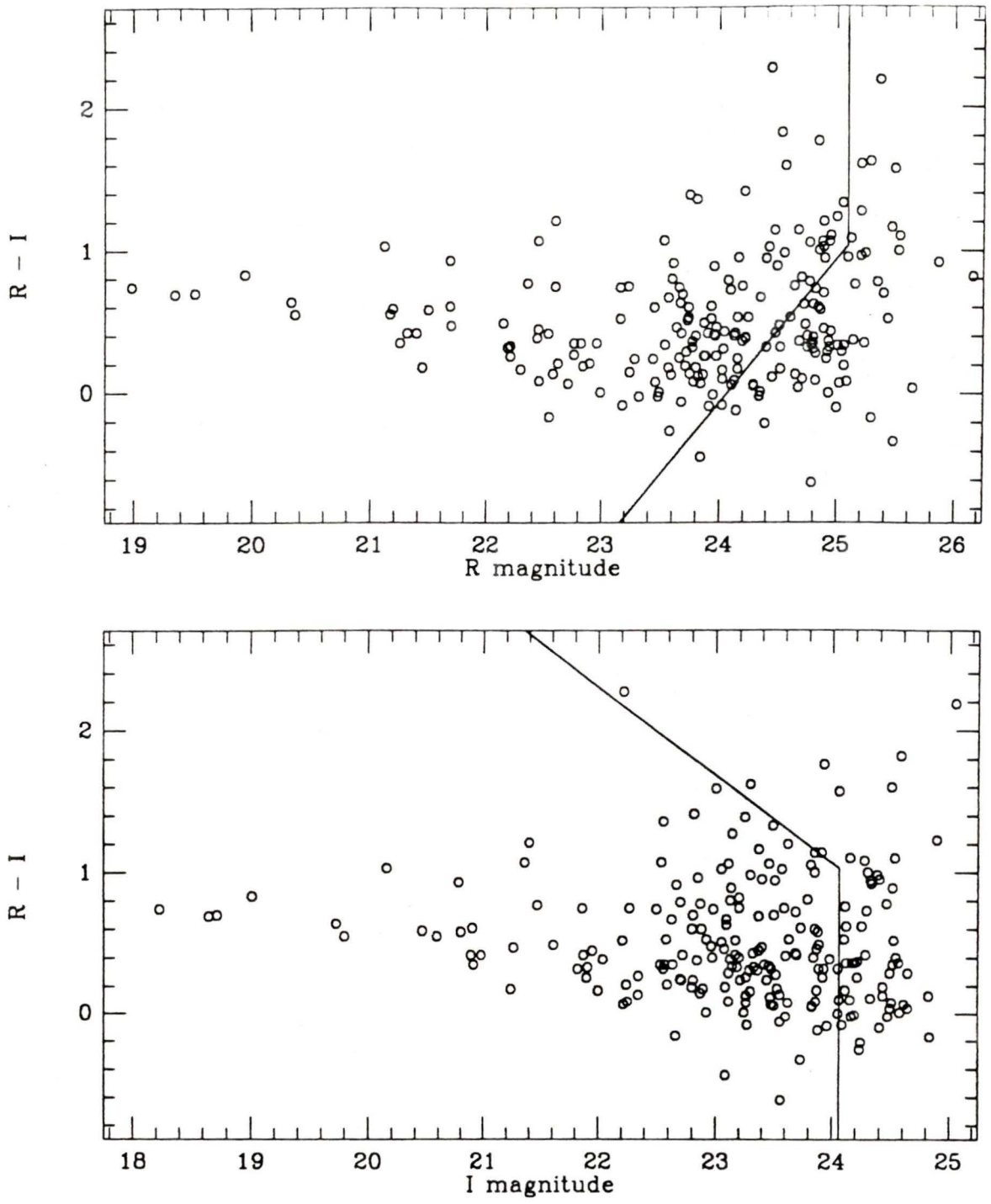

Figure 5.2: $R - I$ vs. R and $R - I$ vs. I . The solid lines are estimates of the 50% completeness limits.

cannot be solely attributed to underweighting the counts. It seems that a portion of the galaxies in the I band have either extremely red colours, or other characteristics that render them undetected in R . Elliptical galaxies at the cluster redshift have red colours but they should still be detected over much of the sample. This is an important feature since in order to examine the evolution of the cluster, an accurate determination must also be made of the galaxies that do not show evolution. We return to this question in Section 5.5.

Figure 5.3 shows the uncorrected colours of all detected stars and galaxies in four ranges of R magnitude. The solid lines indicate the photoelectric stellar main sequence and giant branch for our filter system as taken from Bessell (1979). It should be pointed out that stars with $B - R > 2.0$ do not fit the sequence particularly well. This seems to be caused by differences in the response of photomultipliers and CCDs for complex M star spectra (Schneider *et al.* 1983). The problem is that the effective wavelength of photoelectric R shifts redward by nearly 600Å between spectral types K0 and M0 (Bessell 1979). This results in increased values of $B - R$ and smaller values of $R - I$, which is consistent with the observed discrepancy. This has little effect on the bluer portion of the sequence where the calibration star is located.

Photographic surveys have previously shown a slight blueing trend with magnitude. Its origin could have been the result of K corrections, since blue galaxies suffer less from K dimming and will therefore be enhanced in a magnitude limited sample. Tyson (1988) observed that the blueing trend in $B - R$ extends down to 26 R mag and contends that this effect is too large to be due to K-corrections alone. Theoretical models indicate that a spiral rich sample of evolving galaxies is expected to move to the lower right in

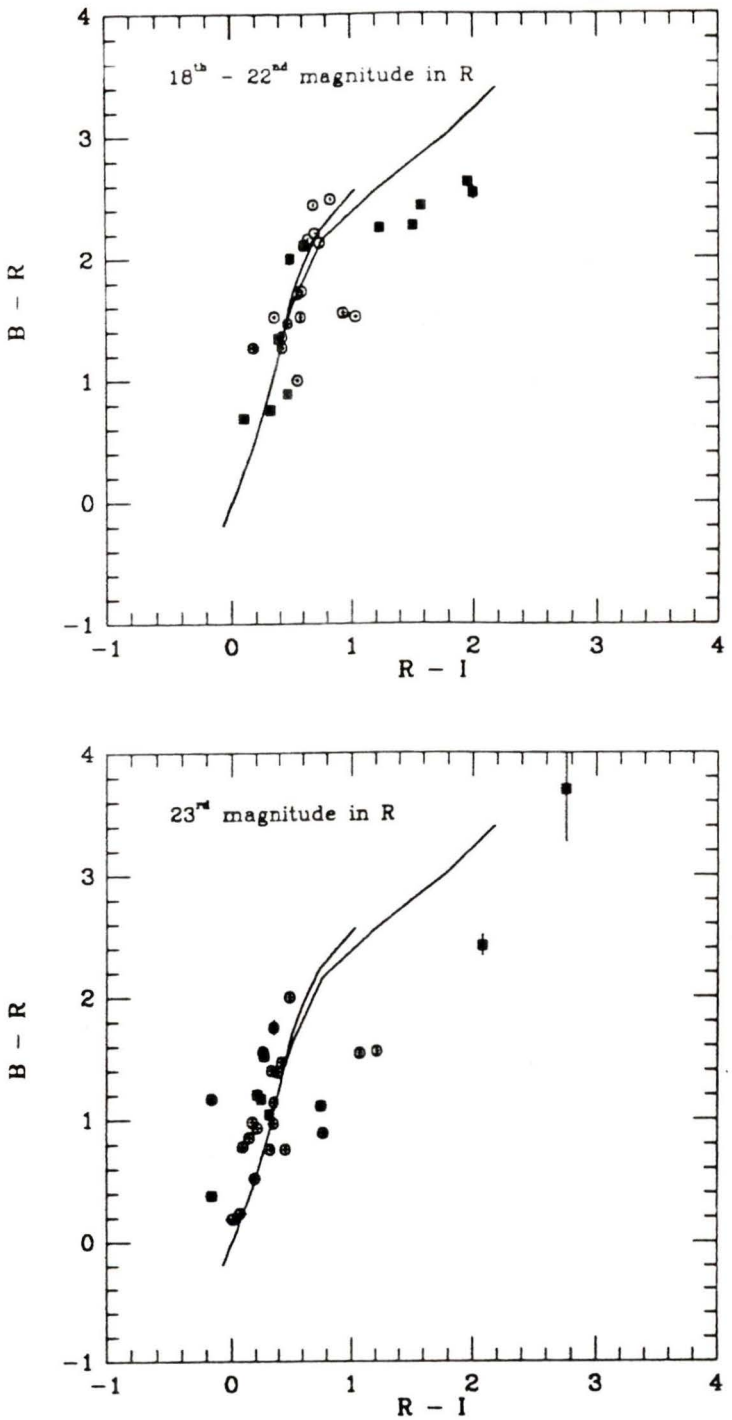

Figure 5.3: $B - R$ vs. $R - I$ for both stars and galaxies. Galaxies are indicated by open circles, stars by filled squares. The solid lines are the main sequence and giant branch as observed photoelectrically.

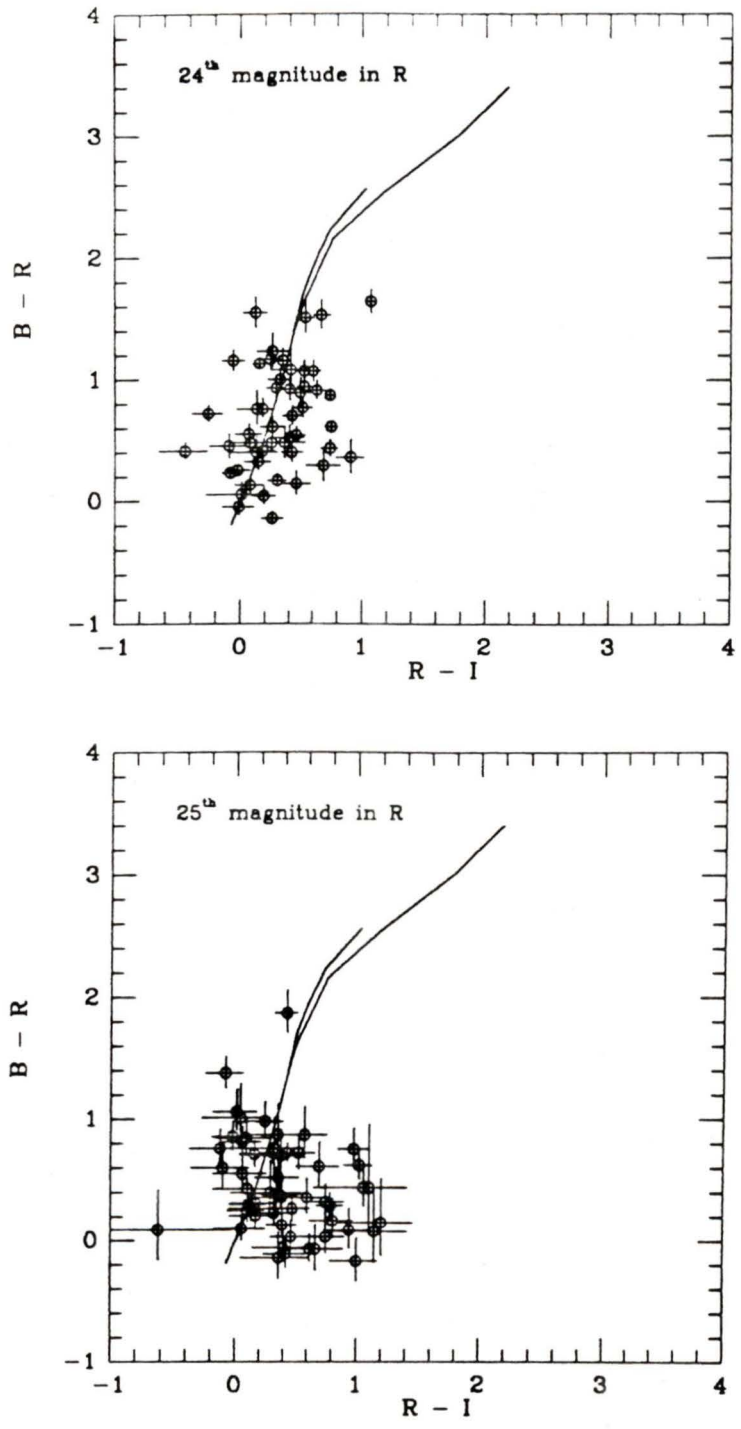

Figure 5.3: (cont.)

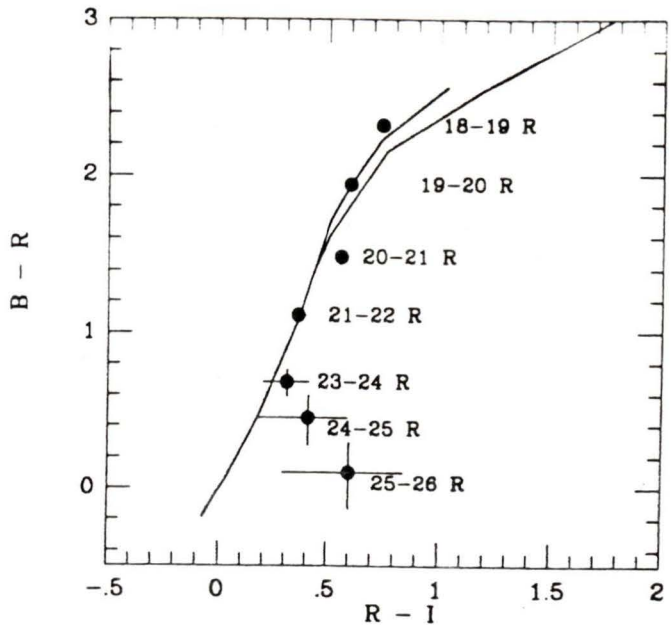

Figure 5.4: Mean $B - R$ vs. $R - I$ as a function of R . The points are for 1 mag bins in R as indicated. The error bars represent the 1σ errors in the mean for galaxies in each bin.

Figure 5.3 with increasing redshift (Bruzual 1981).

Our data initially appear to trend towards the lower left, *i.e.* bluer in both colours. There is some evidence of the expected trend for galaxies in the 24-25 R mag panel. However, in this magnitude range, over 25% of our galaxies still lie on the left side of the stellar sequence; this can be compared with Tyson's work where the fraction is closer to 10%. However, Tyson's data also reach significantly fainter magnitudes, particularly in B . Although the selection effects in $R - I$ work against objects with blue colours, the selection effects in $B - R$ work against objects with red colours. Galaxies that are red in *both* colours will not be seen because of the selection effects caused by the B filter. Hence, the criterion of detection in all filters may cause a trend in one colour as a result of selection effects in a different colour. The mean trends in this sample appear in the statistical colour-colour plot shown in

Figure 5.4.

5.3 A Sample in I

The galaxies in the previous colour-colour diagrams (Figures 5.3-5.4) are included by virtue of their detection in each of the three filters B , R and I . This allows the relatively straightforward calculation of the mean colours, since the simulations give a fair understanding of the selection effects in the individual filters. The mean colours appear to indicate that the general distribution becomes too blue in $R - I$ at magnitudes where the cluster galaxies are believed to be predominant. However, the selection effects may be very strong and the diagrams fail to show a significant clumping in colour distribution that may be indicative of a cluster. There is also a notable absence of objects with colours that match those of early type galaxies at a redshift of $z = 0.9$.

This lack of early type galaxies in the colour-colour diagram may be more indicative of the selection effects than the true distribution of morphological types. Normal elliptical galaxies at the cluster redshift are expected to have colours of $B - R = 3.5$ and $R - I = 1.5$, implying that 50% completeness in B requires an elliptical galaxy to have $R \leq 22.0$, over a magnitude brighter than the bright end of the excess! Therefore the requirement that galaxies be detected in B effectively excludes early type cluster galaxies from the sample.

In order to reduce these selection effects, we have chosen a sample of galaxies with $I \leq 23.5$ that were also detected in the R bandpass, all of which have $R - I$ colours measured with a S/N better than $3:1$. (By "detected", we mean that the galaxy has not only been detected, but also has a Kron magnitude with S/N $\geq 3:1$) Because the I bandpass suffers the least from K

corrections, ordering the galaxies by I magnitude reduces the contamination from flat spectrum galaxies. Early type galaxies are brighter in I than in other filters and the $R-I$ colours for cluster elliptical galaxies should be detectable in both filters over much of the sample. Out of this sample of 120 galaxies, we were also able to obtain the $B-R$ to a S/N $\geq 3:1$ for all but 12 objects. The magnitudes, colours and spectral energy distributions (SED), which include the narrow band fluxes, for all 120 galaxies in this sample are given in Appendix A.

The criterion that the galaxies be detected in R greatly reduces the completeness of the sample. Only for objects with $I \leq 22.0$ is the R detection complete. For the complete list of galaxies with $I \leq 23.5$, 70 are not detected in R and attempts to determine their colour resulted in fewer than half having $R-I$ colours with S/N $\leq 3:1$ (and still fewer in $B-R$). Hence the requirement that the galaxies be detected in R effectively eliminates all the objects that have poor colour determinations, but at the cost of introducing an additional selection effect. The advantage is that the selection is reasonably well defined, and from the simulations we can estimate the expected number in the sample using only objects with a large signal-to-noise ratio. However, it is apparent from Figure 4.7 that the matched counts underestimate the straight I counts. The nature of this discrepancy is examined in Section 5.5.

5.4 Cluster Galaxies

In order to make a determination of cluster membership, we have calculated the redshifted colours for our filter system, using the spectral energy distributions of Coleman *et al.* (1980). For this we adopted a somewhat primitive

smoothing function instead of using the combination of filter transmission and CCD response. However, we found this was able to reproduce the results of Coleman *et al.* to within ±0.05 mag for both colours and K corrections; this is sufficient for our purposes.

We also determined the colours for Bruzual's (1981) evolutionary models at $z = 0.9$, transforming his photographic *JFN* into our *BRI* system through Coleman's spectral energy distributions. The models are for an exponential rate of star formation and the μ term indicates the fraction of gas that would remain after 10^9 yr (1 Gyr) if the gas from dying stars is not returned back into the system. For $\mu > 0.7$, or constant rates of star formation, the evolutionary curve appears indistinguishable from the morphological sequence and the distinction does become not significant until $\mu \leq 0.5$. The colours for $\mu < 0.5$ are not supplied directly by Bruzual (1981), but were interpolated from his Figure 42j. Hence, the star formation rates are not indicated; the blue end of the curve goes off scale at a point corresponding to $\mu \approx 0.2$

The colours are shown in Figure 5.5 for galaxies out to $z = 1.3$. While several of the colours are multi-valued between type and redshift, this diagram is fairly effective at distinguishing relatively nearby galaxies from those at the cluster redshift, particularly for early type systems. This is because the large 4000Å break in early type galaxies lies between the *R* and *I* filters at $z = 0.9$.

Narrow band filters were also used in conjunction with broad band colours to aid in determining cluster membership. The narrow band data were originally part of a survey designed to detect high redshift primeval galaxies (see Ch.2), and hence were not taken at ideal wavelengths for the study of galaxies at $z = 0.9$. (A narrow filter at 7100Å to detect redshifted [OII] 3726/3729Å line would have been particularly informative.) At the cluster

redshift, the 9500Å filter contains both Hβ and the [OIII] 4959/5007Å doublet. Unfortunately, this filter suffers a bright limiting magnitude, somewhat poorer seeing and a 500Å equivalent width that gives a much weaker indication of the presence of an emission line. The 8100Å filter contains the G band absorption feature, but may also be affected by Hγ in either absorption or emission. Likewise the 7500Å filter contains the H and K calcium lines but also includes [NeIII] + Hϵ. The 6800Å filter does not appear to match any common features and the 6300Å filter contains [NeIII] and [NeV] lines that are generally quite weak.

The 6300Å and 6800Å filters are expected to lie near the continuum levels for cluster galaxies, but the [OII] 3726/3729Å line lies in the R band over the range $0.5 \geq z \geq 0.9$, and although this line lies near the edge of the filter at the cluster redshift, its effective wavelength corresponds to the peak sensitivity of the CCD. The presence of this line is common in deep spectroscopic field surveys (Koo 1988, Ellis 1987) and this line is often strong enough to distort the observed colours of galaxies (Tyson 1988). The sense of this change is to the upper right in Figure 5.5, *i.e.* redder in $B - R$ and bluer in $R - I$. This may be the cause of some of the noise in the diagram since evolution will tend to shift galaxies to the blue in both colours.

The other effect that this would have is to increase the signal in the R band relative to the 6300Å and 6800Å bands. Combined with the presence of [OIII] in the 9500Å filter this could restrict this combination of features to galaxies near the cluster redshift. However, this combination is rarely seen with the notable exception of 3C 217. Our confidence in the 9500Å filter drops rapidly with magnitude, partly because of the aforementioned reasons, and also because the wavelength of the 9500Å band is far enough away from the I filter that it can be difficult to distinguish between a continuum rise

and the presence of a weak emission line.

The radio galaxy 3C 217 is of particular interest since it is the only object of known redshift in the field. From its position in Figure 5.5, the galaxy has colours that resemble a late type spiral galaxy at low redshift. However, the SED shows emission in the 9500Å filter and both R and I fluxes higher than the narrow bands. The high I value is probably relative to metal and/or Balmer absorption in the 7500Å and 8100Å filters while the high R value is most likely from an [OII] emission line. The level of the R flux above the narrowband filters implies that this line may brighten R by ~ 0.4 mag, corresponding to a line strength of 1.3×10^{-15}ergs cm^{-2}s^{-1} which is high but still comparable to some radio galaxies that show strong [OII] emission. For example, the radio galaxy 3C 266 ($z = 1.27$) has an [OII] strength of 4.1×10^{-15}ergs cm^{-2}s^{-1} (Spinrad and Djorgovski 1984). This is several times greater than the implied line strength in 3C 217, even without correcting for the higher redshift of 3C 266. Removal of the [OII] contribution from the R mag would shift the position of 3C 217 in Figure 5.5 towards the lower right, *i.e.* towards the $z = 0.9$ locus.

Figure 5.5 plots the colours of the galaxies with $I \leq 21.6$; most of these galaxies appear to be foreground spiral galaxies with $z \leq 0.5$. Eight galaxies have colours or SED's that indicate potential cluster membership, and three of these are brighter than 3C 217. Galaxy 9 has an SED very similar to 3C 217 except for the absence of emission in the 9500Å filter. Galaxy 7 has an SED similar to the two dimmer galaxies, 18 and 19, all having colours indicative of cluster spiral galaxies. Galaxy 10 is somewhat bluer than these galaxies in $R - I$; however, the strength of the R band relative to the 6300Å and 6800Å filters indicates that the colours may be affected by the [OII] emission line. It does seem that these galaxies are likely to be

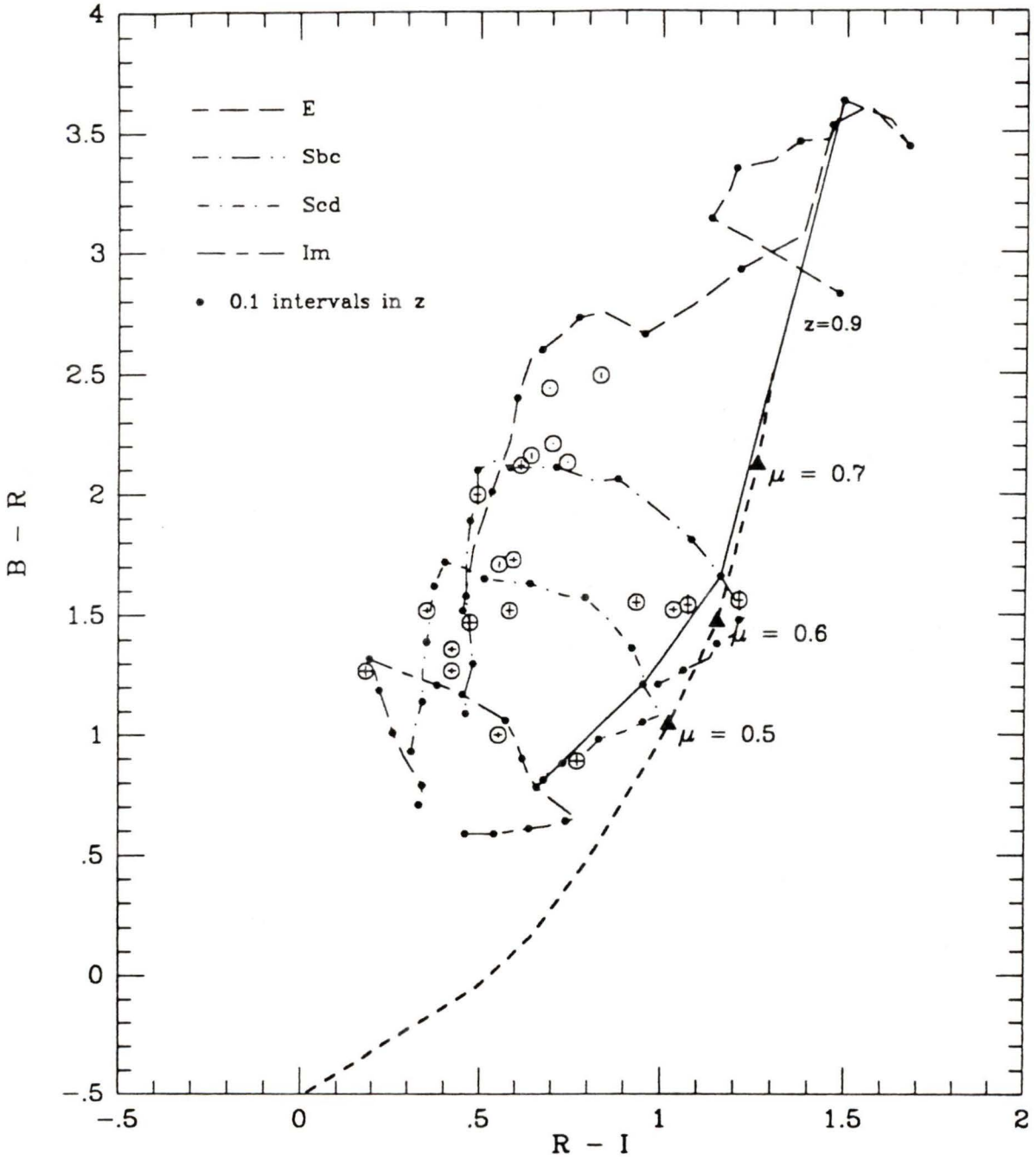

Figure 5.5: $B - R$ vs. $R - I$ for galaxies with $I < 21.6$. The broken lines are the redshifted colours for unevolving galaxies of the type indicated (Coleman *et al.*). The redshift range is $0.0 \leq z \leq 1.3$ and the colours move clockwise with increasing redshift. The solid line indicates the locus of $z = 0.9$ unevolving galaxies and the heavy dashed line indicates Bruzual's evolutionary models for galaxies at $z = 0.9$.

cluster members although they do appear unexpectedly luminous. Galaxy 17 has broadband colours similar to 3C 217 and appears to contain [OII] emission in the R band but lacks the strong signal in the 9500Å filter.

Figure 5.6 contains galaxies in the range $21.7 \leq I < 22.6$ corresponding to the beginning of the excess of galaxies found in the number counts. The field population in this panel tends towards later type spiral and irregular galaxies, and a few objects have colours that are too blue for normal galaxies in either one or both colours. Five galaxies appear to have colours matching normal cluster members, including galaxy 41 which has colours resembling an Sa or S0 galaxy. Galaxy 27 has an SED that shows some evidence of a break between R and I , with R raised above the narrow band flux, but again the 9500Å flux appears low.

The last three panels consist of the galaxies that appear in the I band N(m) diagram for the bins centered on 22.75, 23.00 and 23.25 (all of which show a significant excess over the expected field density). Unfortunately, the photometric uncertainty of these galaxies becomes a significant factor and the information available from the narrow band filters is greatly limited. The trend to bluer galaxies also makes it harder to determine cluster membership since any break between the R and I filters would be small and difficult to detect.

In Figure 5.7, only galaxies 56, 58 and 60 have normal cluster colours and galaxy 58 is the reddest cluster galaxy indicated thus far. 54 and 63 may also be potential members. Most of the galaxies have colours that are too blue to be normal systems at any redshift. Unlike Figure 5.6 where the galaxies tend to be too blue in $R - I$, this panel shows three galaxies that are blue in $B - R$. These galaxies have colours that fit better to Bruzual's model with $\mu > 0.5$ indicating high rates of star formation. Some additional blue

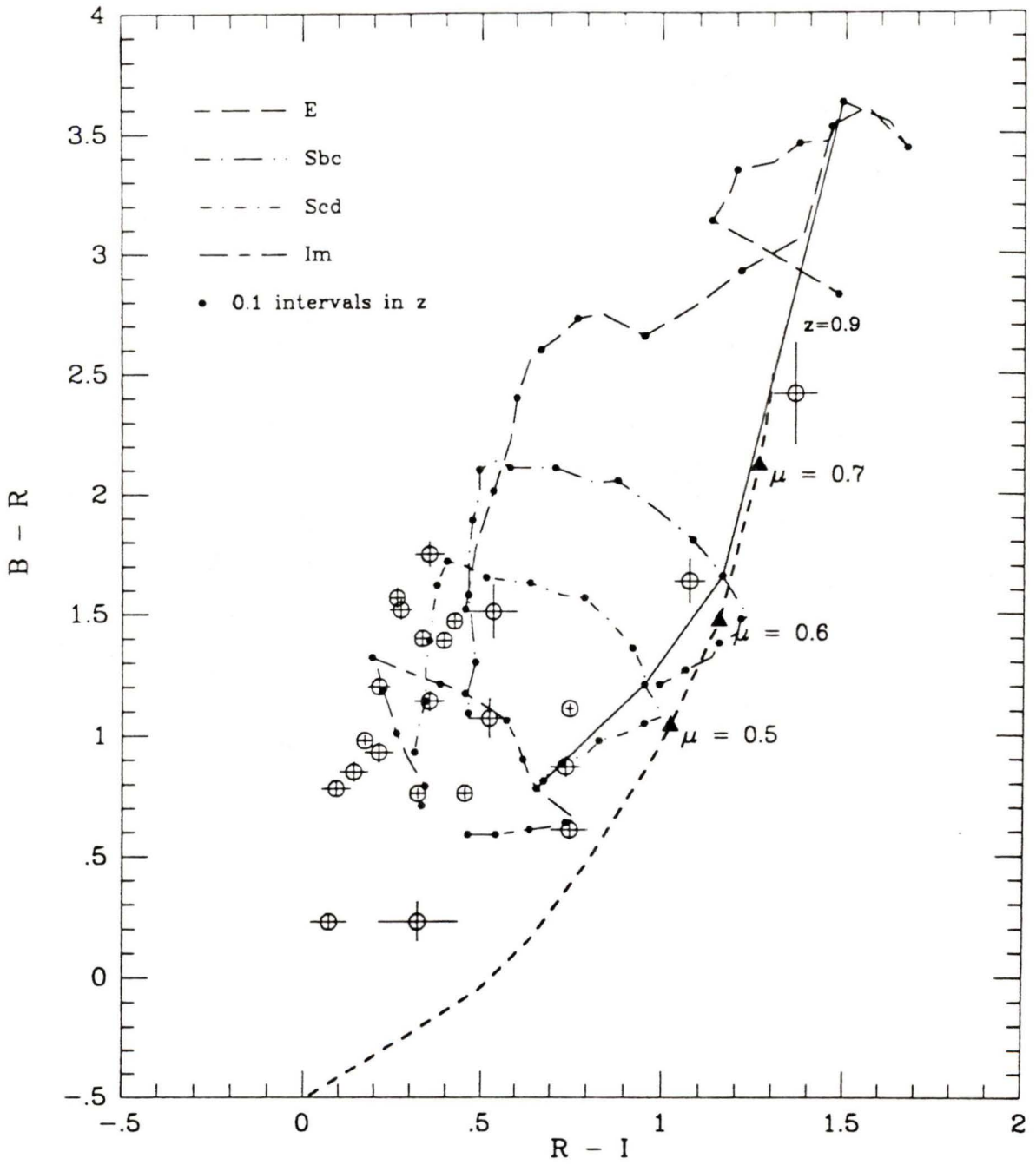

Figure 5.6: $B - R$ vs. $R - I$ for $21.7 < I < 22.6$. Symbols are the same as for Figure 5.5.

galaxies also appear to have SED's indicating cluster membership. Galaxies 46, 54 and 63 might be potential members but they lack evidence of [OII] emission that would explain their position above the $z = 0.9$ locus. Galaxy 48 is interesting for its flat $R - I$ colours and unusual SED.

Figure 5.8 shows an even greater tendency towards galaxies that are too blue in $B - R$. Many of these appear to be actively evolving systems with a high rate of star formation. Very few objects have normal cluster colours although galaxy 85 is the first galaxy with colours matching a cluster elliptical galaxy. Galaxies 70 and 83 are also potential members except that both lie more than 2σ from the locus. Galaxy 75 is unusual because of its extremely flat $R - I$ colour and high flux in the 9500Å filter.

Figure 5.9 shows a few more galaxies with normal cluster colours, galaxies 94, 100, 118, 119 and possibly 109 being potential cluster members. There is also an increase in the number of galaxies with flat $R - I$ colours although there are still many galaxies that are blue in $B - R$. Approximately one third of the galaxies appear to have a high flux through the 9500Å filter, although the uncertainty is high.

The high signal to noise ratio of the objects in Figures 5.5 and 5.6 allows us to estimate the fraction of cluster members. It would be difficult to distinguish between cluster galaxies and those at higher redshift; however the latter are not expected to be a significant contaminant at these magnitudes. From Tyson's absolute number densities, 17 ± 4 field galaxies are expected in Figure 5.5. Out of 21 galaxies in the panel, we estimate that there are 8 cluster members which leaves 13 field galaxies. This result agrees, given the errors, with the expected number of field galaxies.

In Figure 5.6, 24 field galaxies are expected, although we suspect that 7 of these are cluster members. Again, the numbers are probably consistent to

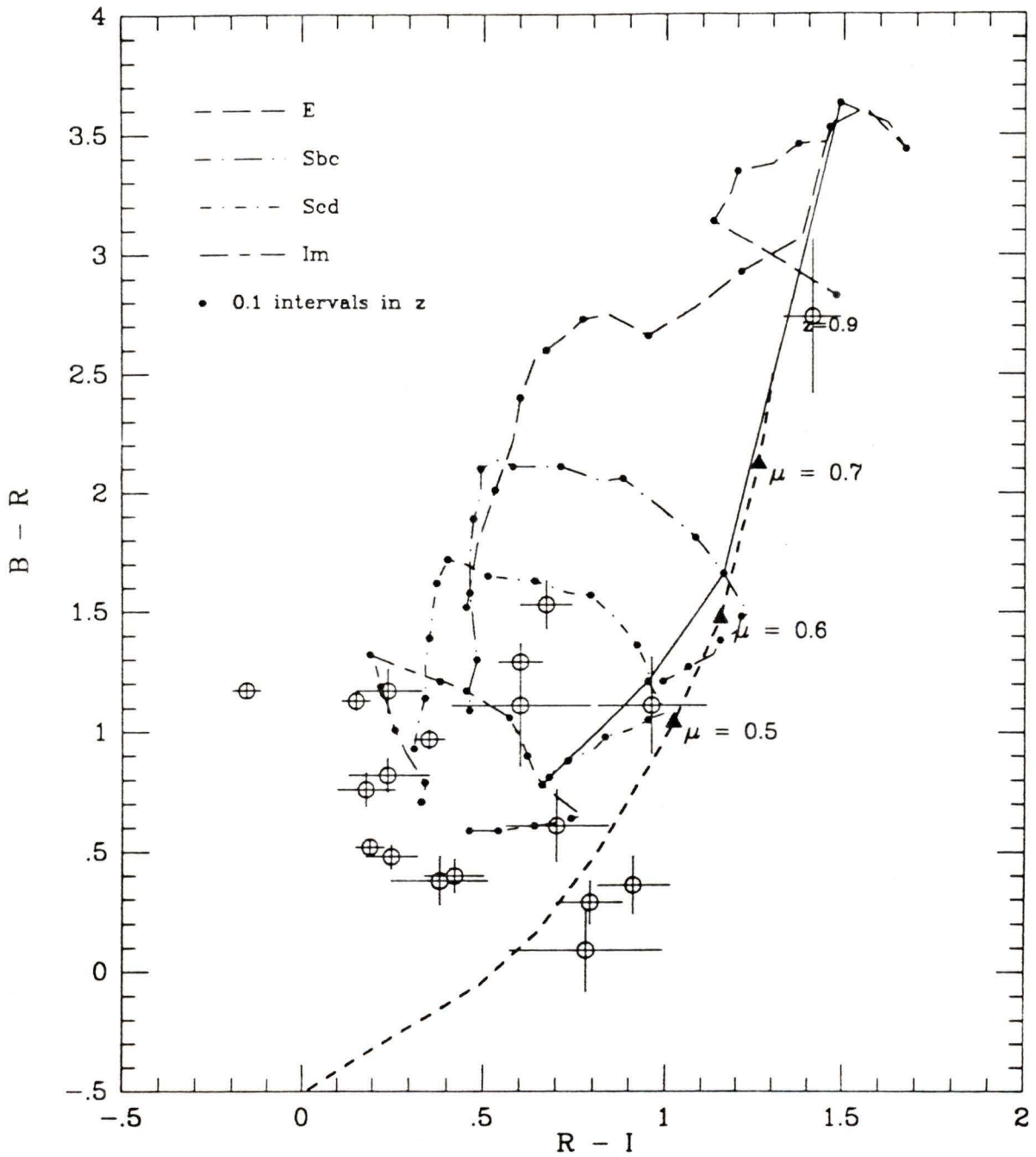

Figure 5.7: $B - R$ vs. $R - I$ for $22.6 < I < 22.9$. Symbols are the same as for Figure 5.5.

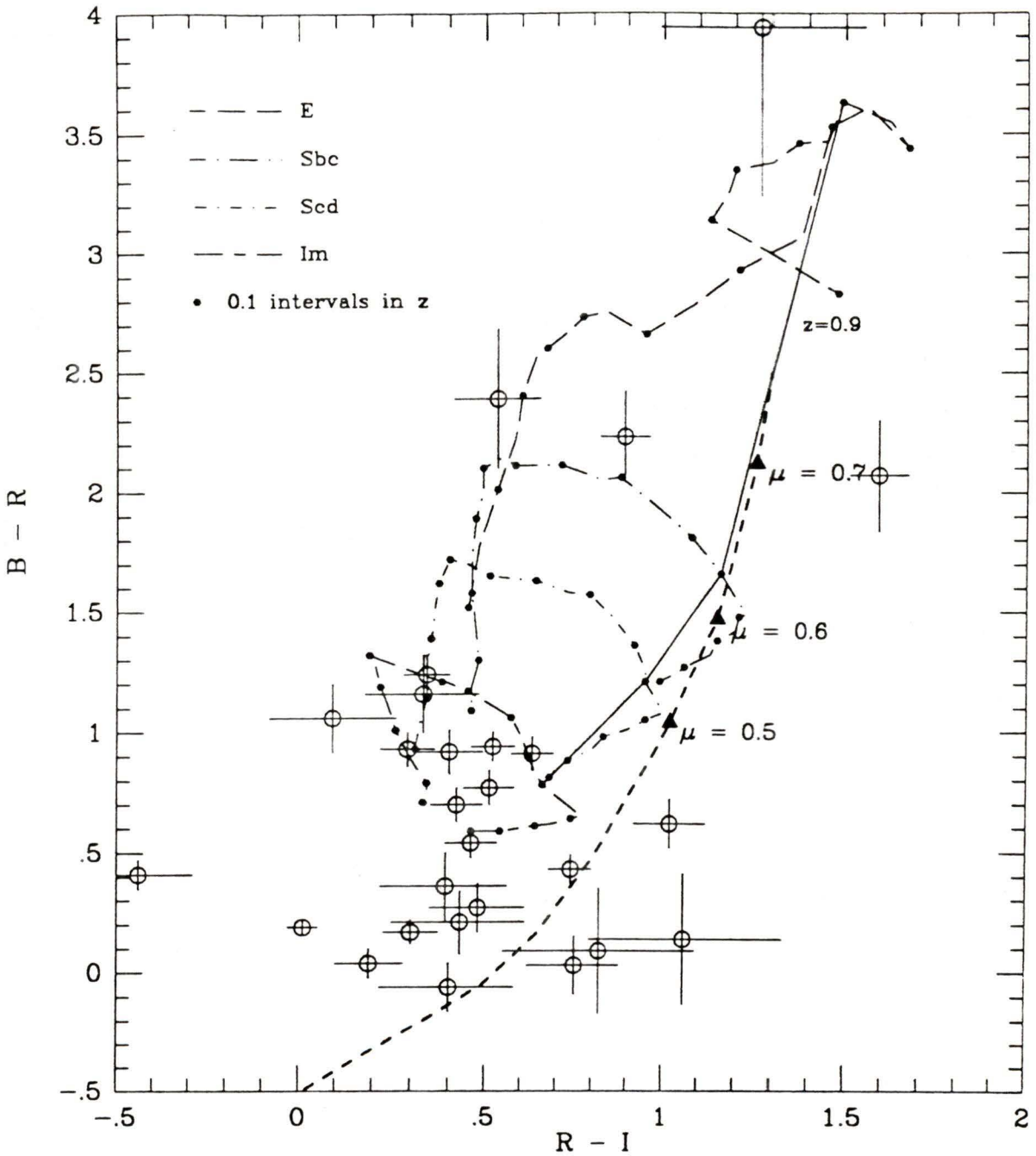

Figure 5.8: $B - R$ vs. $R - I$ for $22.9 < I < 23.2$. Symbols are the same as for Figure 5.5.

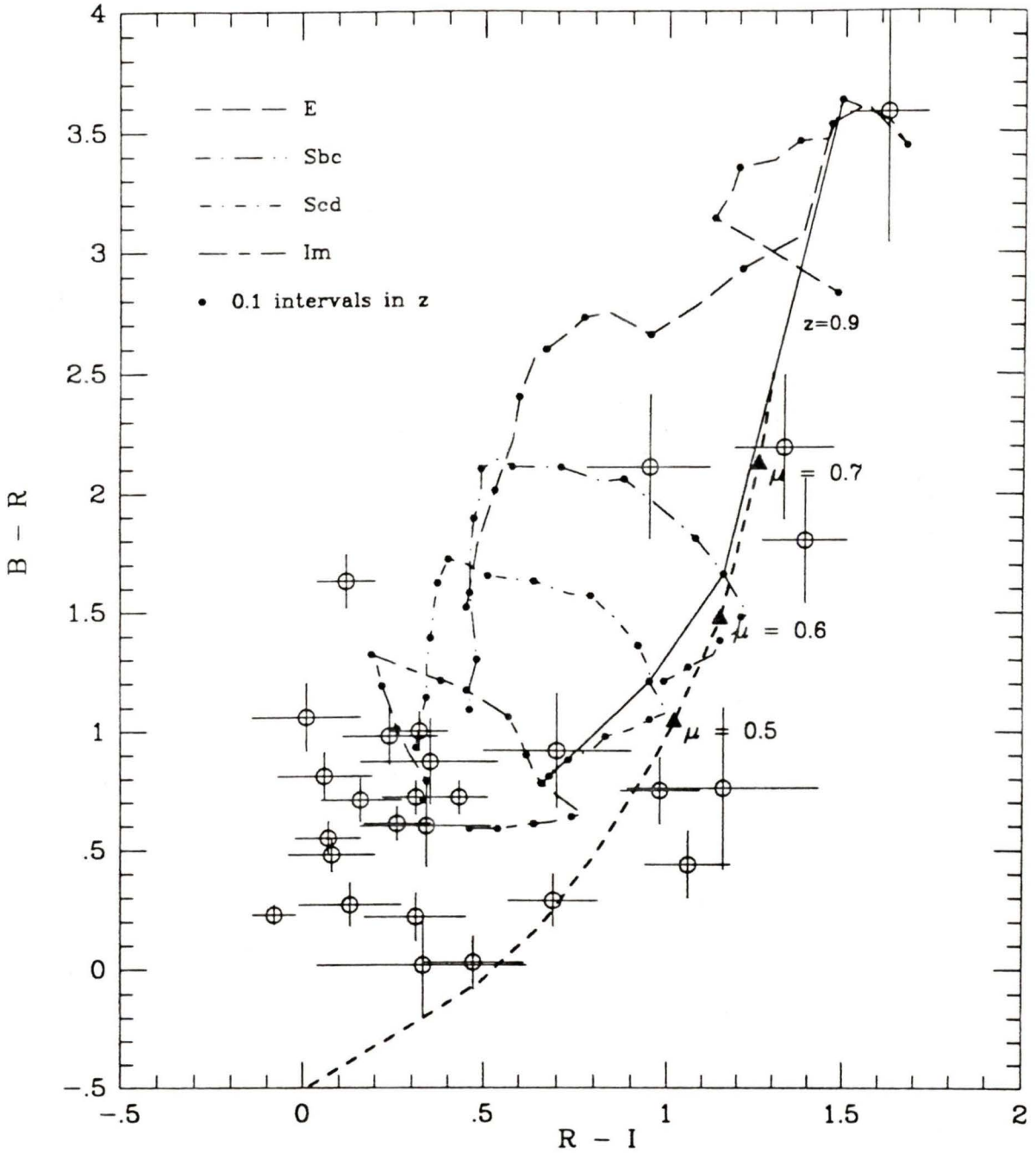

Figure 5.9: $B - R$ vs. $R - I$ for $23.2 < I < 23.5$. Symbols are the same as for Figure 5.5.

within the uncertainties. These numbers do appear to rule out the possibility that the excess counts at fainter magnitudes can be explained by shifting the zero point of Tyson's density normalization. A minimal 0.2 dex shift implies 27 and 38 field galaxies in Figures 5.5 and 5.6 respectively, which does not appear compatible with our estimates of the field in these panels.

The field content for the sample, as estimated from the colours, is shown in Figure 5.10. This shows the bright end of the field content to be somewhat low in comparison with Tyson's field counts. However, at these magnitudes uncertainties in the colours are typically ± 0.05 mag and the SED's are extremely helpful in making identifications, *i.e.* the broadband colours of 3C 217 would classify it as having the colours of a field spiral galaxy.

The three faintest bins, corresponding to Figures 5.7-5.9, have a relatively higher field content. This may be real or it may be the result of our inability to distinguish blue cluster galaxies because of the poorer S/N in both the broadband and narrowband filters. In particular, the effect of the [OII] line on the R flux becomes indistinguishable as the noise in the narrowband filters increases. Although this may result in a few cluster galaxies being assigned to the field, we are confident that the field content has been adequately determined and it appears unlikely to have been underestimated.

5.5 Missing Galaxies

The selection of the sample required that the galaxies be detected in R in addition to satisfying the magnitude limit imposed in I . This was because we required the galaxies to have a well determined value of $R - I$; the simulations allowed us to determine the weighting of the galaxies based on this colour. However, as noted in Section 5.2, the requirement that the galaxies

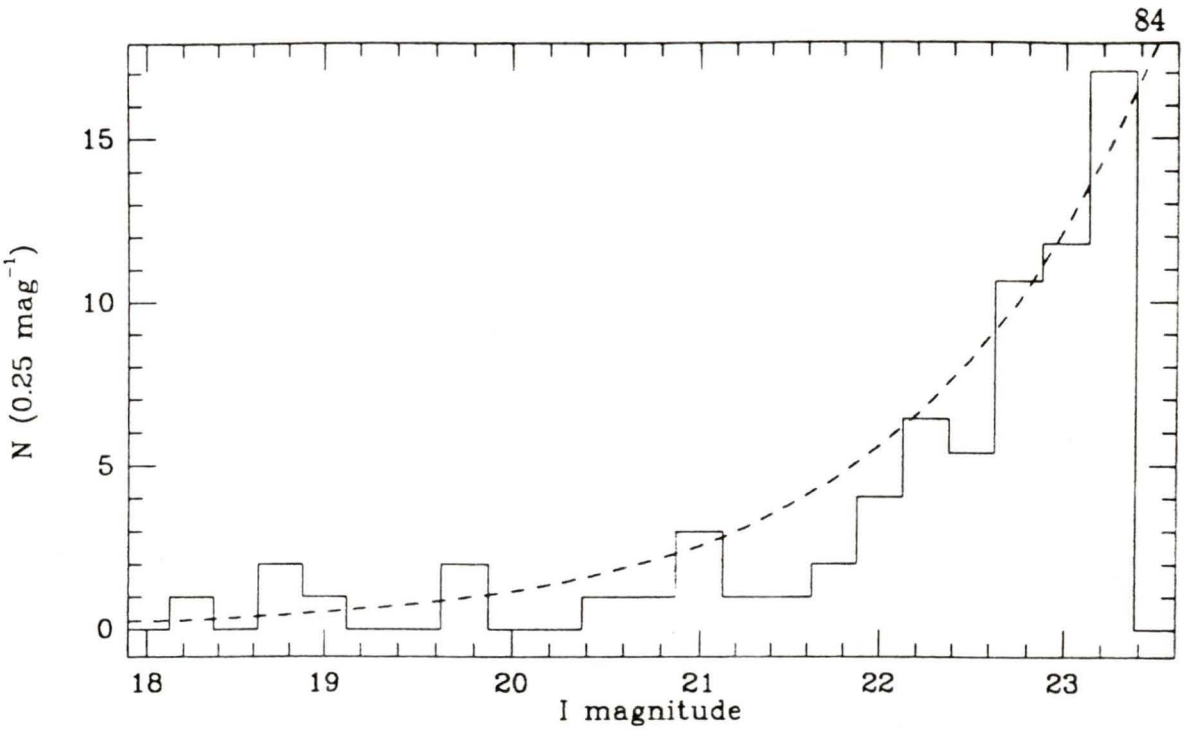

Figure 5.10: Field galaxies with $I < 23.5$. Tyson's field counts are shown as the dashed curve.

be detected in R produces a stronger selection effect on the distribution than accounted for by the simulations. The sense of the selection primarily affects galaxies with large $R - I$ colours, and elliptical galaxies at the cluster redshift are very red. Therefore, it is critical that we investigate those galaxies that are only detected in the I band to avoid the possibility of overestimating the evolution in the cluster. However, it does not seem that these galaxies would have strong selection effects against them in I since the all the objects have a S/N $\geq 5:1$. Therefore we can be reasonably certain that the sample in I is complete.

Of the 190 galaxies with $I < 23.5$, 70 are not detected in R . Most of these galaxies are quite faint; 60 have I magnitudes that would place them in the final two magnitude bins. Not all of these would need to be detected to account for the discrepancy between the matched counts and the I counts,

since the weighting for the matched counts is naturally higher. The *weighted* difference between the two number counts is $\sim$ 55 galaxies, most of which is attributable to the final two bins. Somewhat fewer galaxies actually need to be detected, although the exact number depends on the their magnitude and colour.

In order to determine colours for these objects (or at least upper limits), we performed aperture photometry on the B and R frames using the position of the galaxy in the I frame as the input position. The photometry routine was then allowed to iterate until a stable centroid was found. If a stable centroid could not found within one seeing disk of the input position, the aperture was fixed at the input position. We were able to obtain a S/N $\geq 3:1$ for 27 galaxies in $R-I$. Of these, only one object has an $R-I$ colour red enough to be a cluster elliptical galaxy. The remainder have colours compatible with the galaxies seen in Figures 5.7-5.9.

The size of the galaxies appears to be an important consideration in determining whether they are detected in both filters. Figure 5.11 diplays the r_{-2} value for the entire sample of galaxies with $I < 23.5$. The galaxies that are not found in R are shown to be much less compact and presumably have lower surface brightness than the majority of galaxies that are found in both filters. However, it is not readily apparent if these galaxies are not found in both filters because they are extended, or if they represent a population of extended galaxies that are not found in R because of their red colour.

Since these are low surface brightness objects, the calculation of centroid position is more susceptible to noise or other factors which could result in computed centroids for different filters that lie outside the matching radius. Increasing the matching radius radius by 1 pixel results in finding counterparts for 9 of the 70 galaxies from the existing R detection lists. All but one

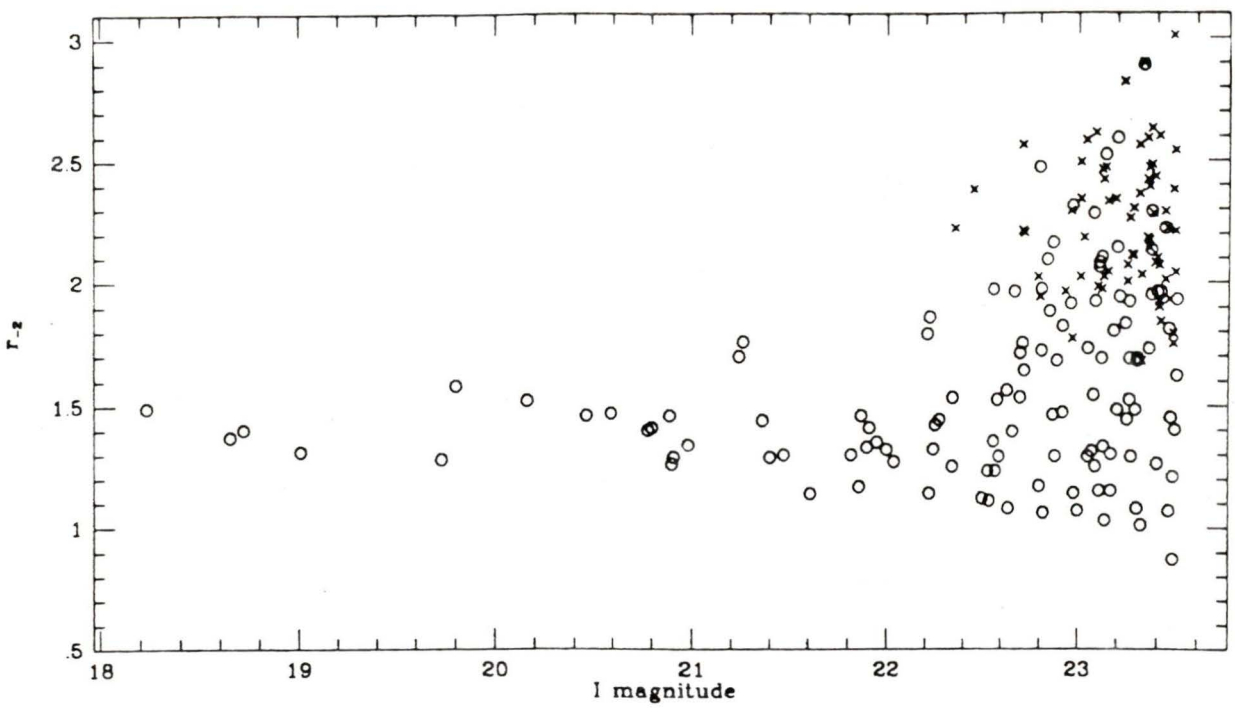

Figure 5.11: r_{-2} vs. I for galaxies with $I < 23.5$. The circles represent galaxies detected in both R and I, crosses are galaxies detected only in I.

of these have colours with good signal to noise using the photometry scheme described above, suggesting that most of the matches are real. Increasing the matching radius still further produces more matches but the fraction of spurious matches will also increase.

In the simulations, measuring colours requires that the objects are not only detected in both filters but also have centroid positions within the matching radius. For galaxies that are bright in I with flat $R - I$ colours, the matching criterion is the major source of incompleteness since the objects are close to complete in the individual filters. For the objects that are found only in I, the majority that have estimated colours with good S/N are fairly flat in $R - I$ and it appears that most of them can be accounted for by the weighting applied to the matched objects. Also, the bulk of the single filter objects have $R - I$ colours with poor S/N, or simply upper limits. This in-

dicates that there are more red galaxies than are represented in the matched filter objects

In some cases, the centroid position is the critical factor, but this factor alone is insufficient to explain the discrepancy in the counts. A further consideration is that at high redshifts, the angular size of galaxies increases as $(1+z)^2$ while surface brightness dims by $(1+z)^{-4}$. Therefore, we expect the cluster galaxies to show greater extension and lower surface brightness than the closer field galaxies. Simulations by Infante (1987) suggest that by $z = 0.9$, the low surface brightness of elliptical galaxies would render them difficult to detect. Hence, not only are there selection effects against cluster elliptical galaxies because of their colour, but also because of their low surface brightness at high z.

For the above reasons, cluster elliptical galaxies are expected to be difficult to detect in any filter other than I. However, since these galaxies should have a $B - I \sim 5$, the measurement of a significant signal in B would rule out the galaxy as a cluster elliptical. In order to estimate how many elliptical galaxies are in this sample, we adopt the criterion that the objects have a 3σ lower limit consistent with their expected B mag. We also require that the $R - I$ colour be within 3σ of the expected value. This produces a list of 41 galaxies that would qualify as clusters ellipticals. If these galaxies have been "unfairly" discriminated against because of their low surface brightness, their inclusion in the sample would easily account for the discrepancy in the number counts once the weighting is applied.

In the main sample, only two galaxies have colours resembling those expected for cluster elliptical galaxies ; both are quite faint ($I = 23.14, 23.30$) and they have large uncertainties in their $B - R$ colour. If the above criteria were applied to this sample, an additional four galaxies would be classified as

elliptical. Since all of these galaxies have colours matching early type cluster members, the criterion appears to provide an acceptable limit for red cluster galaxies. However it is clear that there are many times more red galaxies found only in I than are represented by these six galaxies (even after applying the weighting).

There is still the question of how many of the "missing" galaxies are cluster elliptical galaxies. On the one hand, because of their red colours and low surface brightness, the selection effects will be more severe for cluster elliptical galaxies than for other galaxies. On the other hand, all of the galaxies that are not found in R have fairly high values of r_{-2}, and from the strength of the distribution in Figure 5.11, it appears that compactness is the determining factor independent of the colour. However, the fraction of objects that are estimated to have fairly flat $R - I$ colours, resembling bluer cluster members or field objects, are well represented in the main sample and their lack of detection in both filters is accounted for by the applied weighting. It is only the redder galaxies that appear to be severely under-represented in the main sample and hence the implication is that the discrepancy in the number counts is entirely due to a population of elliptical galaxies.

5.6 Luminosity Evolution

For the objects that show colours similar to those expected for cluster members, we could determine the absolute magnitudes in a fairly straightforward manner by applying the K correction in the I band for the perceived galaxy type. However, a more general approach can be made by translating the I mag at $z = 0.9$ directly into a rest frame B mag. Since the effective wavelengths are closely matched, this provides a weaker dependence on galaxy

type (*i.e.* colour). The following relationship was estimated using the redshifted Coleman *et al.* SED's,

$$M_{B_0} = I \ - 0.37(R - I) + 1.45 - 5\log d_L \tag{5.1}$$

where d_L is the luminosity distance given by equation 4.1 (p. 50). The advantage is that there is only 0.3 mag difference between the corrections for E and Im type galaxies whereas the difference in I band K corrections is about 1.2 mag.

Using the above relation, the observed brightness of 3C 217 corresponds to an absolute restframe magnitude of $M_{B_0} = -20.8$. The removal of 0.4 mag from the R band (due to the [OII] contribution), results in colours that indicate a star formation rate of order $\mu = 0.5$ according the Bruzual's models. Sandage's (1973) mean brightest cluster elliptical galaxy, for $H_0 =$ 100 km s^{-1}Mpc^{-1}, has an absolute restframe magnitude of $M_{B_0} = -20.9 \pm 0.4$ (rms). Although the absolute magnitude of 3C 217 is comparable to this value, Bruzual indicates that star formation in the $\mu = 0.5$ model contributes $\sim$ 1.0 mag to the luminosity. This means that by the present epoch, 3C 217 will be dimmer than Sandage's value for the brightest cluster elliptical galaxy. The difference might be made up for by galaxy mergers that occur during the time since the light that we observe left 3C 217 ($\sim$ 60% of the age of the Universe).

The three galaxies (7, 9 and 10) that are brighter than 3C 217 have absolute restframe magnitudes of $M_{B_0} = -21.73$, -21.12 and -21.07 respectively, and colours resembling those of spiral galaxies at the cluster redshift. NGC 4321 has been considered typical of the brightest cluster spiral (Coleman *et al.* 1980) with an absolute restframe magnitude of $M_{B_0} = -20.1$. This rules out the possibility that these three bright galaxies are spiral because of the

strong luminosity evolution required. They are more likely to be elliptical galaxies undergoing evolution both in luminosity and in colour, with star formation rates corresponding to a Bruzual model of $\mu = 0.5$-0.6. These galaxies also do not require any further luminosity enhancement from mergers to retain their status as brightest cluster members.

Aside from the luminosity of these galaxies, the other curious feature is their tight spatial grouping; all three are located within a circle of radius $15''$, or ~ 80 kpc at the cluster redshift. Furthermore, this group is located towards the edge of the field, about 600 kpc away from 3C 217. One possible scenario is that these galaxies form a subcluster on the edge of the main cluster. Over time, the three galaxies will become less luminous as their gas reserves are exhausted and star formation ceases, whereas 3C 217 may continue to increase in luminosity, being resupplied with fresh gas and perhaps entire galaxies, by virtue of its position at the cluster centre.

The other possibility is that these three galaxies, and not 3C 217, are at the cluster centre and galaxy 7 is the brightest cluster member. When a cluster possesses a powerful radio source, and either contains a single optically dominant galaxy or shows a strong central concentration, the brightest member is normally the radio source (Riley 1975). Neither of these conditions is in evidence in this case, but further observations of the surrounding fields would be required to establish the centroid and orientation of the cluster. Spectroscopic observations would also be required to confirm that these three bright galaxies are cluster members.

Luminosity evolution is implied for the brightest cluster members simply because of their bright absolute magnitudes. This may also be the case for several of the lower rank, blue members ($I \leq 22.5$), but these galaxies are not bright enough to require luminosity evolution using the above arguments.

The colour of these galaxies also appears closer to that of the non-evolving sequence of Coleman *et al.* (1980) than the evolving sequence of Bruzual. However, this may be in part due to the effects of an [OII] emission in the R band, which would tend to shift galaxies up above the evolutionary sequence. This is certainly the case for the brightest galaxies.

The most luminous galaxies that clearly lie along Bruzual's evolutionary sequence (corresponding to $\mu \sim 0.4$) have absolute restframe magnitudes of $M_{B_0} \approx -19.1$. In contrast, the brightest red galaxy in the sample has $M_{B_0} = -19.5$ and the faintest red galaxy in the sample has $M_{B_0} = -18.7$. Therefore, in a restframe B magnitude system, these evolving galaxies are not overly bright considering that the implied star formation rates would increase their luminosity by over 1 mag.

The brightest red galaxy in the sample has an absolute magnitude near the bright end of luminosity function for early type galaxies determined for the Virgo cluster (Binggeli *et al.* 1988). At the magnitude of the faintest red galaxy, the luminosity function for Virgo elliptical galaxies still continues to rise although the luminosity function for Virgo S0's and early type spiral galaxies is very close to the peak. This is of some interest since fainter than the limit of this sample ($I = 23.5$), the number counts begin to decrease. However, our counts drop much faster than the S0 luminosity function and hence the more likely explanation is that early type galaxies have a brighter completeness limit because of their low surface brightness (Koo 1986).

5.7 Colour Evolution

In order to determine the extent of evolution, we divide the galaxies into red and blue populations. The blue portion is defined as those galaxies with

colours bluer than the redshifted colours of an Sbc galaxy. The Butcher and Oemler (1984) definition of blue galaxies corresponds to galaxies with restframe $B - V \leq 0.7$. Our definition is roughly consistent since Sbc galaxies have a restframe colour of $B - V = 0.6$, the difference having no effect on the sample selection. On the other hand, it is clear that the cutoff should be no bluer since the two brightest cluster galaxies have Sbc colours and show evidence of luminosity evolution which presumably also affects their colour.

A few of the redder objects found in both filters lie in the red sample but most of the red sample consists of galaxies that were found only in the I filter. These were the galaxies that had upper limits on their colours that matched the selection criterion for elliptical galaxies. Not all of these red galaxies were required and the galaxies were chosen by tightening the selection criterion until there were enough galaxies to account for the discrepancy in the number counts - *i.e.* adding these galaxies to the matched filter number counts yielded approximately the same value as for the single filter counts. Since most of these galaxies lack good colour information, an average colour of $R - I = 1.4$ was adopted in calculating their weighting and absolute magnitude. This is slightly bluer (0.1 mag) than cluster elliptical galaxies in order to reflect a mix of E and S0 galaxies.

Figure 5.12 shows the magnitude distribution for the entire cluster sample. Determining the evolution from apparent I magnitude would result in a blue fraction of $\sim 50\%$. In order to compare these observations directly with those of Butcher and Oemler (1984), we need to transform the I magnitude into a restframe V. The relationship was estimated as

$$M_{V_0} = I \ - 1.10(R - I) + 1.58 - 5\log d_L \tag{5.2}$$

using the approach in the previous section although the dependence on the

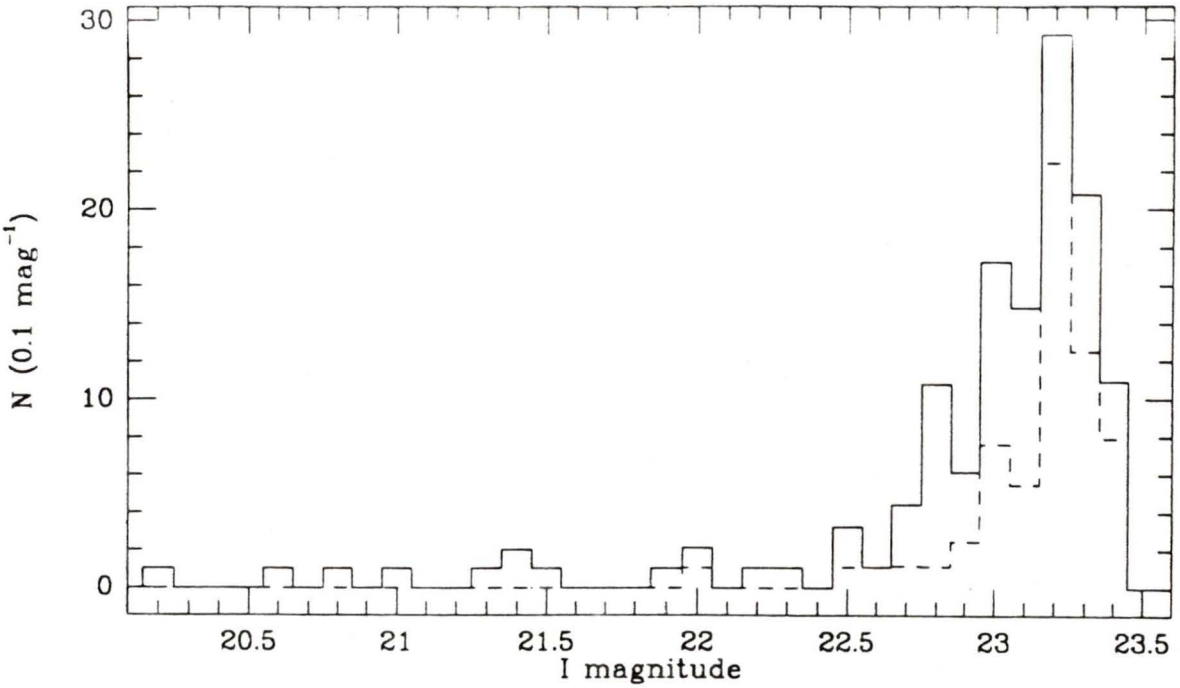

Figure 5.12: Number of cluster galaxies as a function of I . The solid line indicates the entire cluster sample, the dashed line is the red population.

colour term is much stronger.

Figure 5.13 shows the magnitude distribution as a function of absolute V magnitude. The strength of the K corrections for the red sample is immediately apparent whereas many of the evolving galaxies have small K corrections and appear relatively dimmer. The blue fraction is determined from the galaxies with $M_{V_0} \leq -18.4$ since this the last bin that contains a red population that is complete. This results is a blue fraction of 0.26 ± 0.06. The uncertainty represents the range provided by the uncertainty in the actual colour of of the red population and the standard deviation in the $R-I$ dependence of the V transformation.

This value is comparable to that seen in the highest redshift BO clusters but appears incompatible with the formal extension of the Butcher-Oemler effect out to higher redshifts. BO (1984) claim an increase in the fraction

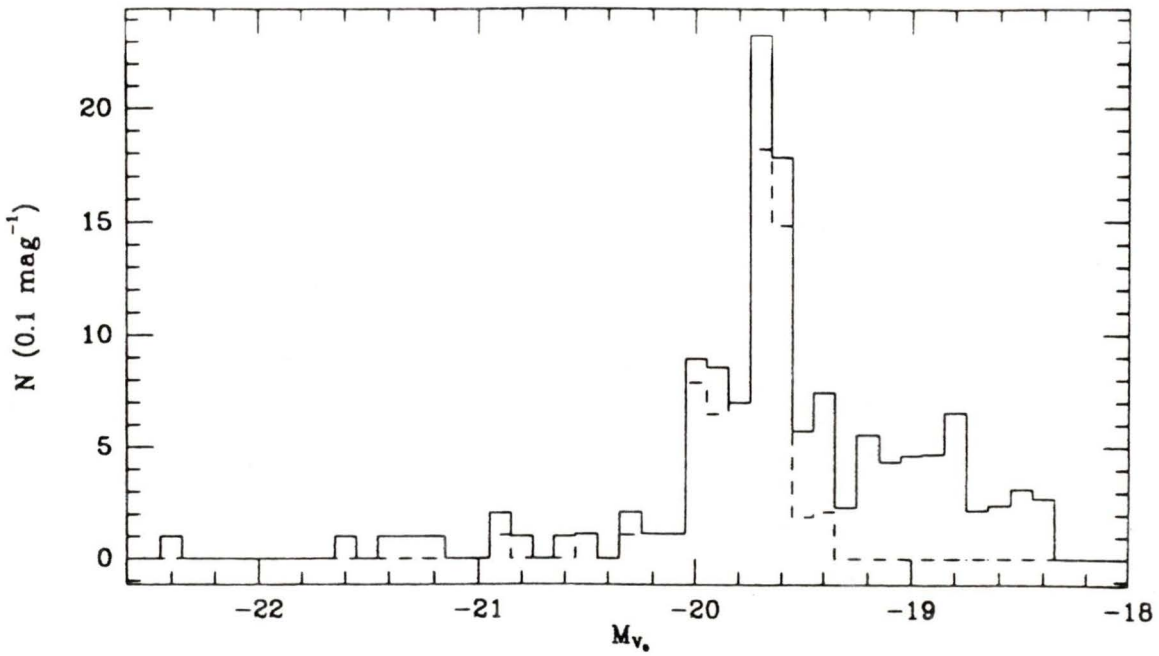

Figure 5.13: Number of cluster galaxies as a function of M_{V_0}. The solid line indicates the entire cluster sample, the dashed line indicates the red population. The sample is incomplete beyond $M_{V_0} = 18.4$.

of blue galaxies in clusters from 0.03 locally to 0.25 by $z = 0.5$. Hence we would expect to see a blue fraction of 0.40 by $z = 0.9$.

There are several possible explanations for this discrepancy. The largest source of potential error is in the determination of the red population. There are several strong arguments which support the assumption that galaxies found only in I are in fact cluster elliptical galaxies, but there is no substitute for good data. Additional observations $\sim$ 1.0 mag deeper in R , or alternatively, observations in a longer wavelength filter, would be required to confirm the nature of this population.

Differences in the sampling might also result in changes in the observed blue fraction. BO (1984) clusters were surveyed out to a radius of 3.0 Mpc whereas our sample covers an area corresponding to a radius of only about 0.5

Mpc. Since early type galaxies tend to have a higher concentration towards the cluster centre, our small sample area may survey only the portion of the cluster with the richest population of elliptical galaxies . However, the final BO samples are chosen from a smaller radius (based on the number density profile), typically $1 - 2'$ for clusters with $z \geq 0.3$. The corresponding metric sizes are actually smaller than our surveyed area and hence this may actually cause us to observe too many blue galaxies.

Another difference in our sample is that our limiting absolute magnitude is $M_{V_0} \approx -19.4$ (corresponding to the limit of the red population), whereas the limit used by BO is a magnitude fainter at $M_{V_0} = -18.5$. This might perhaps cause us to detect too many red galaxies, but in fact the opposite will occur. Models (*e.g.* Bruzual 1981) predict that evolution in luminosity will accompany, and dominate, evolution in colour, so that a brighter cutoff would result in the inclusion of relatively more evolving galaxies. For our sample, a limiting magnitude 0.7 mag brighter ($M_{V_0} = -20.1$), would result in an increase in the blue fraction of $\approx 70\%$.

It appears that sample differences cannot be responsible for our low fraction of blue galaxies. Therefore, if our identification of the population of elliptical galaxies is essentially correct, the low blue fraction implies that evolution will not become dominant among cluster members until redshifts $z \geq 2$. Another interpretation is that since the blue fraction is very similar to that seen in the highest redshift BO clusters, it is possible that evolution increases only out to $z \leq 0.5$, but remains fairly constant at higher redshifts. However, this only a single cluster and there is easily enough scatter among the Butcher-Oemler clusters to allow for some red clusters at high redshift (*e.g.* Cl 0016+16). The true situation can be clarified only by observations of other high redshift clusters.

Chapter 6

Conclusion

There is little doubt that this study reveals the existence of a cluster at a redshift of $z = 0.9$, despite the lack of central condensation. The only obvious clues are the presence of 3C 217 and an overall number density enhancement of a factor of ~ 2 over the field. However, the N(m) diagrams for all three broadband filters show an increase in counts that is steeper than Euclidean and a peak excess well above that predicted for a field sample. The excess counts are also shown to increase in both size and slope at longer wavelengths, opposite to what is observed in the field. These features can be understood in terms of the wavelength dependence of the K corrections for a distant cluster of galaxies.

A Schechter function provides a good fit to the excess counts in B and R . These were determined to have characteristic luminosities of $M_B{}^* = -19.9 \pm 0.5$ and $M_R{}^* = -20.2 \pm 0.4$ after applying distance and K corrections corresponding to $z = 0.9$. These values of M^* are in good agreement with published values, further supporting the existence of a cluster, although the uncertainty in applying a single K correction to a population of galaxies

does not allow stronger conclusions to be drawn. The I band data do not provide as good a fit, despite smaller K corrections, and the best fit appears to require that large numbers of faint galaxies go undetected.

For galaxies that are detected in two filters, the number counts show that the B and R filters contain roughly comparable populations since the counts remain virtually unchanged from those in the individual filters. However, the number counts of galaxies detected (and matched) in both R and I show a large reduction compared with the counts determined from individual filters, suggesting that these filters are sensitive to different galaxy populations. The I band suffers the least from K dimming and hence will be more sensitive to early type galaxies at the cluster redshift. Of the galaxies not found in I , many have blue $B - R$ colour suggesting a population of flat spectrum objects that are simply too faint to be seen in I .

Once the presence of the cluster was established, an investigation of evolution was undertaken. In order to distinguish between field and cluster galaxies, the expected colour of galaxies in the $B - R$ vs. $R - I$ plane was determined for the redshift range $0.0 \leq z \leq 1.3$ using the spectral energy distributions from Coleman *et al.* (1980). Since these colours neglect the effects of evolution, the colours corresponding to evolutionary models at $z = 0.9$ were also determined (Bruzual 1981). Spectral energy distributions using the broadband and narrowband fluxes were also compared to those of Coleman *et al.* to aid in identification.

The predicted colours were then compared with the colours observed for a sample of galaxies with $I < 23.5$. Despite the high field contamination, removal of the field content appeared fairly straightforward for all but the faintest, bluest galaxies. The number of field galaxies based strictly on colour showed good agreement with the field counts observed by Tyson (1988).

Although field contamination was one of the major problems in the original Butcher-Oemler work (1978), the use of two colour indices and the fact that the cluster is at high redshift (and hence the colours are well separated from the majority of field objects) rendered this somewhat less of a concern.

The majority of cluster galaxies found by this method have fairly blue colours and evolution among them is strongly indicated. However, more than a third of galaxies in the sample were detected only in I and these galaxies possess large angular sizes in addition to apparently red colours, as would be expected for cluster elliptical galaxies. Ignoring these galaxies would lead to an overestimate of the fraction of blue galaxies in the sample. A sample of the red galaxies was taken based on the discrepancy seen in the number counts and this was added to the main sample.

The entire sample was divided into red and blue populations using a blue criterion equivalent to that used by Butcher and Oemler (1984). Transforming the sample to the absolute V magnitude system resulted in considerable brightening of the red population relative to the blue. From this we determined the blue fraction of $f_B = 0.26 \pm 0.06$. This does not appear to be consistent with the $f_B = 0.40$ expected from the formal extension of the Butcher-Oemler effect out a redshift of $z = 0.9$. Our value for the blue fraction suggests less evolution over the last 50% of the age of the Universe, and requires the bulk of galaxy evolution to have occurred at redshifts ≥ 2.

This result remains somewhat tentative because of the indirect method used for determining the population of elliptical galaxies. However, if the population of elliptical galaxies has been correctly determined, other interpretations are still possible. Our value of the the blue fraction is similar to that found in the bluer, high redshift clusters in the BO (1984) sample. This could imply that evolution remains fairly constant in the range $0.5 \leq z \leq 0.9$

and drops off only at redshifts of $z \leq 0.5$. However, these observations are of a single cluster and there is easily enough scatter in the BO sample to allow for some red clusters at high redshifts. Deeper observations are required to confirm the red population in this cluster and observations of other high redshift clusters are required before any clear trends can be established. These observations are certainly within the limits of existing ground based telescopes and would represent a significant increase in the lookback time over which the evolution in clusters has been observed.

Spectroscopy of several of the cluster candidates is also required to confirm their redshift. The observations of the brightest galaxies in the high redshift BO clusters yielded several unusual E+A galaxies that are not represented locally. There may be other previously undetected galaxy types waiting at even higher redshifts. A decade ago, fewer than a dozen galaxies with redshifts of $z \geq 0.5$ were known, most of which were powerful radio galaxies. The situation today is much improved but radio galaxies still dominate the high redshift sample. Since these galaxies are obviously peculiar, their spectral evolution may be very different from the large majority of galaxies. With the small size of this field, multi-aperture spectroscopy could be used obtain spectra for many of the cluster candidates in a single frame, justifying the large amount of telescope time required for objects of this magnitude. This would yield important information on the spectral evolution of normal galaxies at high redshift. It may also be possible to measure the velocity dispersion of the cluster and to test Cold Dark Matter theories which predict cluster formation should occur at $z \leq 1.0$.

The next generation of telescopes, detectors and spectrographs will surely allow astronomers to study clusters of galaxies at redshifts $z = 1$ or even greater, in addition to the clusters at $z \sim 0.5$ that are currently known.

Each foray out to greater distances and lookback times widens the range over which we observe the evolution of galaxies and brings us closer to the epoch of galaxy formation.

REFERENCES

Bessell, M.S., 1979, *Pub.A.S.P.*, **91**, 589.

Binggeli, B., Sandage, A., and Tammann, G.A., 1988, *Ann. Rev. Astr. Ap.*, **26**, 509.

Bruzual, G., 1981, Ph.D. Thesis, University of California, Berkeley.

Broadhurst, T.J., Ellis, R.S., Koo, D.C., and Szalay, A.S., 1990, *Nature*, **343**, 726.

Butcher, H., and Oemler, A., 1978, *Ap.J.*, **219**, 18.

Butcher, H., and Oemler, A., 1984, *Ap.J.*, **285**, 426.

Cappi, A., Chincarini, G., Conconi, P., and Vettolani, G., 1989, *Astr. Ap.*, **223**, 1.

Coleman, G.D., Wu, C., and Weedman, D.W., 1980, *Ap.J. Suppl.*, **43**, 393.

Couch, W.J., Ellis, R.S., Carter, D., and Godwin, J., 1983, *M.N.R.A.S.*, **205**, 1287.

Dressler, A. and Gunn, J.E., 1982, *Ap.J.*, **263**, 533.

Dressler, A. and Gunn, J.E., 1983, *Ap.J.*, **270**, 7.

Dressler, A., 1986, in *Spectral Evolution of Galaxies*, ed. C. Chiosi and A.

Renzini (Dordrecht:Reidel), p. 375.

Ellis, R.S., 1987, in *IAU Symposium No. 124, Observational Cosmology* , ed. A. Hewitt, G. Burbidge, and L.Z. Fang (Dordrecht:Reidel), p. 367.

Felten, J.E., 1985, *Comments Ap.*, **11**, 53.

Gunn, J.E., and Stryker, L.L., 1983, *Ap.J. Suppl.*, **52**,121.

Hall, P., and McKay, C.D., 1984, *M.N.R.A.S.*, **210**,979.

Hubble, E., 1936, *Realm of the Nebulae*, Yale University Press.

Infante, L., 1985, MSc. Thesis, University of Victoria, Victoria.

Infante, L., 1987, *Astr. Ap.*, **183**,177.

Infante, L., Pritchet, C.J., and Quintana, H. 1986 *A.J.*, **91**, 217.

Jarvis, J.F., and Tyson, J.A. , 1981, *A.J.*, **86**, 476.

Kirshner, R.P., Oemler, A., Schechter, P.L., and Shectman, S.A., 1983, *A.J.*, **88**, 1285.

Koo, D.C., 1981, Ph.D. Thesis, University of California, Berkeley.

Koo, D.C., 1985, *A.J.*, **90**, 418.

Koo, D.C., 1986, *Ap.J.*, **311**, 651.

Koo, D.C., 1988, in *Towards Understanding Galaxies at Large Redshifts*, ed. R.G. Kron and A. Renzini (Dordrecht:Kluwer), p. 275.

Kron, R.G., 1980, *Ap.J. Suppl.*, **43**, 305.

Kron, R.G., 1982, *Vistas Astr.*, **26**, 37.

Laing, R.A., Longair, M.S., Riley, J.M., Kibblewhitte, E.J., and Gunn, J.E., 1978, *M.N.R.A.S.*, **183**, 547.

Mathieu, R.D., and Spinrad, H., 1981, *Ap.J.*, **251**, 485.

Mattig, W., 1959, *Astr. Nach.*, **284**, 1.

Oegerle, W.R., and Hoessel, J.G., 1989, *A.J.*, **98**, 1523.

Oke, J.B., and Gunn, J.E., 1983, *Ap.J.*, **266**, 713.

Penston, M.J., Penston, M.V., and Sandage, A., 1971, *Pub.A.S.P.*, **83**, 868.

Peterson, B.A., Ellis, R.S., Kibblewhite, E.J., Bridgeland, M.T., Hooley, T., and Horne, D., 1979, *Ap.J. Lett.*, **233**, L109.

Pritchet, C.J., and Hartwick, F.D.A., 1987, *Ap.J.*, **320**, 464.

Riley, J.M. 1975, *M.N.R.A.S.*, **170**, 53.

Sandage, A., 1983, *Ap.J.*, **183**, 711.

Schechter, P.L., 1976, *Ap.J.*, **203**, 297.

Schild, R.E., 1984, *Ap.J.*, **286**, 450.

Schneider, D.P., Gunn, J.E., and Hoessel, J.G., 1983, *Ap.J.*, **264**, 337.

Shanks, T., Stevenson, P.R.F., Fong. R., and MacGillivray, H.T., 1984, *M.N.R.A.S.*, **206**, 767.

Spinrad, H., and Djorgovski, S., 1984, *Ap.J. Lett.*, **285**, L49.

Stryker, L.L., 1986, private communication.

Tinsley, B., 1980, *Ap.J.*, **241**, 41.

Tyson, J.A., and Jarvis, J.F., 1979, *Ap.J. Lett.*, **230**, L153.

Tyson, J.A., 1988, *A.J.*, **96**, 1.

Walker, G.A.H., Johnson, R., Christian, C.A., Waddell, P., and Kormendy, J., 1984, *Proc. S.P.I.E.*, **501**, 353.

Appendix A

Galaxies in Figures 5.5 – 5.9

No.	α (h m s)(1950)			δ (° ′ ″)(1950)			I	$R-I$	$B-R$
1	09	05	44.50	38	00	35.7	18.23	0.74	2.13
2	09	05	42.59	38	01	59.7	18.65	0.69	2.44
3	09	05	44.36	38	00	00.7	18.72	0.70	2.21
4	09	05	36.61	37	59	51.1	19.01	0.83	2.49
5	09	05	39.31	38	01	35.1	19.73	0.64	2.16
6	09	05	38.53	37	59	23.6	19.80	0.55	1.71
7	09	05	39.18	38	01	20.4	20.16	1.03	1.52
8	09	05	45.94	38	01	22.1	20.46	0.59	1.73
9	09	05	36.93	38	01	19.8	20.59	0.55	1.00
10	09	05	38.82	38	01	12.7	20.78	0.93	1.55
11	09	05	38.75	37	59	26.4	20.80	0.58	1.52
12	09	05	44.32	38	01	53.6	20.89	0.42	1.27
13	09	05	41.06	38	01	16.9	20.90	0.61	2.12
14	09	05	45.94	38	01	04.5	20.91	0.35	1.52
15	09	05	41.38	38	00	29.5	20.98	0.42	1.36
16	09	05	40.89	37	59	51.6	21.24	0.18	1.27
17	09	05	40.03	38	01	48.0	21.26	0.47	1.47
18	09	05	43.74	38	00	24.8	21.36	1.07	1.54
19	09	05	37.68	38	01	04.3	21.40	1.21	1.56
20	09	05	43.76	38	01	32.9	21.47	0.77	0.89
21	09	05	45.71	38	00	28.7	21.61	0.49	2.00
22	09	05	43.28	37	59	46.8	21.82	0.32	0.76
23	09	05	43.86	38	01	57.7	21.86	0.75	1.11
24	09	05	40.08	38	00	07.2	21.87	0.42	1.47
25	09	05	41.26	38	01	29.8	21.90	0.26	1.57
26	09	05	38.67	38	01	28.8	21.91	0.33	1.40
27	09	05	36.85	38	01	04.0	21.95	0.45	0.76
28	09	05	40.45	38	01	20.9	22.00	0.17	0.98
29	09	05	39.84	37	59	16.6	22.04	0.39	1.39
30	09	05	39.04	38	01	16.2	22.21	0.52	1.07
31	09	05	43.65	38	01	44.2	22.22	0.07	0.23
32	09	05	42.64	37	59	20.7	22.22	2.27	0.89
33	09	05	40.39	37	59	35.5	22.24	0.21	1.20
34	09	05	37.56	37	59	30.7	22.25	0.09	0.78
35	09	05	46.18	38	01	56.7	22.27	0.75	0.61
36	09	05	40.71	38	00	18.0	22.34	0.27	1.52
37	09	05	40.59	37	59	43.0	22.34	0.14	0.85
38	09	05	37.39	38	01	00.5	22.50	0.74	0.87
39	09	05	41.27	38	01	38.6	22.53	0.35	1.75
40	09	05	45.21	38	01	49.3	22.54	1.07	1.64

No.	α (h m s)			δ (° ′ ″)			I	$R-I$	$B-R$
41	09	05	36.31	38	00	28.7	22.56	1.36	2.42
42	09	05	40.78	38	01	29.3	22.56	0.32	0.23
43	09	05	38.16	38	01	46.4	22.57	0.35	1.14
44	09	05	37.71	38	00	47.7	22.58	0.53	1.51
45	09	05	38.14	37	59	40.1	22.59	0.21	0.93
46	09	05	43.56	38	00	39.2	22.63	0.67	1.53
47	09	05	37.95	37	59	16.7	22.64	0.35	0.97
48	09	05	42.14	38	00	09.8	22.66	−0.16	1.17
49	09	05	44.89	37	59	32.9	22.67	0.91	0.36
50	09	05	45.99	38	00	17.5	22.70	0.79	0.29
51	09	05	40.47	37	59	27.0	22.70	0.25	0.48
52	09	05	45.31	38	00	35.2	22.71	0.24	0.82
53	09	05	36.97	38	01	26.4	22.72	0.42	0.40
54	09	05	40.95	38	01	27.6	22.80	0.60	1.11
55	09	05	36.70	38	01	55.7	22.80	0.19	0.52
56	09	05	40.01	38	01	07.3	22.81	0.70	0.61
57	09	05	37.54	38	00	45.8	22.81	0.24	1.17
58	09	05	42.27	38	00	29.1	22.82	1.41	2.74
59	09	05	38.47	38	00	51.7	22.84	0.38	0.38
60	09	05	41.96	38	01	14.2	22.85	0.96	1.11
61	09	05	36.42	38	01	40.0	22.87	0.15	1.13
62	09	05	36.46	38	01	47.4	22.87	0.78	0.09
63	09	05	42.80	38	00	36.8	22.88	0.60	1.29
64	09	05	42.84	37	59	48.7	22.89	0.18	0.76
65	09	05	37.41	38	00	00.1	22.92	0.01	0.19
66	09	05	39.00	37	59	50.6	22.92	0.53	2.39
67	09	05	39.98	38	01	57.9	22.96	0.48	0.27
68	09	05	43.72	38	01	45.9	22.97	0.40	−0.06
69	09	05	38.77	37	59	32.1	22.98	0.74	0.43
70	09	05	42.21	38	01	14.5	23.00	1.59	2.07
71	09	05	43.37	38	00	54.6	23.05	0.51	0.77
72	09	05	42.66	38	01	12.5	23.05	1.02	0.62
73	09	05	40.92	38	01	03.9	23.07	0.46	0.54
74	09	05	43.31	38	00	09.0	23.08	0.19	0.04
75	09	05	44.73	38	01	14.8	23.08	−0.44	0.41
76	09	05	36.93	38	00	12.2	23.09	0.43	0.21
77	09	05	43.27	38	01	18.0	23.09	0.63	0.91
78	09	05	41.56	37	59	51.3	23.11	0.09	1.06
79	09	05	42.91	38	00	45.9	23.11	0.29	0.93
80	09	05	44.21	37	59	29.2	23.11	1.06	0.14

$No.$	α (h m s)			δ ($^\circ$ $'$ $''$)			I	$R-I$	$B-R$
81	09	05	44.17	37	59	50.3	23.12	0.39	0.36
82	09	05	37.08	38	00	26.3	23.12	0.30	0.17
83	09	05	42.23	38	00	56.3	23.13	0.89	2.23
84	09	05	37.61	38	01	31.1	23.14	0.34	1.24
85	09	05	44.01	38	00	33.8	23.14	1.27	3.94
86	09	05	45.94	38	00	07.2	23.17	0.52	0.94
87	09	05	43.72	37	59	41.1	23.17	0.42	0.70
88	09	05	39.31	38	01	46.1	23.18	0.33	1.16
89	09	05	39.12	38	00	50.4	23.20	0.82	0.09
90	09	05	38.23	38	01	17.0	23.20	0.75	0.03
91	09	05	40.02	38	01	21.0	23.20	0.40	0.92
92	09	05	43.11	37	59	19.9	23.21	0.24	0.98
93	09	05	42.88	37	59	31.5	23.24	0.01	1.06
94	09	05	39.54	38	00	34.8	23.25	1.39	1.80
95	09	05	42.95	37	59	21.1	23.26	0.08	0.48
96	09	05	40.09	38	00	31.6	23.26	0.26	0.61
97	09	05	39.33	37	59	30.3	23.26	0.13	0.27
98	09	05	39.91	38	01	04.9	23.27	-0.08	0.23
99	09	05	42.00	38	01	17.2	23.29	0.31	0.72
100	09	05	45.81	37	59	56.5	23.30	1.62	3.58
101	09	05	41.44	37	59	25.1	23.30	0.16	0.71
102	09	05	39.57	38	00	33.3	23.30	0.98	0.75
103	09	05	36.20	38	00	25.6	23.32	0.43	0.72
104	09	05	40.86	38	00	56.4	23.33	0.33	0.02
105	09	05	46.25	38	01	20.9	23.36	0.31	0.22
106	09	05	44.65	38	01	55.0	23.37	1.16	0.76
107	09	05	45.69	37	59	47.0	23.37	0.69	0.29
108	09	05	43.46	38	01	31.4	23.37	0.45	> 2.3
109	09	05	42.62	38	01	04.4	23.40	0.95	2.11
110	09	05	42.52	38	01	14.5	23.40	0.47	0.03
111	09	05	37.17	37	59	46.0	23.42	0.35	0.87
112	09	05	36.69	37	59	40.5	23.44	0.24	> 2.4
113	09	05	40.29	37	59	32.9	23.46	1.06	0.44
114	09	05	42.54	38	01	16.4	23.46	0.34	0.60
115	09	05	45.80	37	59	32.7	23.47	0.12	1.63
116	09	05	38.79	38	00	16.0	23.48	0.07	0.55
117	09	05	43.21	38	01	16.8	23.48	0.32	1.00
118	09	05	41.59	38	01	23.9	23.49	1.33	2.19
119	09	05	42.18	37	59	51.1	23.50	0.70	0.92
120	09	05	39.78	38	00	16.0	23.50	0.06	0.81

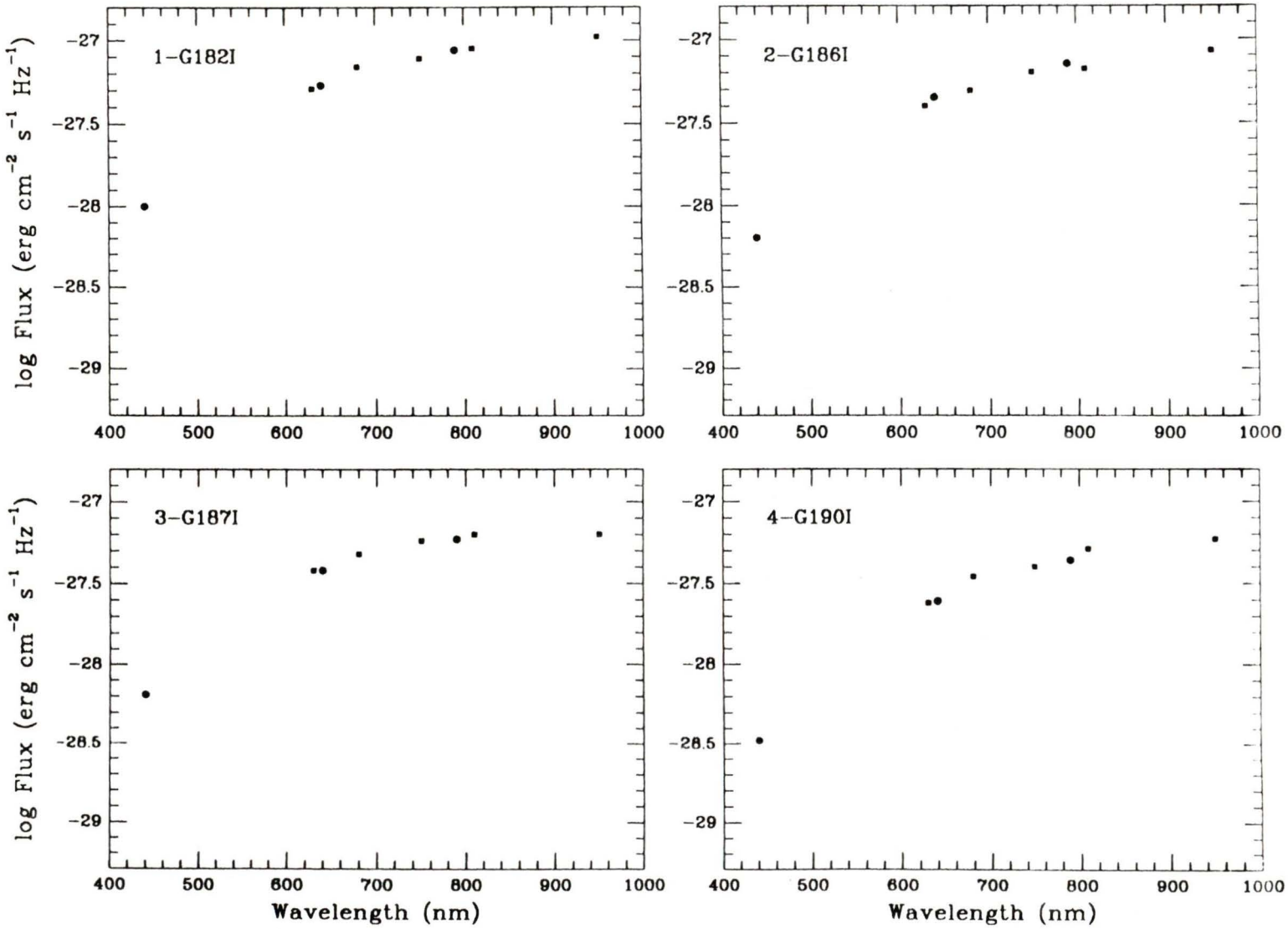

Spectral Energy Distributions

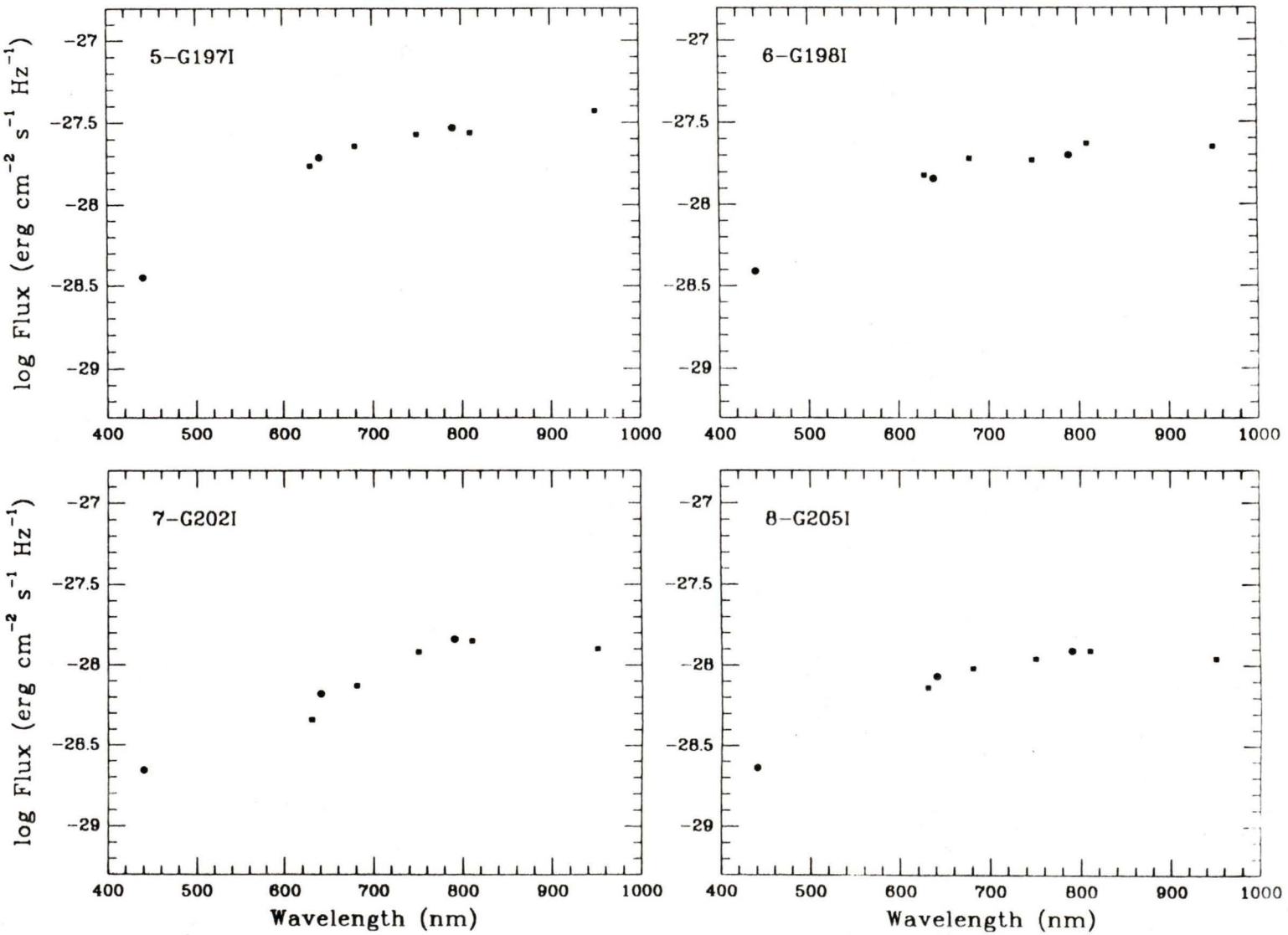
5-G197I
6-G198I
7-G202I
8-G205I
log Flux (erg cm^{-2} s^{-1} Hz^{-1})
Wavelength (nm)
-27
-27.5
-28
-28.5
-29
400
500
600
700
800
900
1000

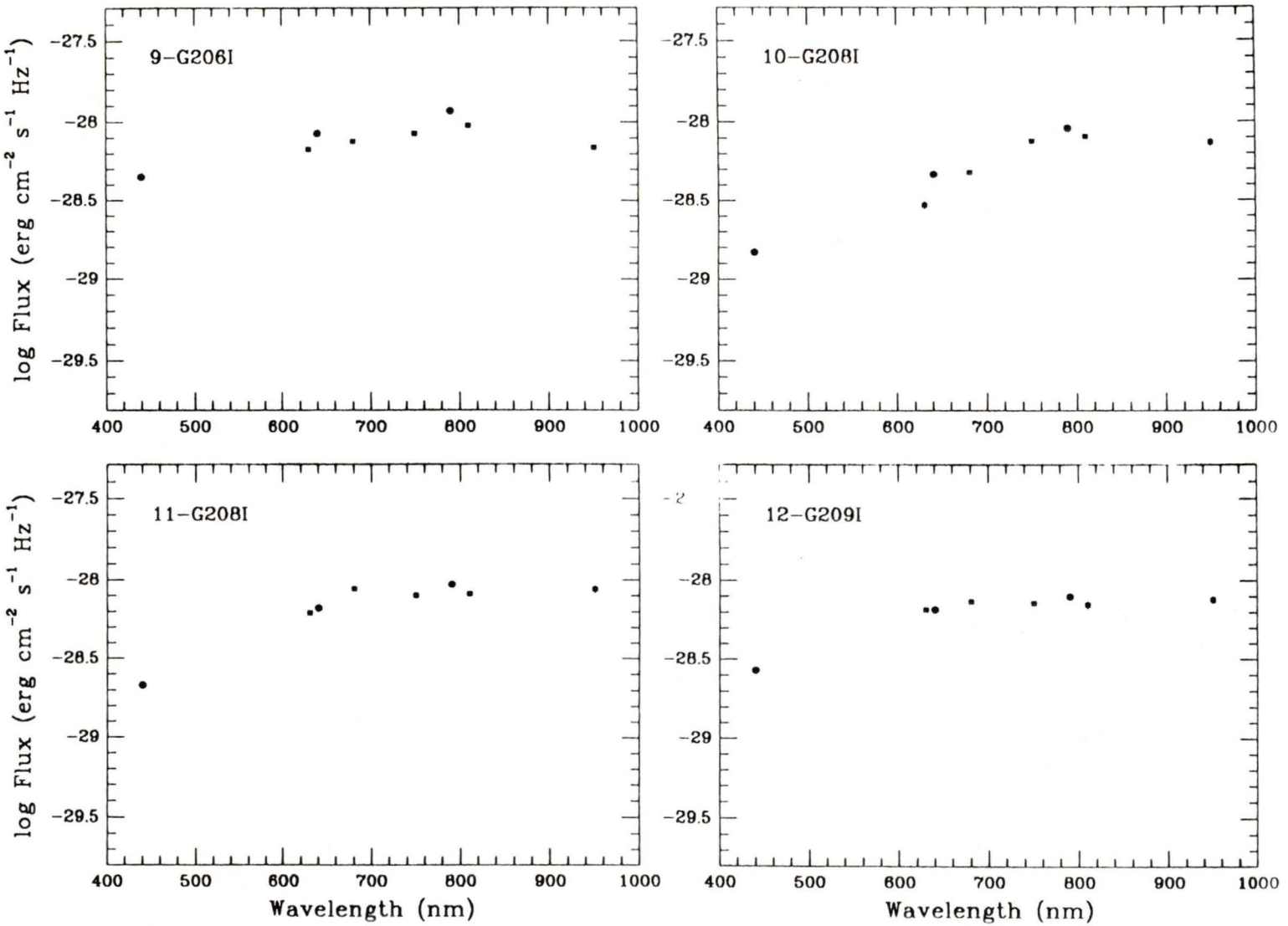
9-G206I
10-G208I
11-G208I
12-G209I
log Flux (erg cm^{-2} s^{-1} Hz^{-1})
Wavelength (nm)
-27.5
-28
-28.5
-29
-29.5
400
500
600
700
800
900
1000

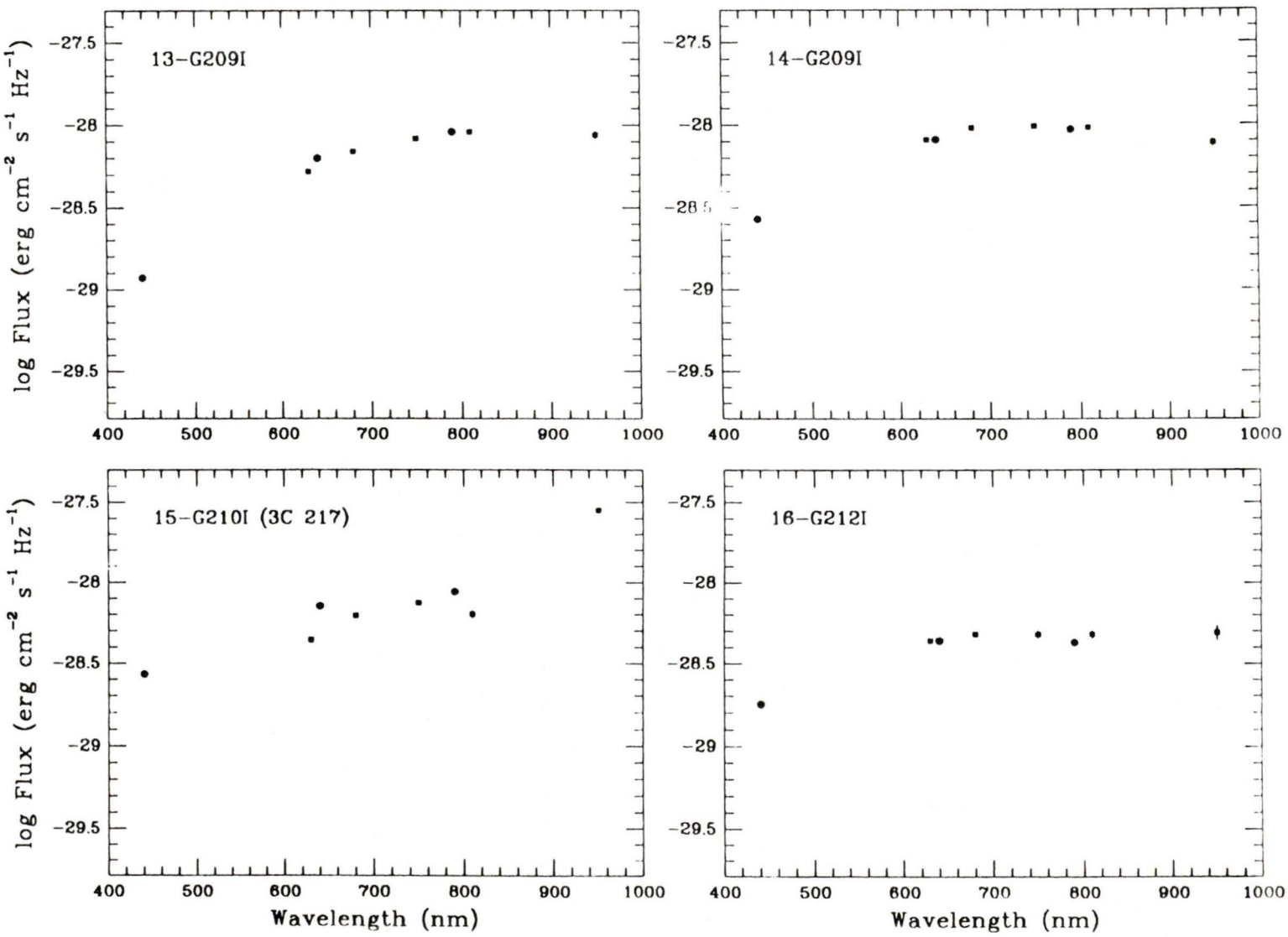
13-G209I
14-G209I
15-G210I (3C 217)
16-G212I
log Flux (erg cm^{-2} s^{-1} Hz^{-1})
Wavelength (nm)
-27.5
-28
-28.5
-29
-29.5
400
500
600
700
800
900
1000

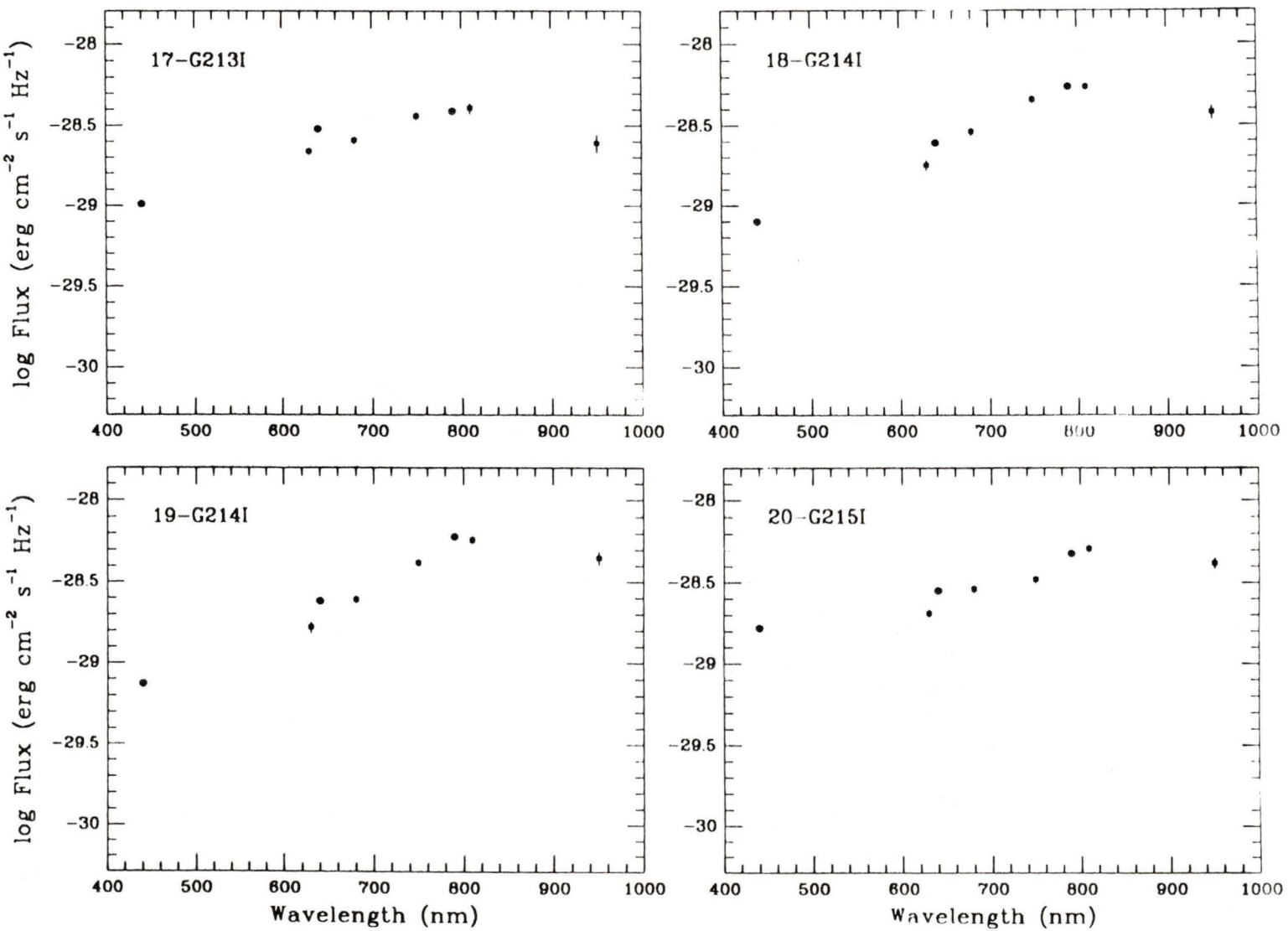
17-G213I
18-G214I
19-G214I
20-G215I
log Flux (erg cm^{-2} s^{-1} Hz^{-1})
Wavelength (nm)
-28
-28.5
-29
-29.5
-30
400
500
600
700
800
900
1000

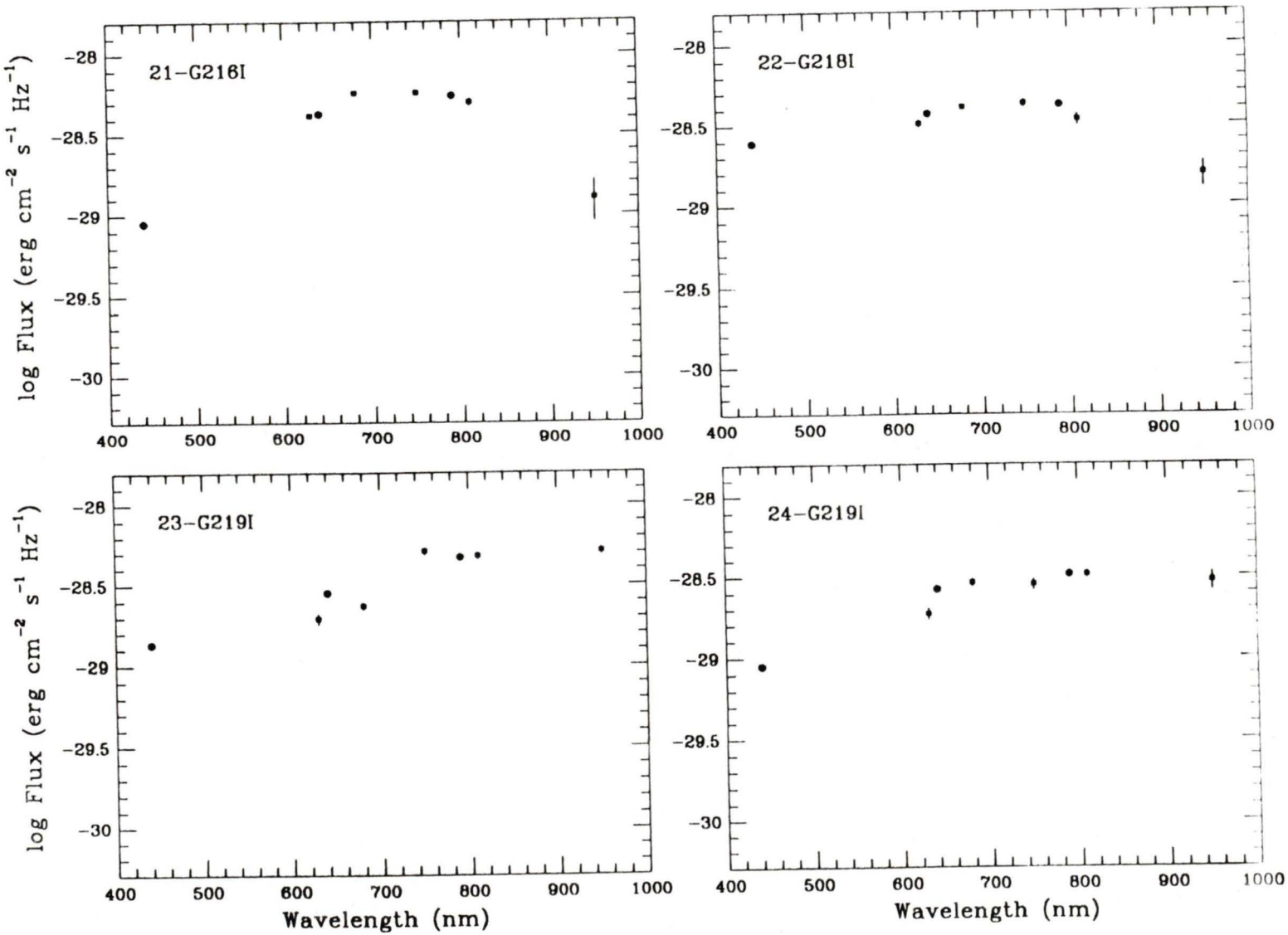
21-G216I
22-G218I
23-G219I
24-G219I
log Flux (erg cm^{-2} s^{-1} Hz^{-1})
Wavelength (nm)
-28
-28.5
-29
-29.5
-30
400
500
600
700
800
900
1000

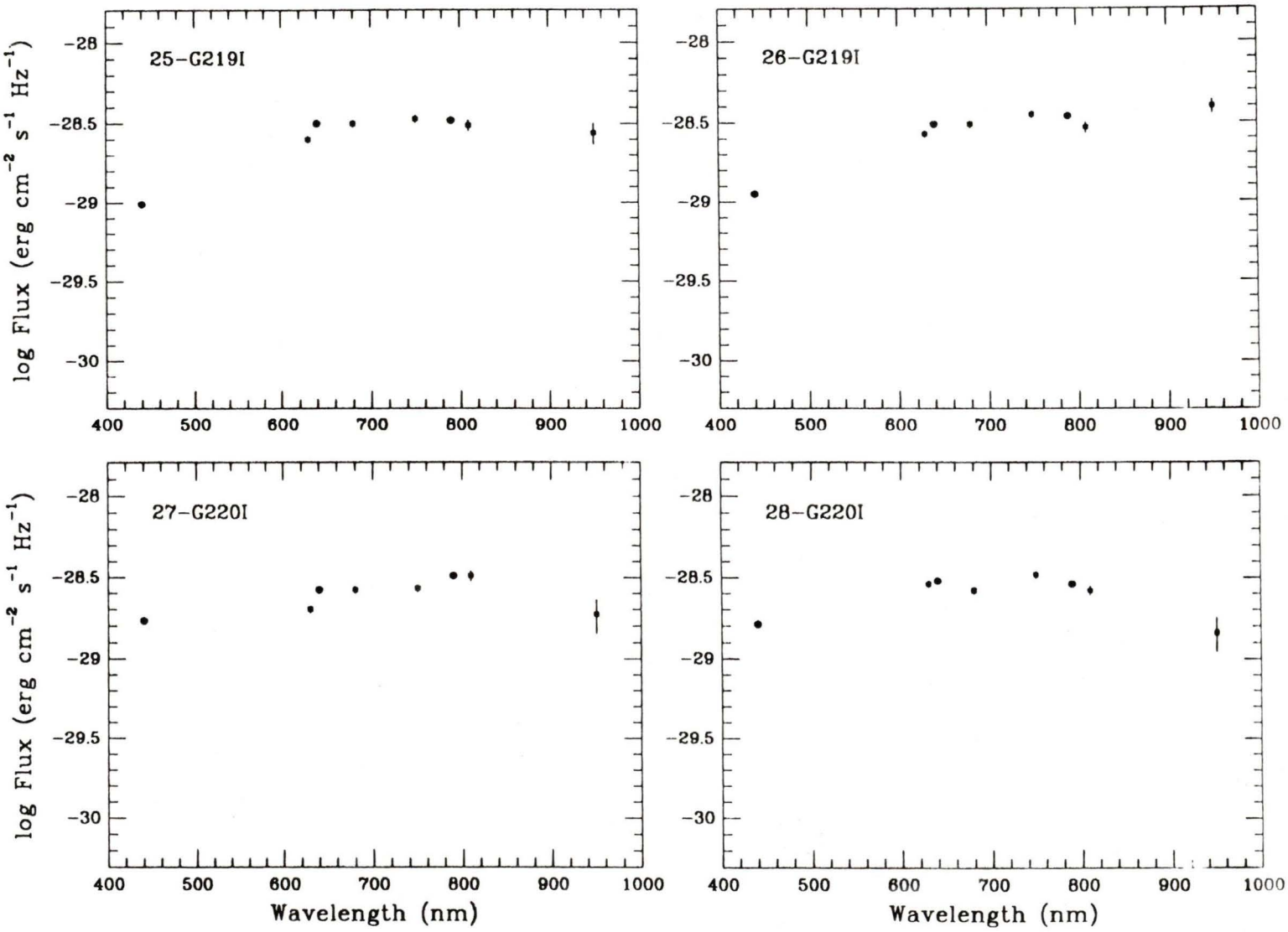
25-G219I
26-G219I
27-G220I
28-G220I
log Flux (erg cm^{-2} s^{-1} Hz^{-1})
Wavelength (nm)
-28
-28.5
-29
-29.5
-30
400
500
600
700
800
900
1000

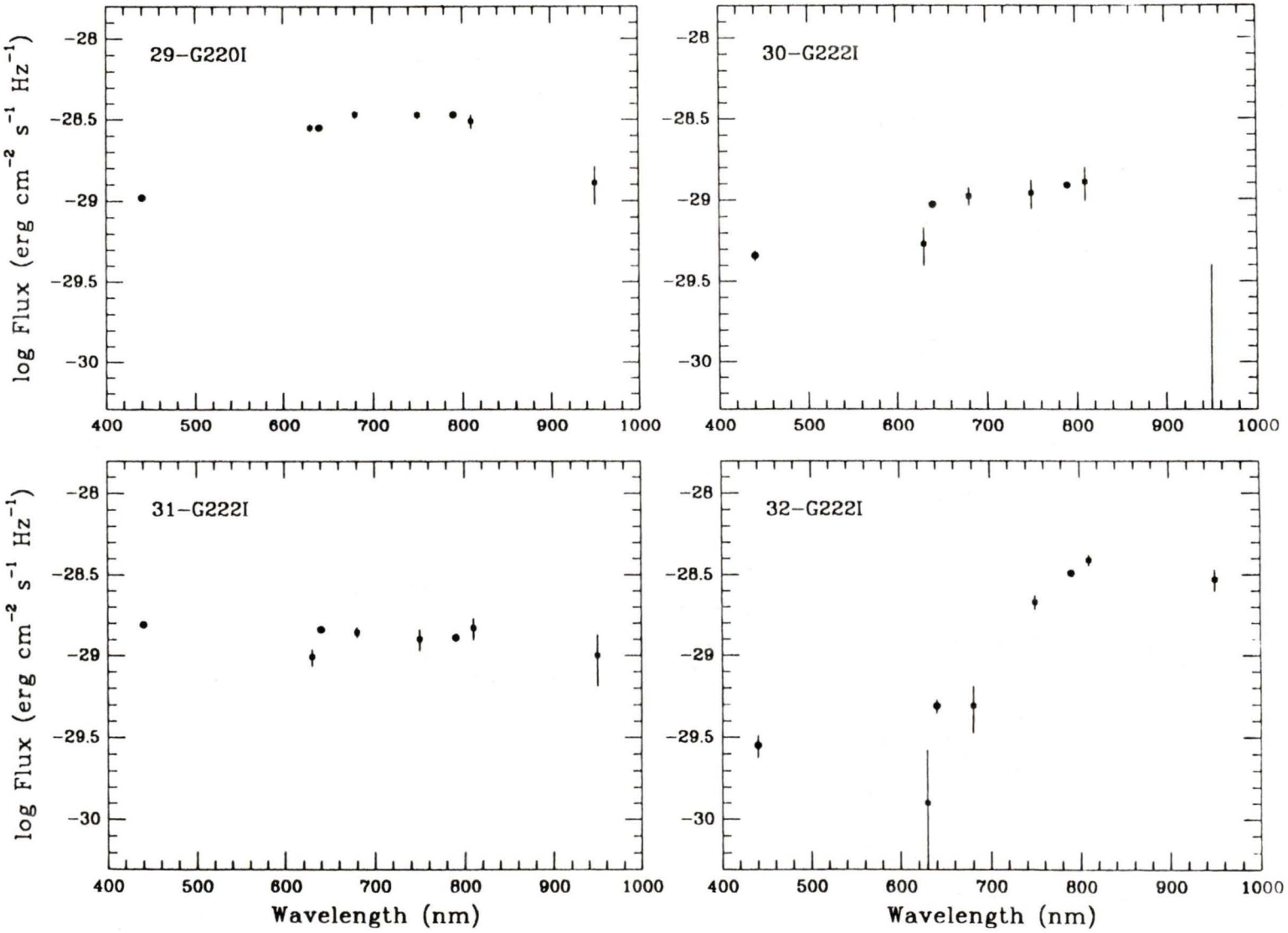
29-G220I
30-G222I
31-G222I
32-G222I
log Flux (erg cm^{-2} s^{-1} Hz^{-1})
Wavelength (nm)
-28
-28.5
-29
-29.5
-30
400
500
600
700
800
900
1000

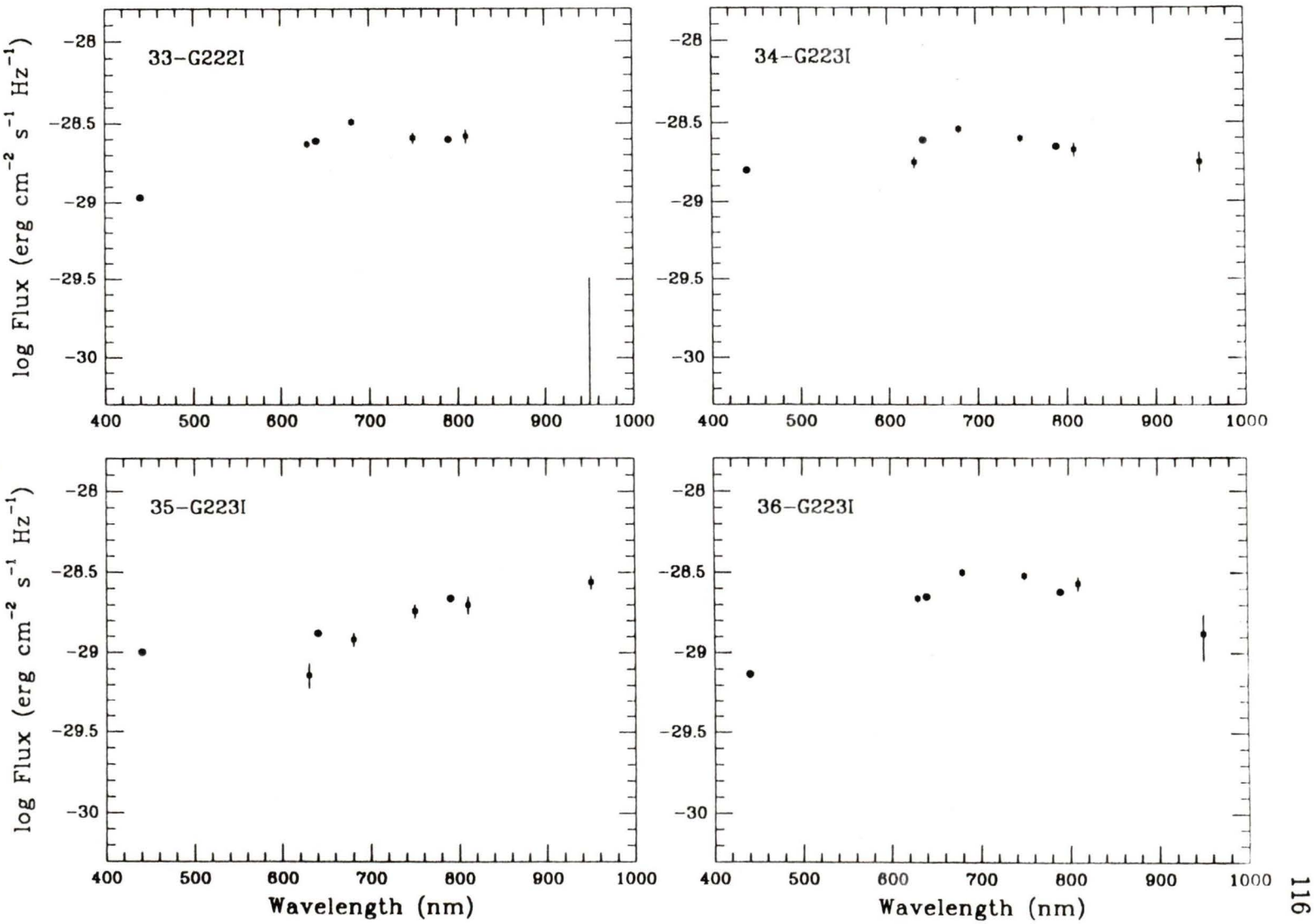
33-G222I
34-G223I
35-G223I
36-G223I
log Flux (erg cm^{-2} s^{-1} Hz^{-1})
Wavelength (nm)
-28
-28.5
-29
-29.5
-30
400
500
600
700
800
900
1000

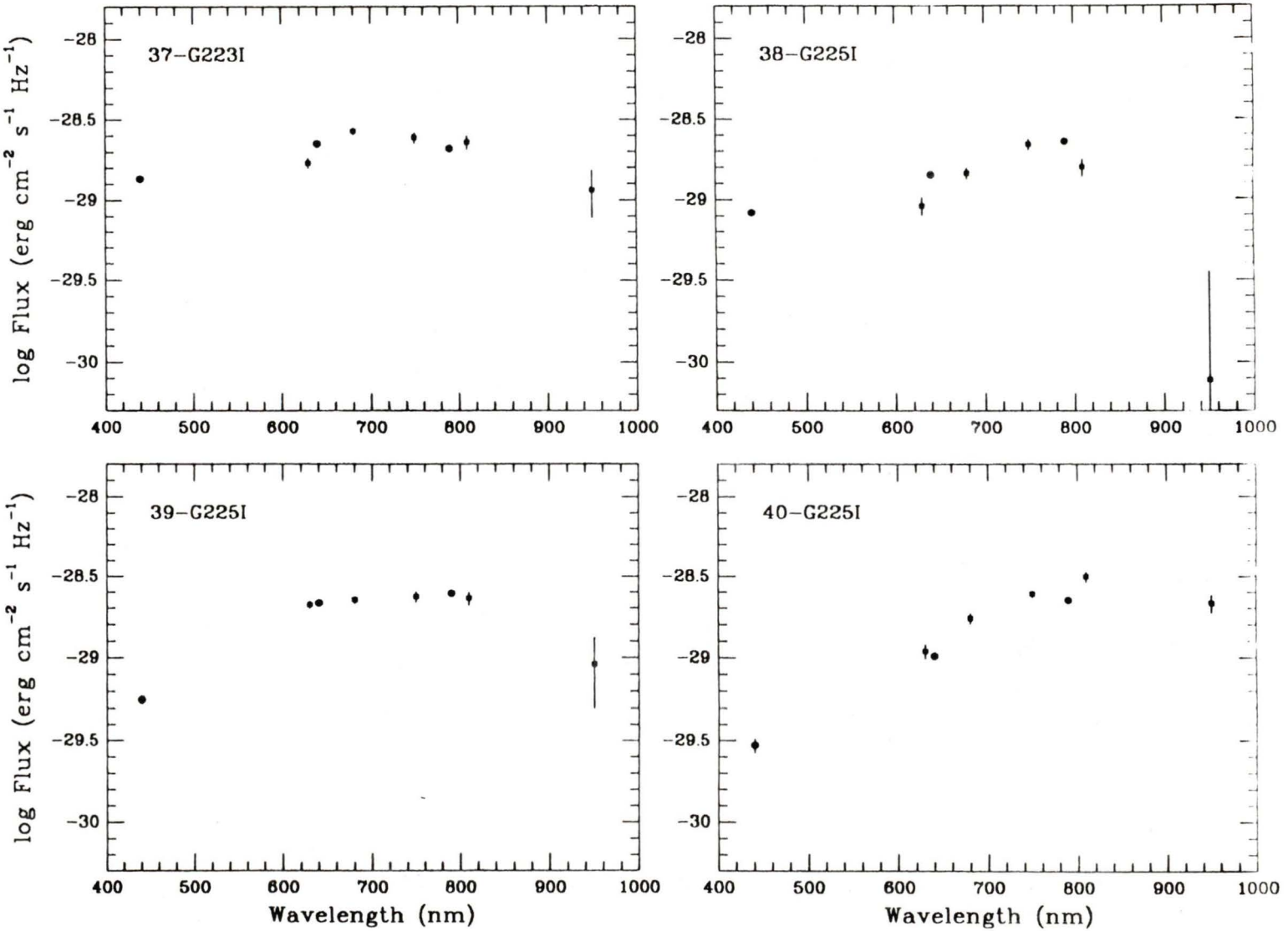
37-G223I
38-G225I
39-G225I
40-G225I
log Flux (erg cm^{-2} s^{-1} Hz^{-1})
Wavelength (nm)
-28
-28.5
-29
-29.5
-30
400
500
600
700
800
900
1000

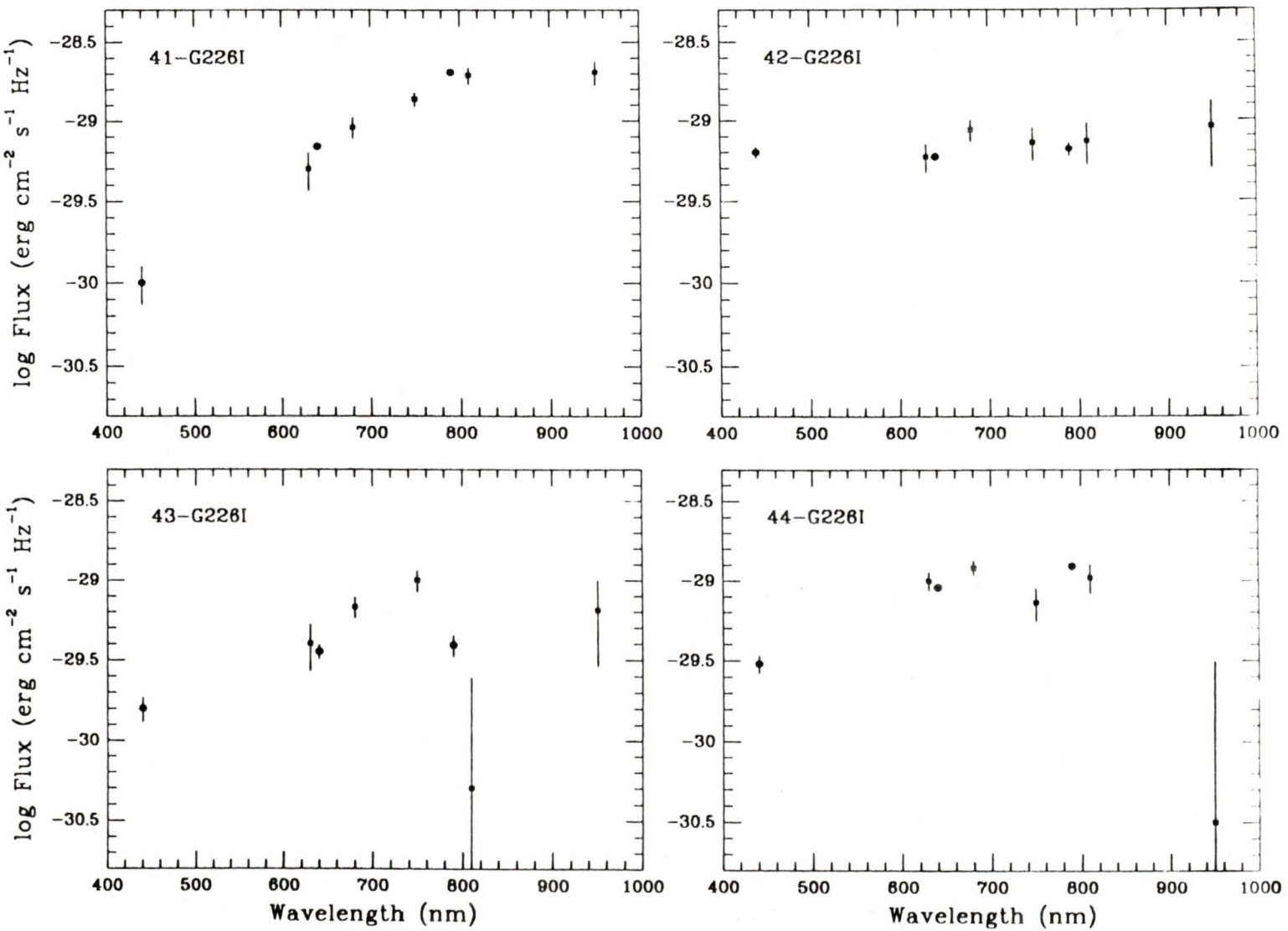
41-G226I
42-G226I
43-G226I
44-G226I
log Flux (erg cm^{-2} s^{-1} Hz^{-1})
Wavelength (nm)
-28.5
-29
-29.5
-30
-30.5
400
500
600
700
800
900
1000

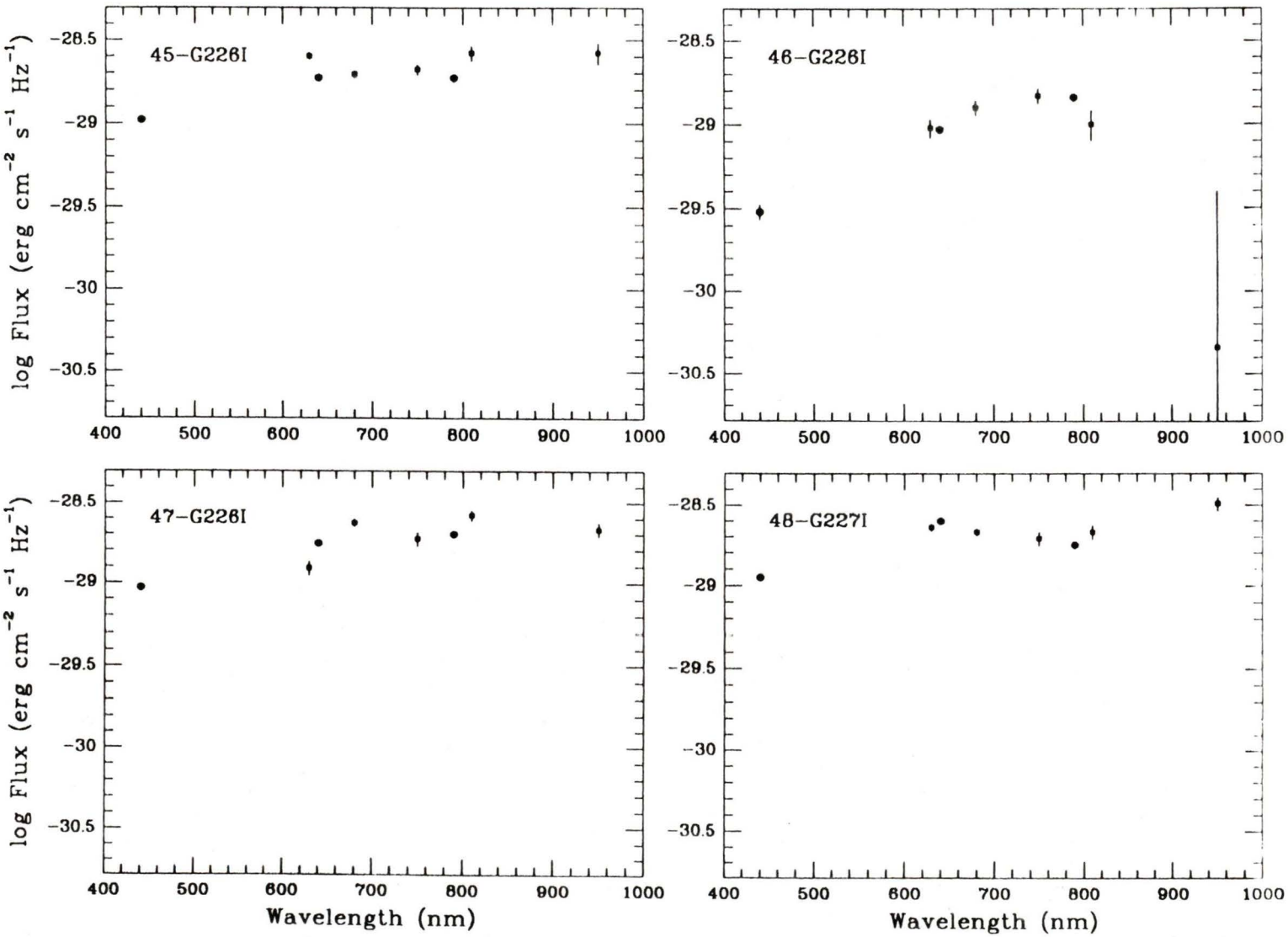
45-G226I
46-G226I
47-G226I
48-G227I
log Flux (erg cm^{-2} s^{-1} Hz^{-1})
Wavelength (nm)
-28.5
-29
-29.5
-30
-30.5
400
500
600
700
800
900
1000

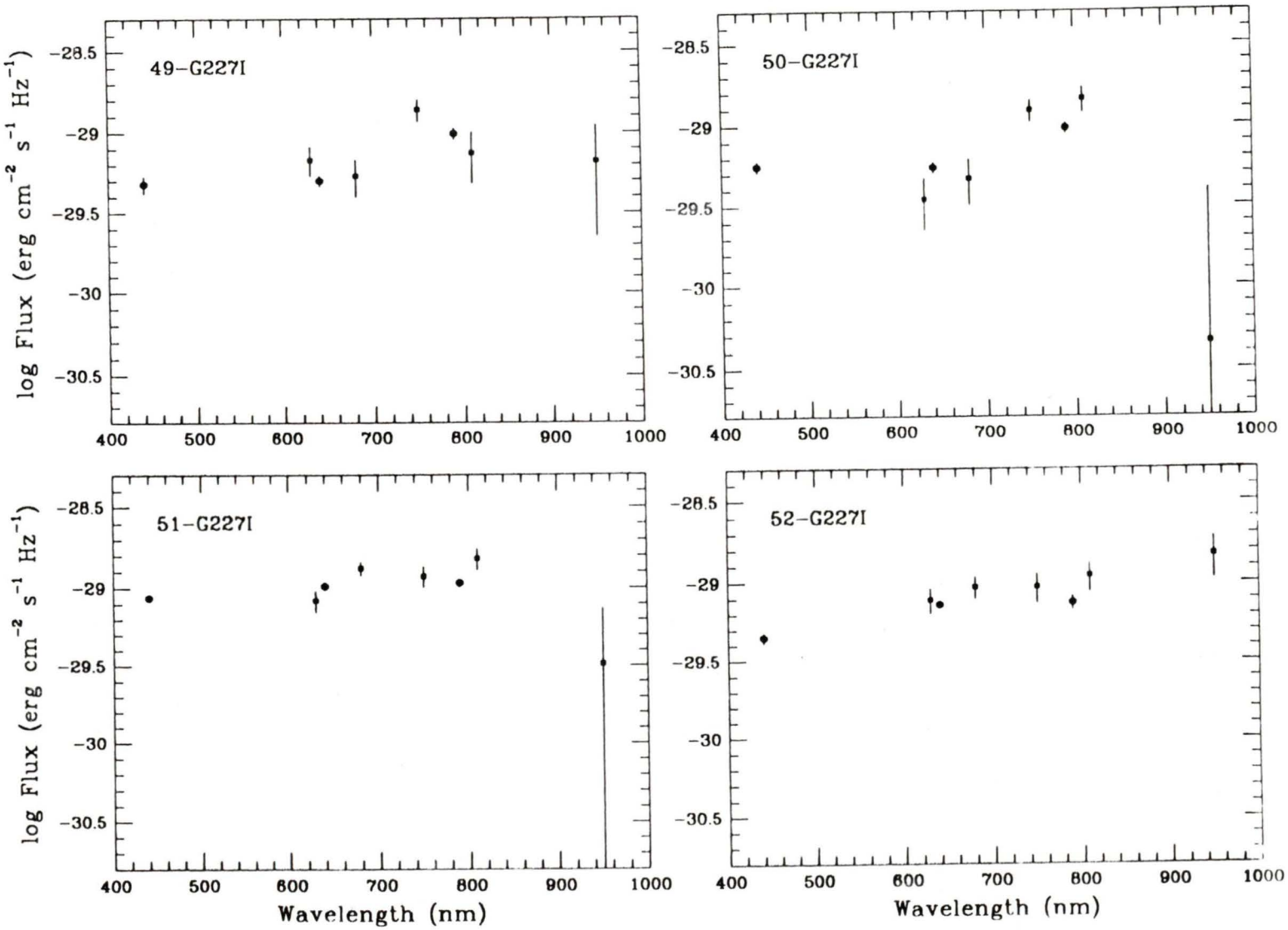
49-G227I
50-G227I
51-G227I
52-G227I
log Flux (erg cm^{-2} s^{-1} Hz^{-1})
Wavelength (nm)
-28.5
-29
-29.5
-30
-30.5
400
500
600
700
800
900
1000

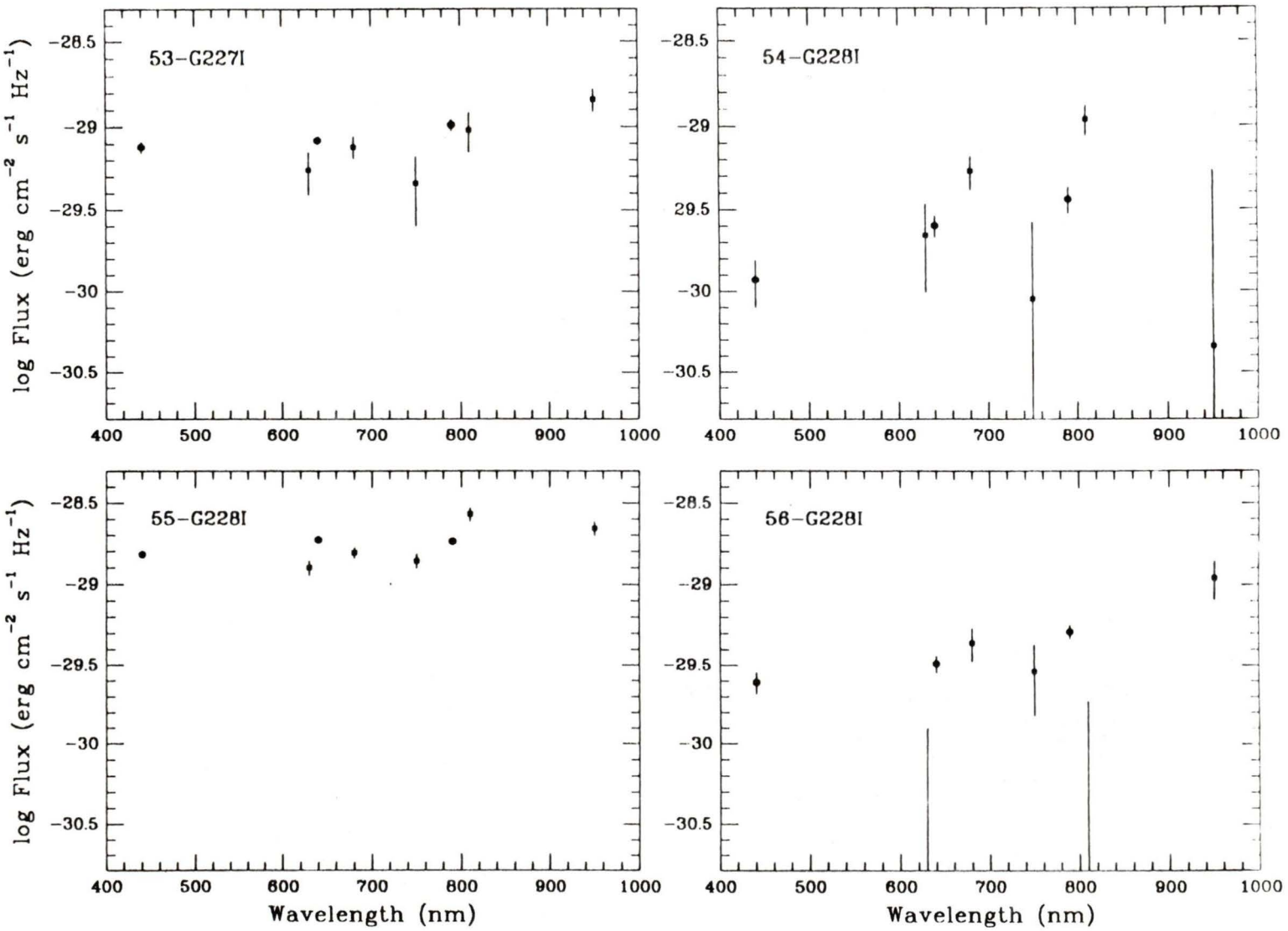
53-G227I
54-G228I
55-G228I
56-G228I
log Flux (erg cm^{-2} s^{-1} Hz^{-1})
Wavelength (nm)
-28.5
-29
-29.5
-30
-30.5
400
500
600
700
800
900
1000

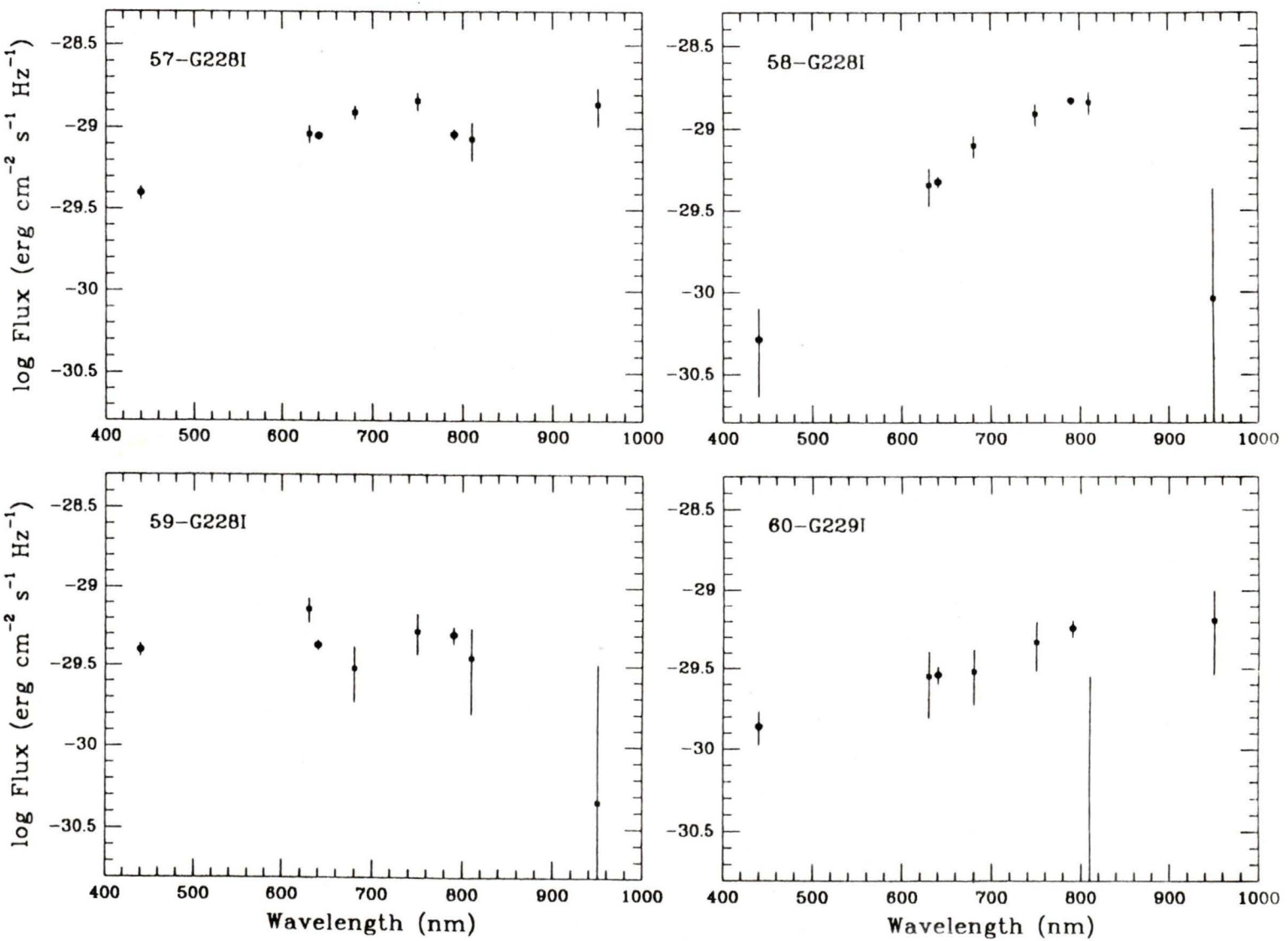
57-G228I
58-G228I
59-G228I
60-G229I
log Flux (erg cm^{-2} s^{-1} Hz^{-1})
Wavelength (nm)
-28.5
-29
-29.5
-30
-30.5
400
500
600
700
800
900
1000

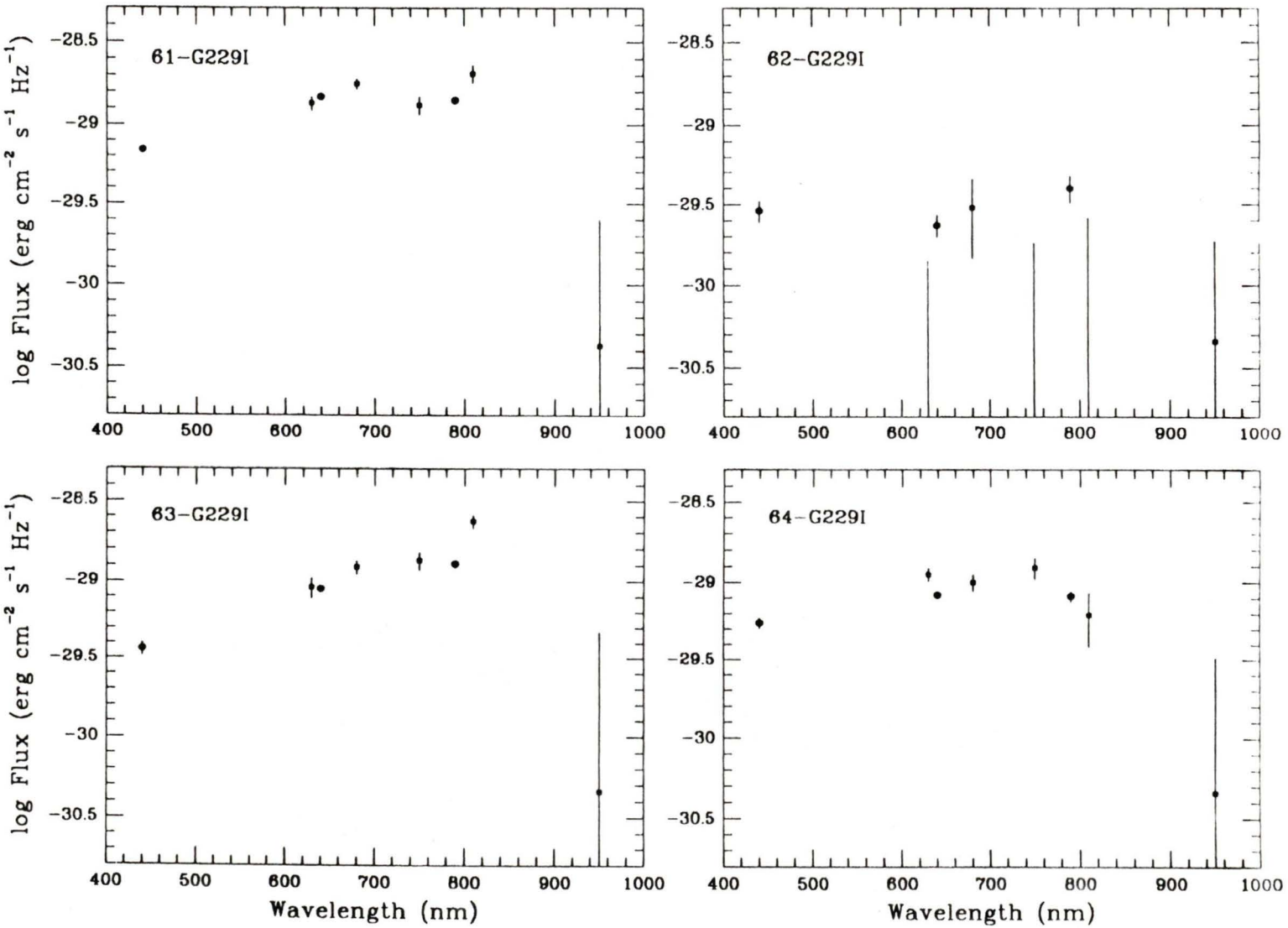
61-G229I
62-G229I
63-G229I
64-G229I
log Flux (erg cm^{-2} s^{-1} Hz^{-1})
Wavelength (nm)
-28.5
-29
-29.5
-30
-30.5
400
500
600
700
800
900
1000

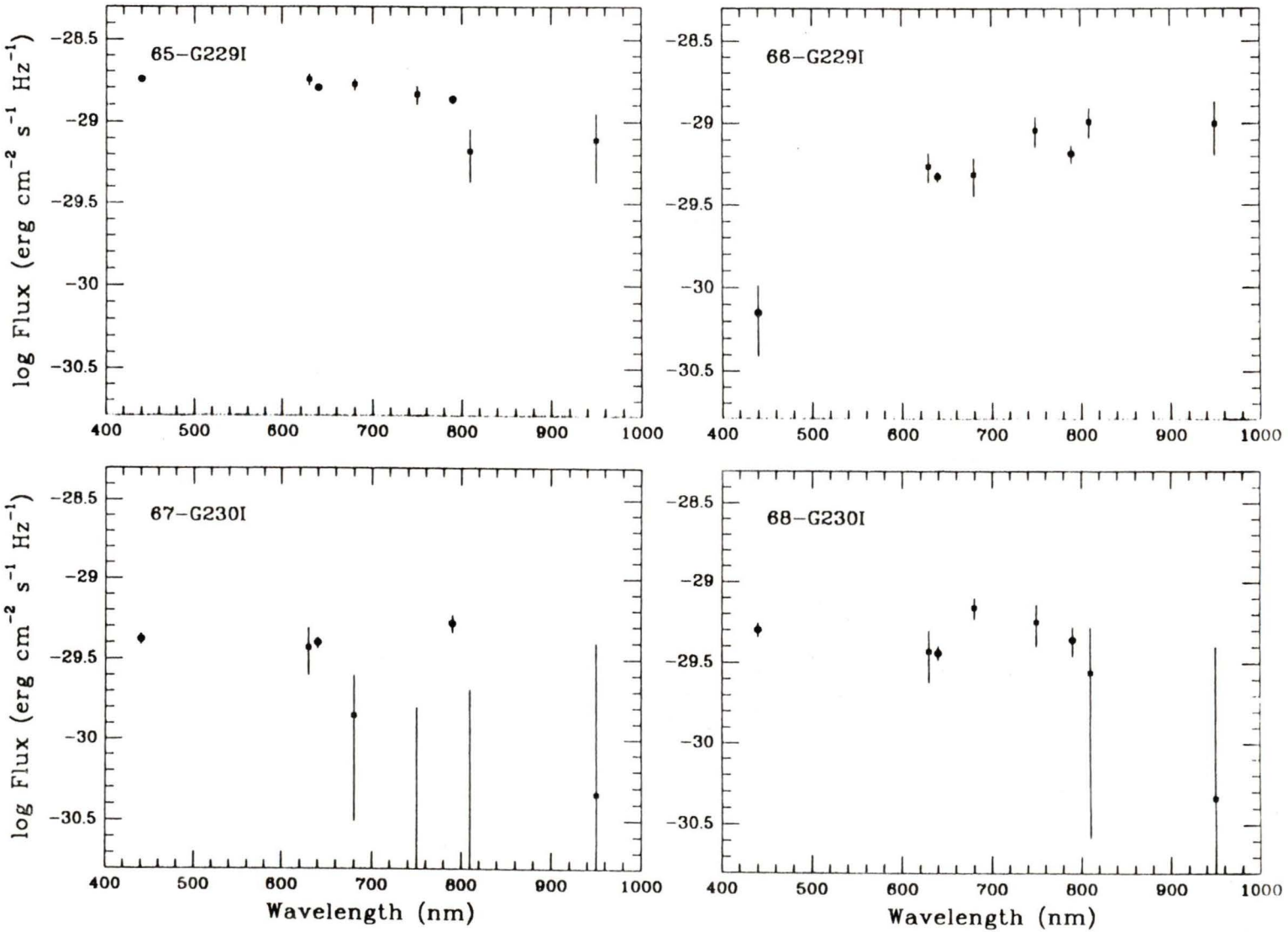
65-G229I
66-G229I
67-G230I
68-G230I
log Flux (erg cm^{-2} s^{-1} Hz^{-1})
Wavelength (nm)
-28.5
-29
-29.5
-30
-30.5
400
500
600
700
800
900
1000

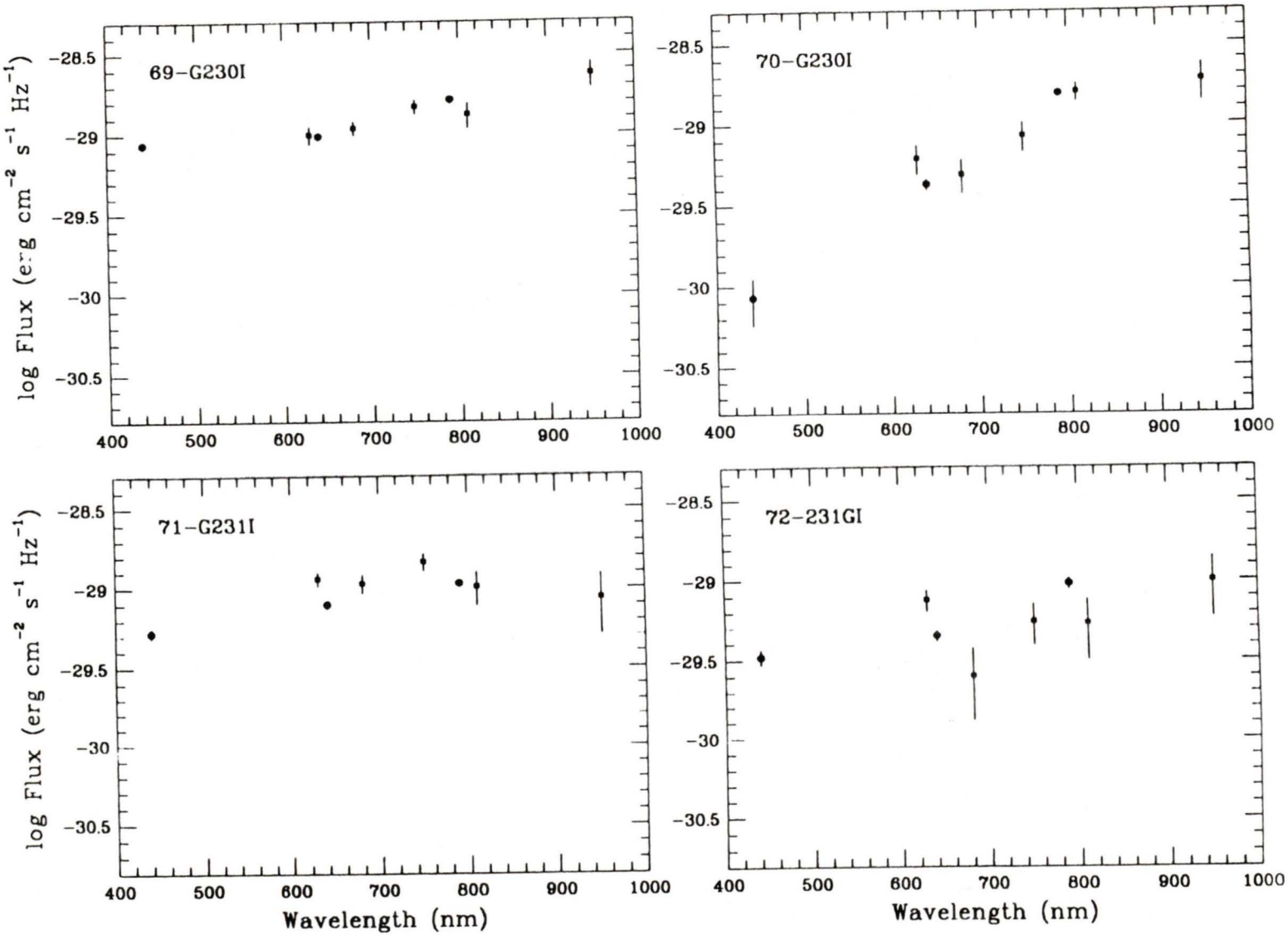
69-G230I
70-G230I
71-G231I
72-231GI
log Flux (erg cm^{-2} s^{-1} Hz^{-1})
Wavelength (nm)
-28.5
-29
-29.5
-30
-30.5
400
500
600
700
800
900
1000

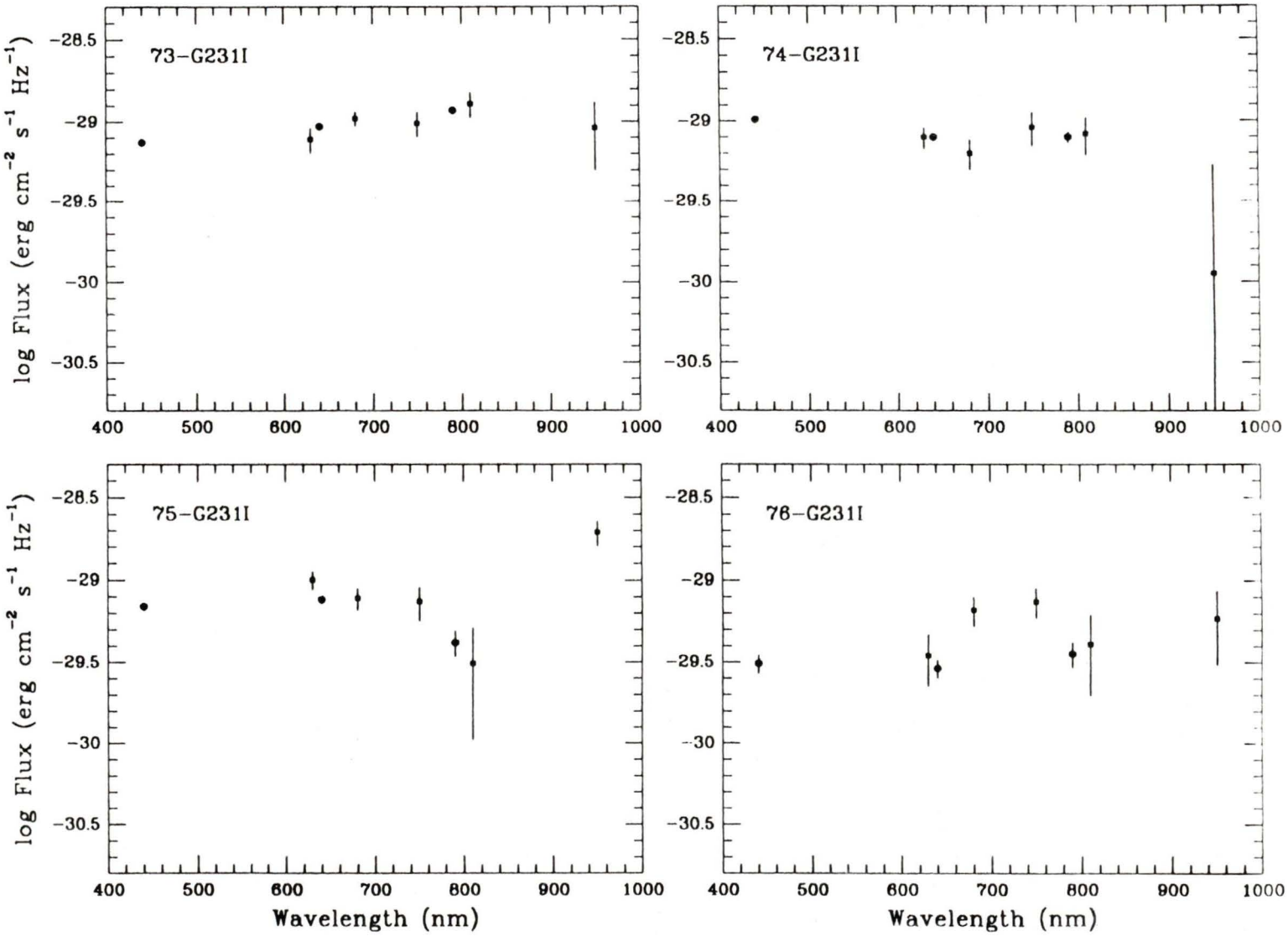
73-G231I
74-G231I
75-G231I
76-G231I
log Flux (erg cm^{-2} s^{-1} Hz^{-1})
Wavelength (nm)
-28.5
-29
-29.5
-30
-30.5
400
500
600
700
800
900
1000

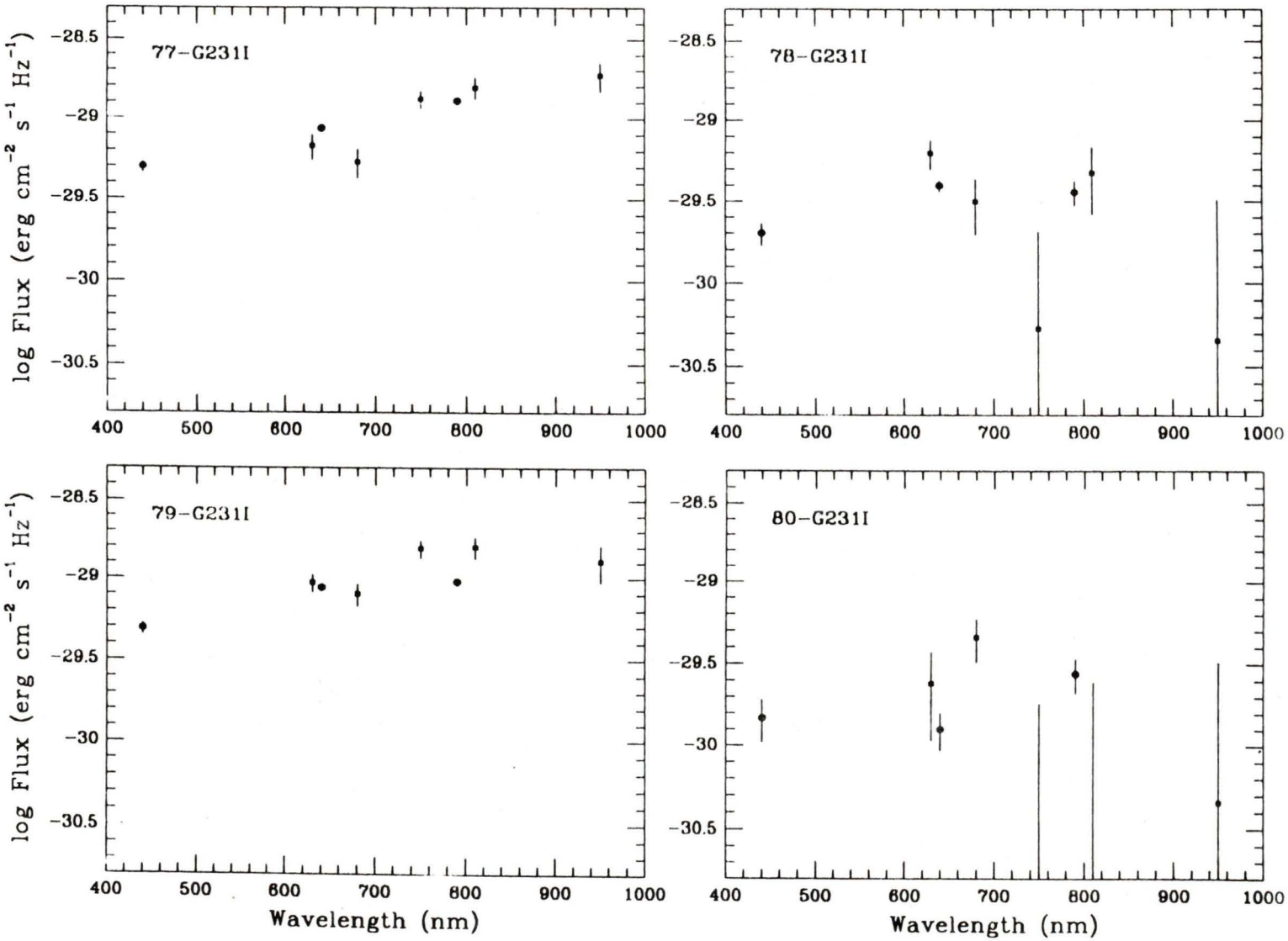
77-G231I
78-G231I
79-G231I
80-G231I
log Flux (erg cm^{-2} s^{-1} Hz^{-1})
Wavelength (nm)
-28.5
-29
-29.5
-30
-30.5
400
500
600
700
800
900
1000

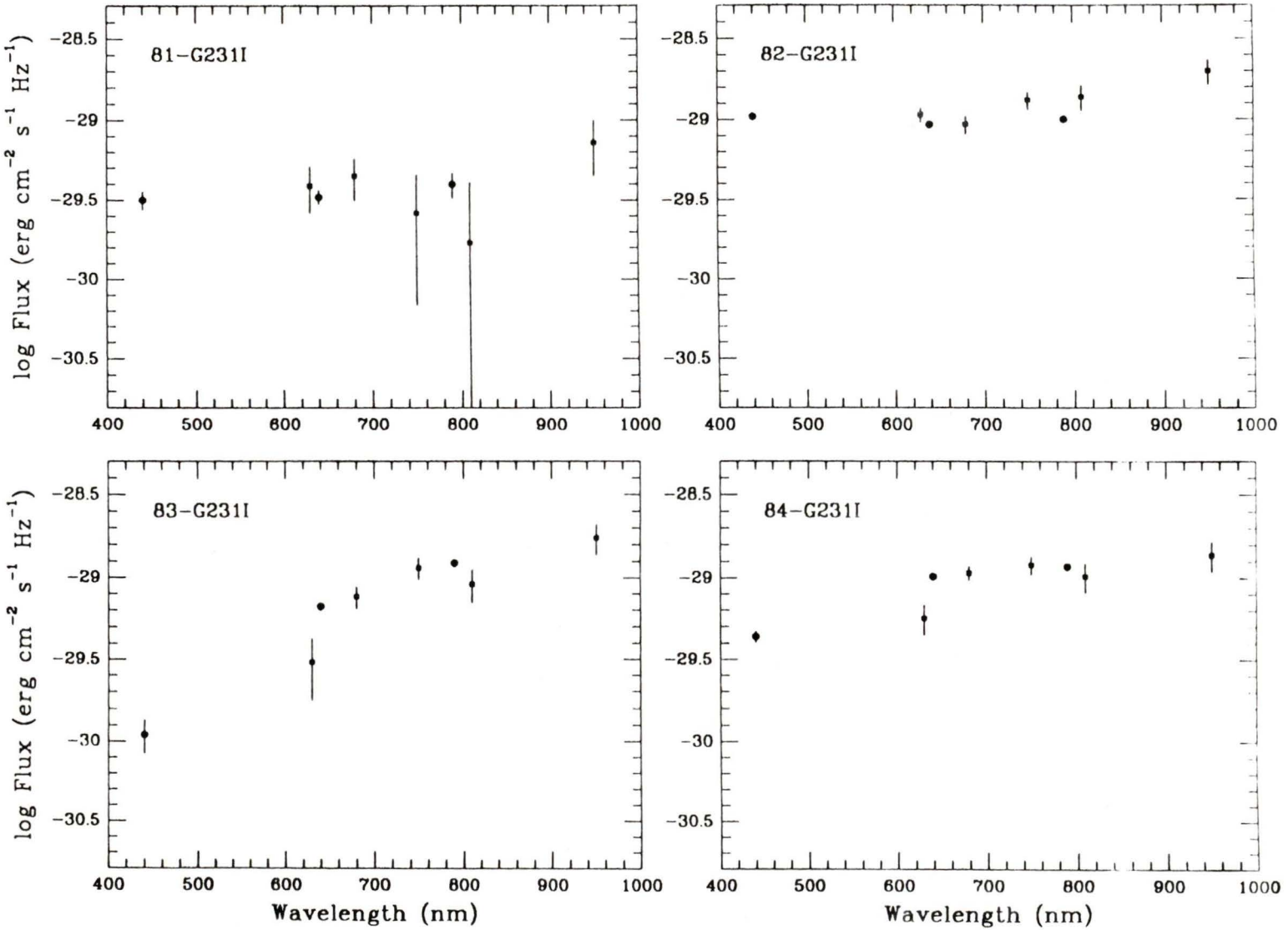
81-G231I
82-G231I
83-G231I
84-G231I
log Flux (erg cm^{-2} s^{-1} Hz^{-1})
Wavelength (nm)
-28.5
-29
-29.5
-30
-30.5
400
500
600
700
800
900
1000

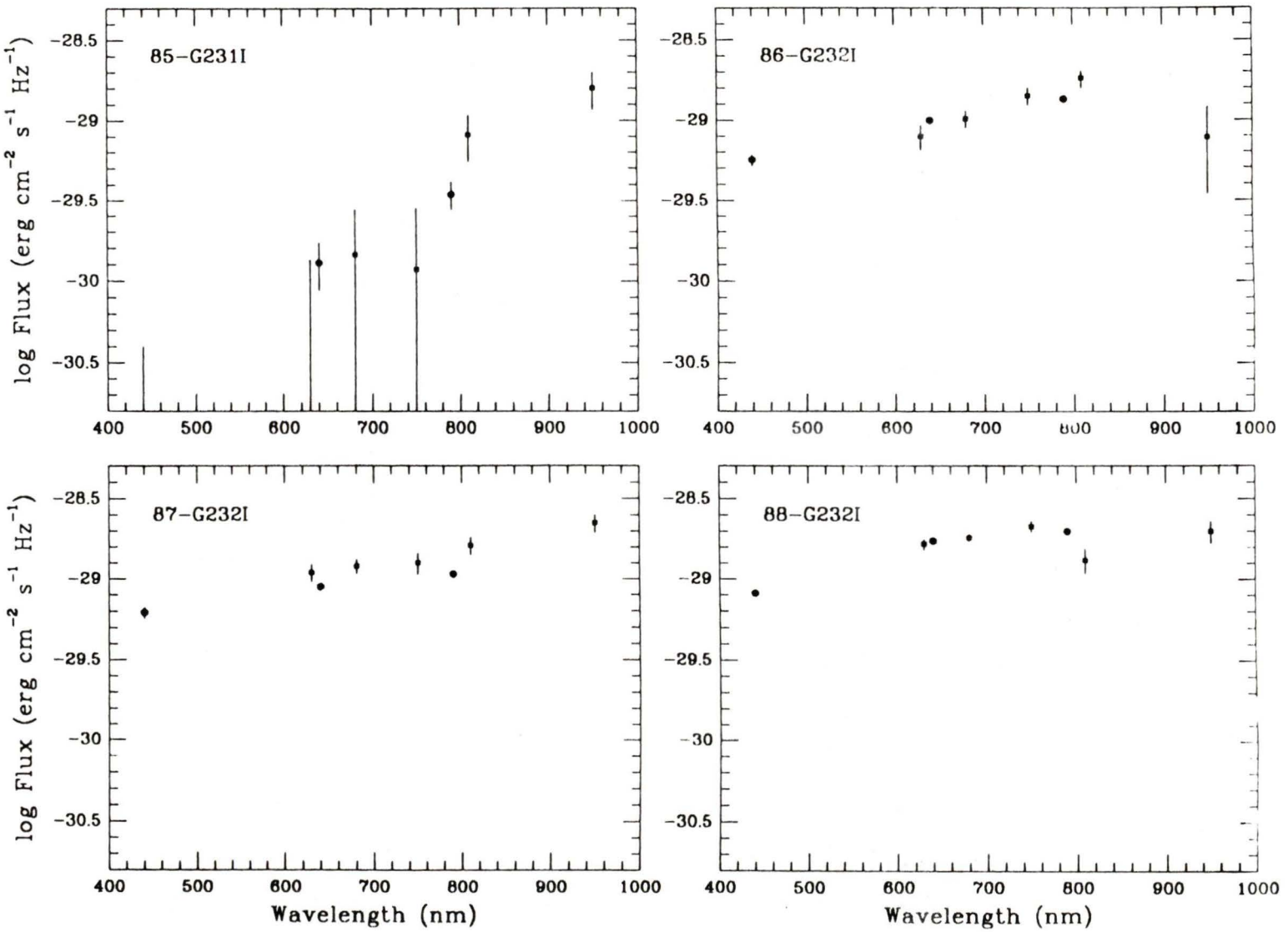
85-G231I
86-G232I
87-G232I
88-G232I
log Flux (erg cm^{-2} s^{-1} Hz^{-1})
Wavelength (nm)
-28.5
-29
-29.5
-30
-30.5
400
500
600
700
800
900
1000

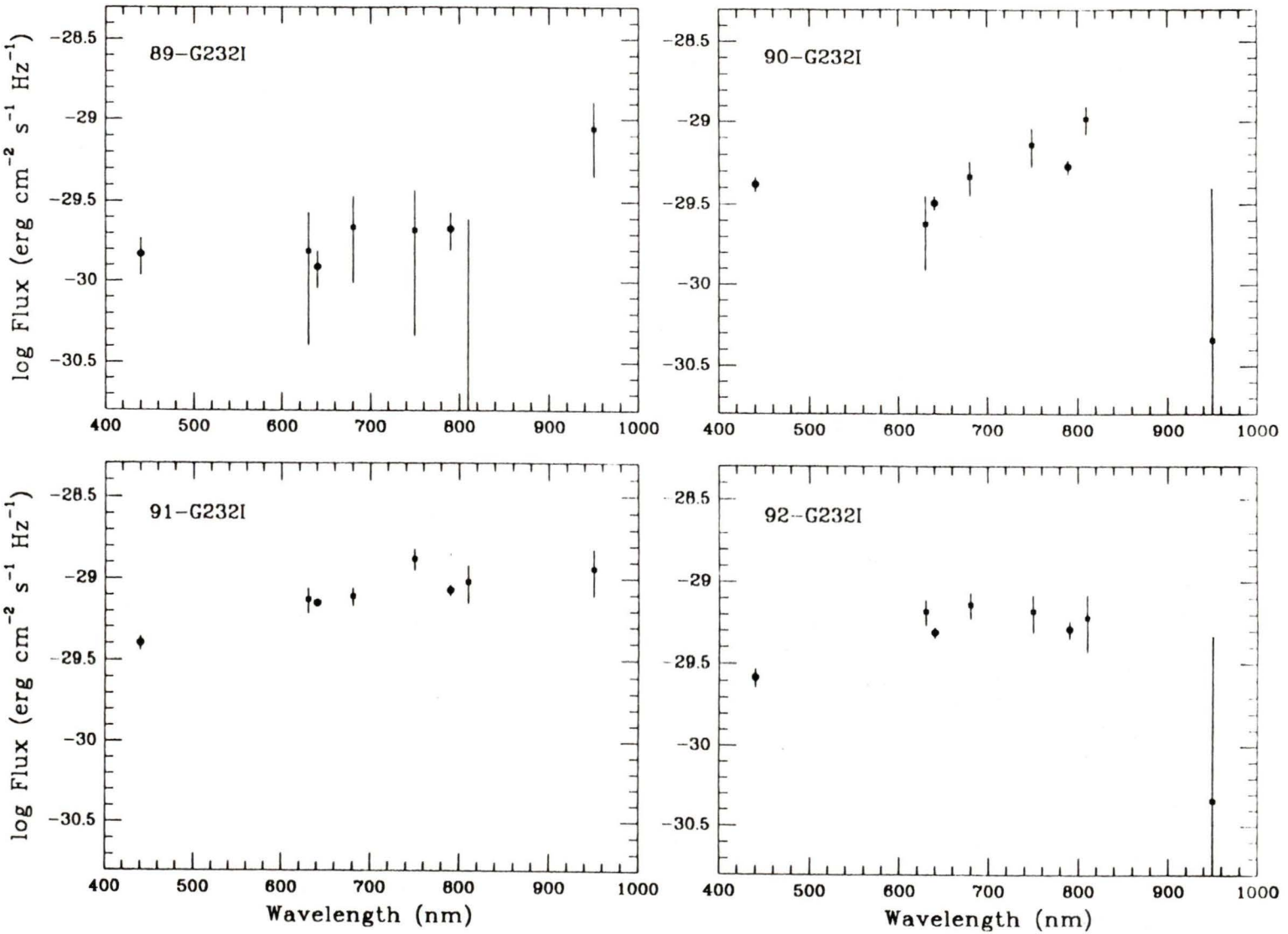
89-G232I
90-G232I
91-G232I
92-G232I
log Flux (erg cm^{-2} s^{-1} Hz^{-1})
Wavelength (nm)
-28.5
-29
-29.5
-30
-30.5
400
500
600
700
800
900
1000

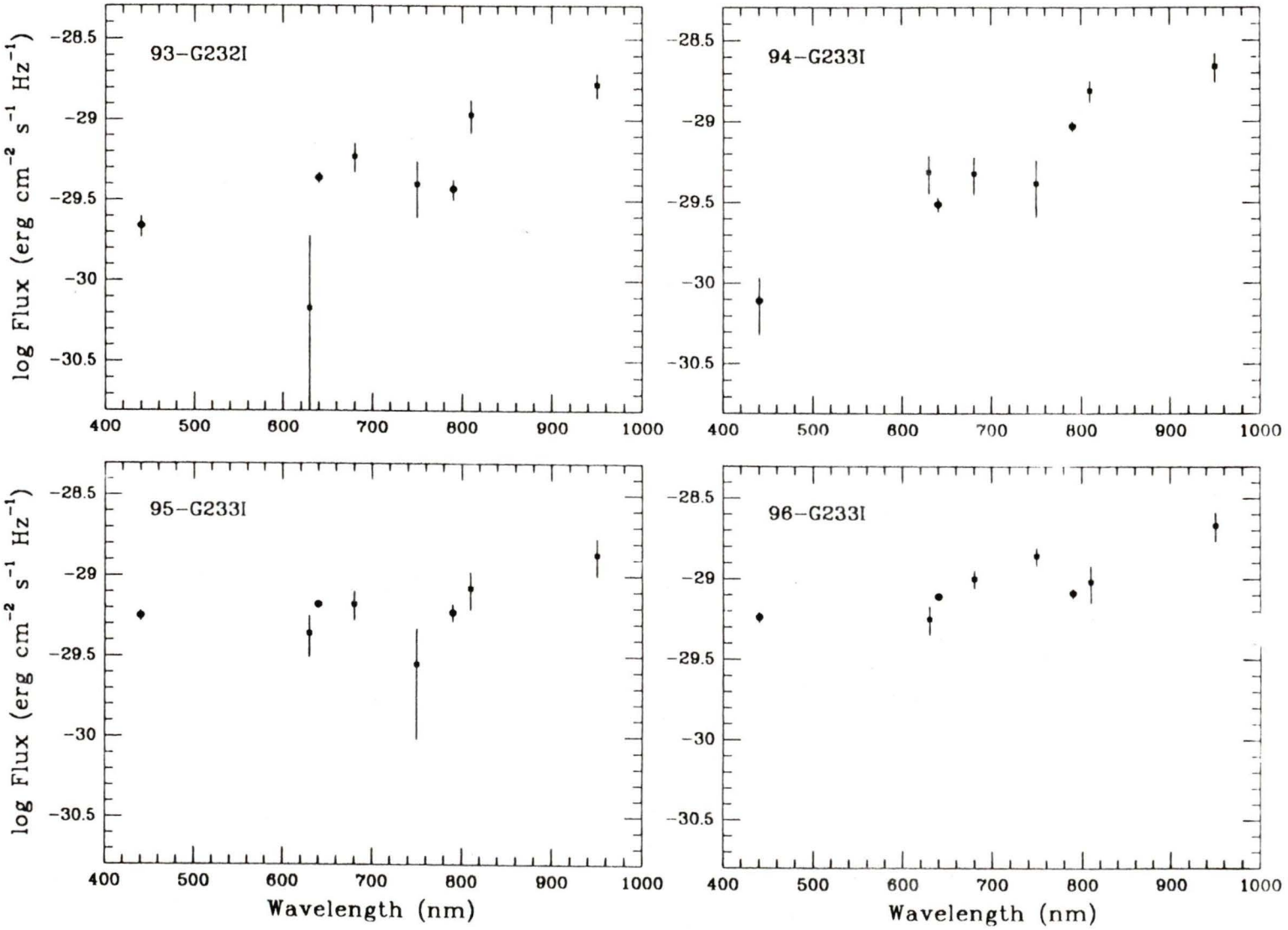
93-G232I
94-G233I
95-G233I
96-G233I
log Flux (erg cm^{-2} s^{-1} Hz^{-1})
Wavelength (nm)
-28.5
-29
-29.5
-30
-30.5
400
500
600
700
800
900
1000

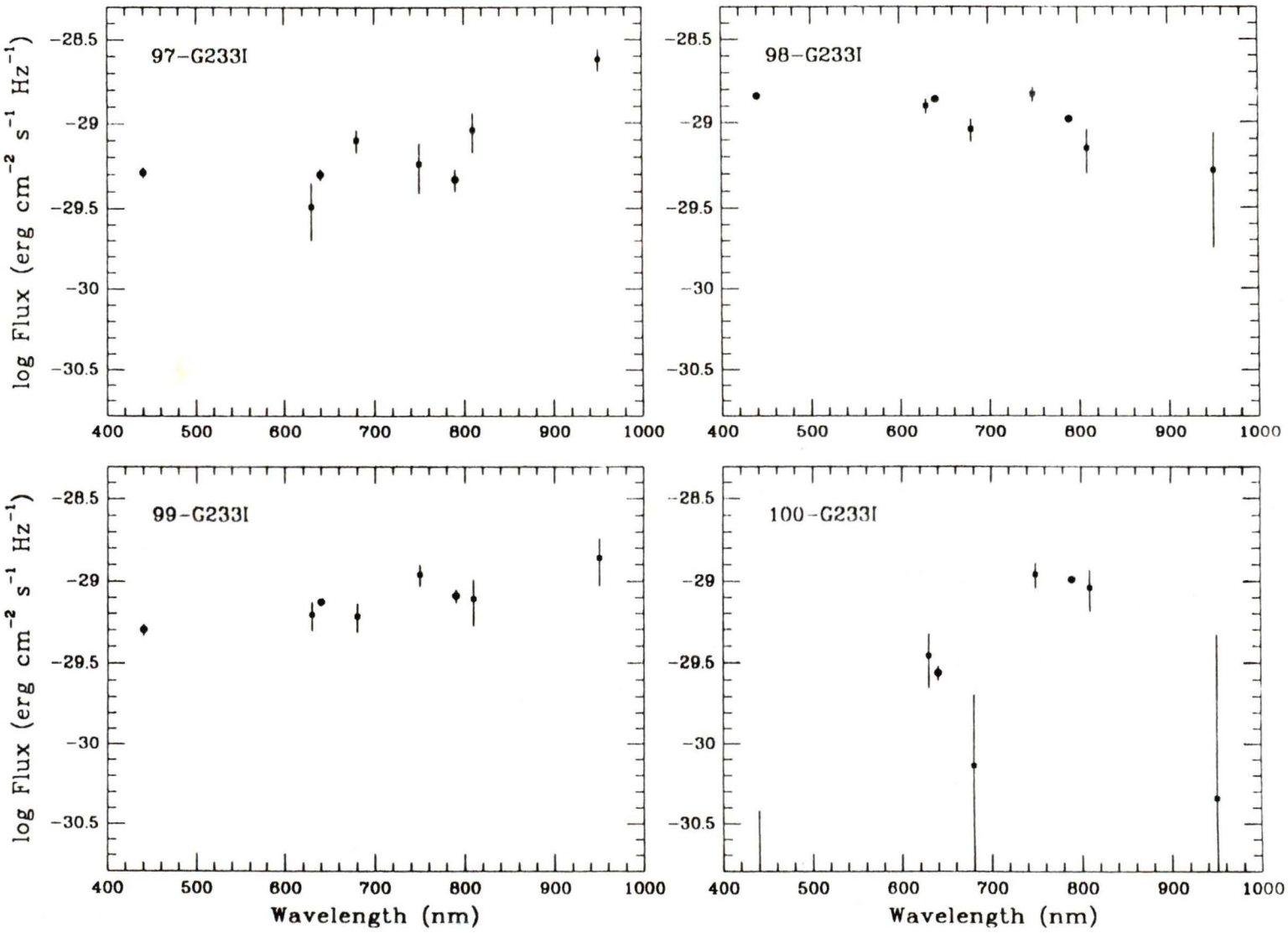
97-G233I
98-G233I
99-G233I
100-G233I
log Flux (erg cm^{-2} s^{-1} Hz^{-1})
Wavelength (nm)
-28.5
-29
-29.5
-30
-30.5
400
500
600
700
800
900
1000

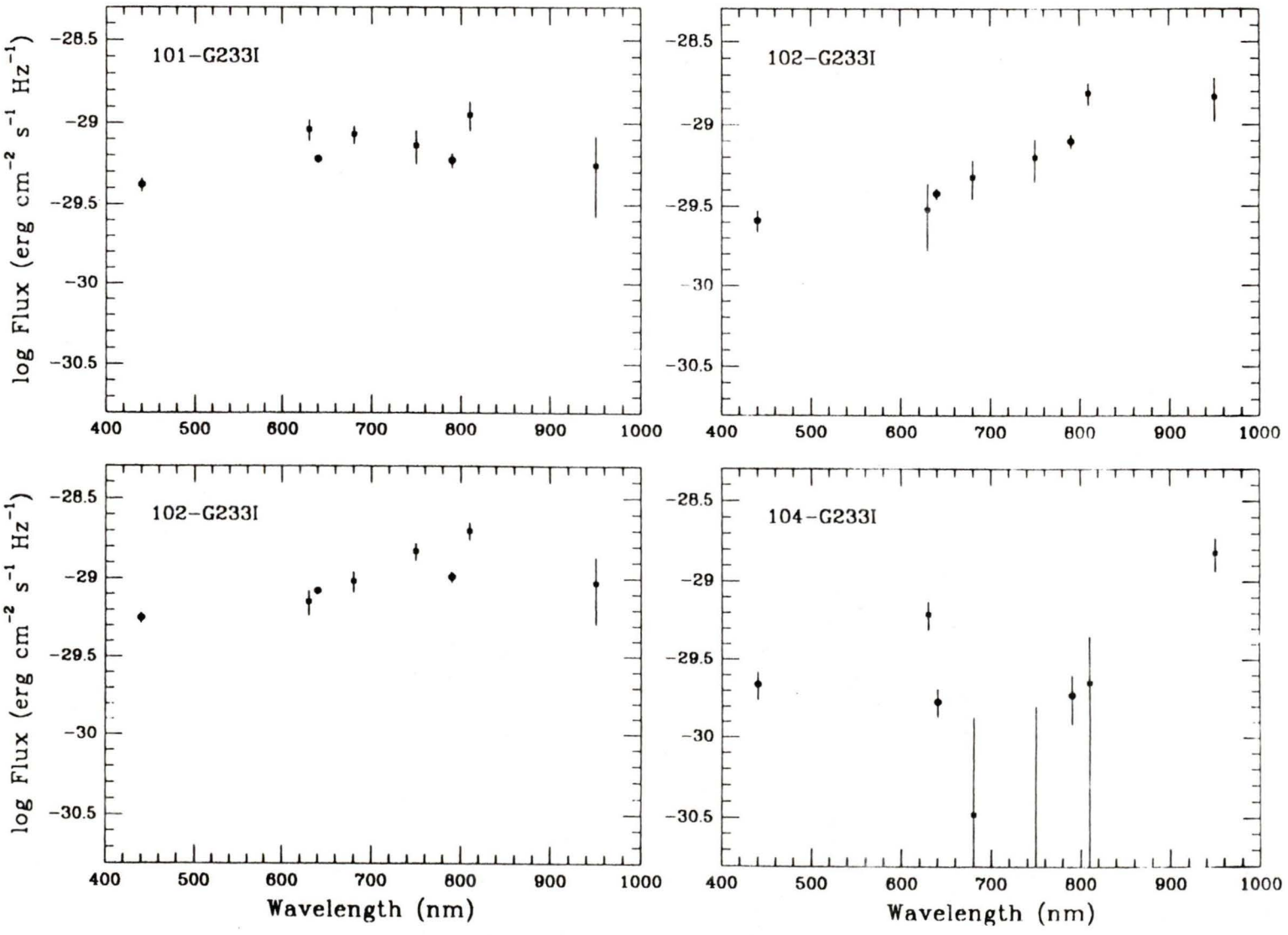
101-G233I
102-G233I
102-G233I
104-G233I
log Flux (erg cm^{-2} s^{-1} Hz^{-1})
Wavelength (nm)
-28.5
-29
-29.5
-30
-30.5
400
500
600
700
800
900
1000

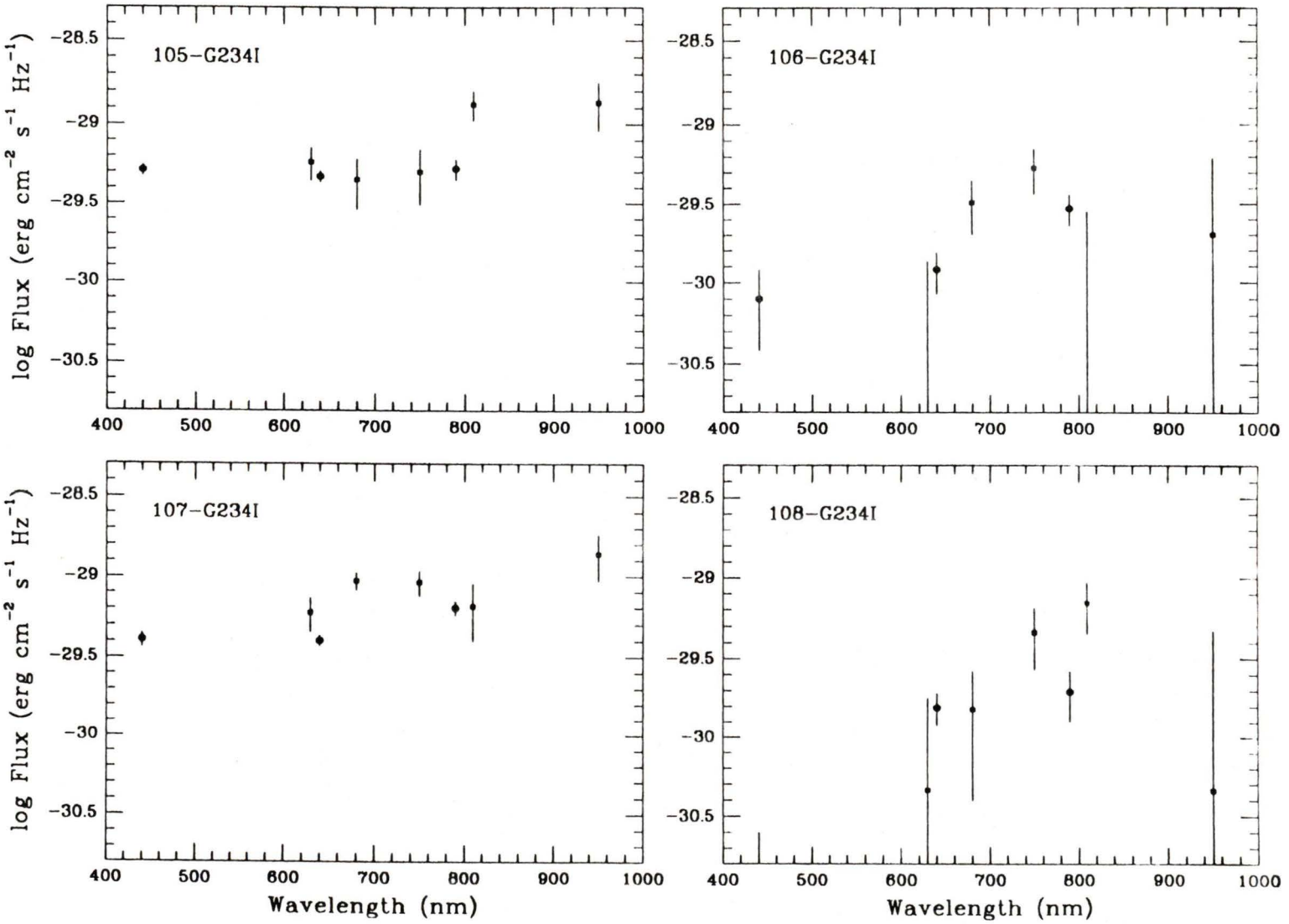
105-G234I
106-G234I
107-G234I
108-G234I
log Flux (erg cm^{-2} s^{-1} Hz^{-1})
Wavelength (nm)
-28.5
-29
-29.5
-30
-30.5
400
500
600
700
800
900
1000

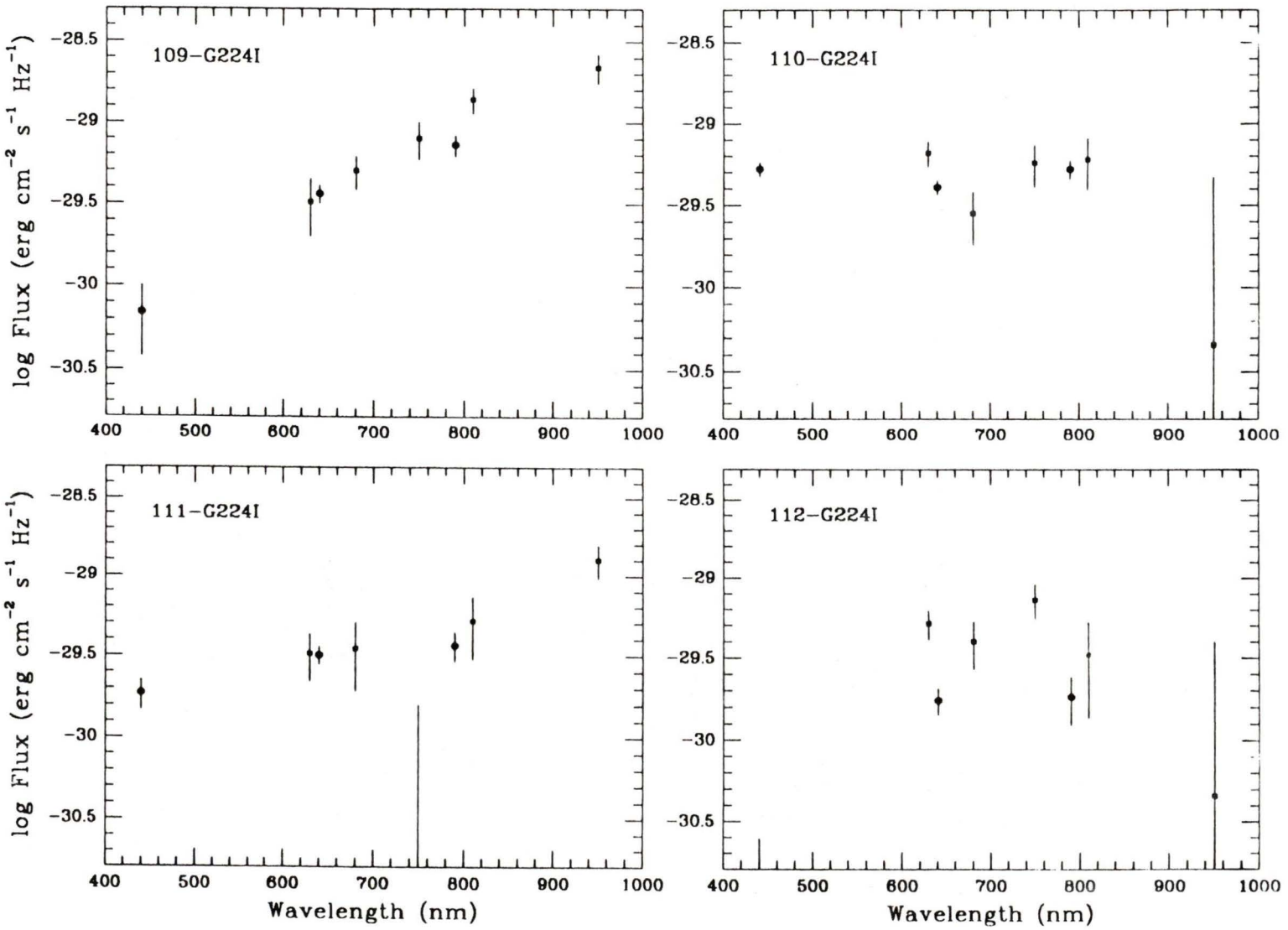
109-G224I
110-G224I
111-G224I
112-G224I
log Flux (erg cm^{-2} s^{-1} Hz^{-1})
Wavelength (nm)
-28.5
-29
-29.5
-30
-30.5
400
500
600
700
800
900
1000

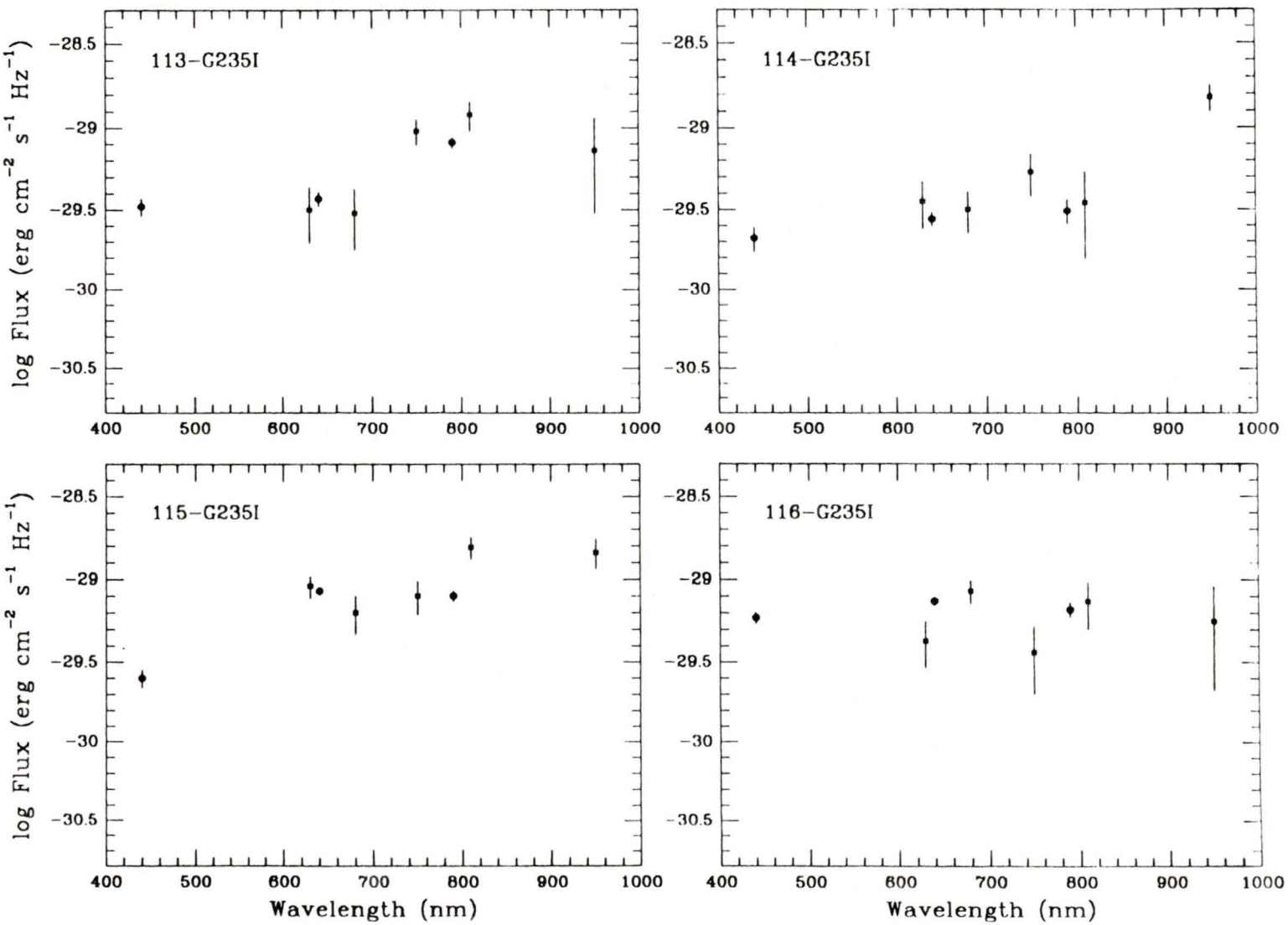
113-G235I
114-G235I
115-G235I
116-G235I
log Flux (erg cm^{-2} s^{-1} Hz^{-1})
Wavelength (nm)
-28.5
-29
-29.5
-30
-30.5
400
500
600
700
800
900
1000

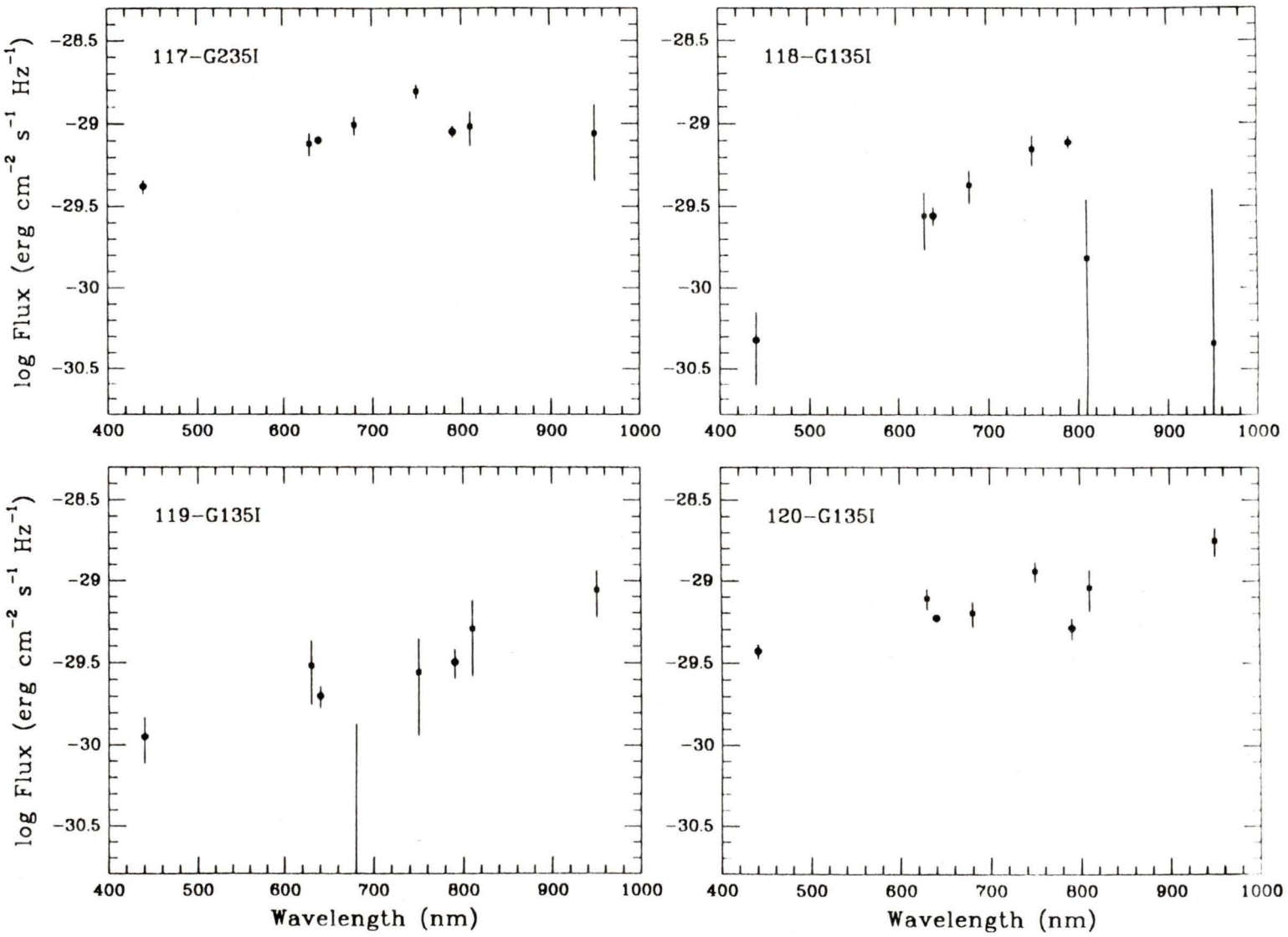
117-G235I
118-G135I
119-G135I
120-G135I
log Flux (erg cm^{-2} s^{-1} Hz^{-1})
-28.5
-29
-29.5
-30
-30.5
400
500
600
700
800
900
1000
Wavelength (nm)

Vita

Surname: **Ross** Given Names: **Gordon Chattan**

Place of Birth: **Vancouver, British Columbia**

Date of Birth:**May 26, 1961**

Educational Institutions Attended, with Dates of Entering and Leaving:

University of Calgary, Calgary	**1979 to 1982**
University of Victoria, Victoria	**1985 to 1990**

Degrees, Diplomas, Etc., Awarded, with Dates and Names of Institutions:

B.Sc. (Honours) **1988** **University of Victoria**

Partial Copyright License

I hereby grant the right to lend my thesis (the title of which is shown below) to users of the University of Victoria Library, and to make single copies only for such users, or in response to a request from the library of any other university or similar institution, on its behalf or for one of its users. I further agree that permission for extensive copying of this thesis for scholarly purposes may be granted by me or a member of the university designated by me. It is understood that copying or publication of this thesis for financial gain shall not be allowed without my written permission.

Title of Thesis:

A Cluster of Galaxies at z = 0.9

[redacted]

Author: Ross, Gordon Chattan

Date, September 4, 1990